Springer Series in Materials Science 259

Amin TermehYousefi

Nanocomposite-Based Electronic Tongue

Carbon Nanotube Growth by Chemical Vapor Deposition and Its Application

Springer

Springer Series in Materials Science

Volume 259

Series editors

Robert Hull, Troy, USA
Chennupati Jagadish, Canberra, Australia
Yoshiyuki Kawazoe, Sendai, Japan
Richard M. Osgood, New York, USA
Jürgen Parisi, Oldenburg, Germany
Tae-Yeon Seong, Seoul, Republic of Korea (South Korea)
Shin-ichi Uchida, Tokyo, Japan
Zhiming M. Wang, Chengdu, China

The Springer Series in Materials Science covers the complete spectrum of materials physics, including fundamental principles, physical properties, materials theory and design. Recognizing the increasing importance of materials science in future device technologies, the book titles in this series reflect the state-of-the-art in understanding and controlling the structure and properties of all important classes of materials.

More information about this series at http://www.springer.com/series/856

Amin TermehYousefi

Nanocomposite-Based Electronic Tongue

Carbon Nanotube Growth by Chemical Vapor Deposition and Its Application

Springer

Amin TermehYousefi
Department of Mechanical Engineering,
Faculty of Engineering
University of Malaya
Kuala Lumpur
Malaysia

and

Department of Human Intelligence Systems,
Graduate School of Life Science and
Systems Engineering
Kyushu University of Technology
Kitakyushu
Japan

ISSN 0933-033X ISSN 2196-2812 (electronic)
Springer Series in Materials Science
ISBN 978-3-319-66847-5 ISBN 978-3-319-66848-2 (eBook)
https://doi.org/10.1007/978-3-319-66848-2

Library of Congress Control Number: 2017951163

© Springer International Publishing AG 2018
This work is subject to copyright. All rights are reserved by the Publisher, whether the whole or part of the material is concerned, specifically the rights of translation, reprinting, reuse of illustrations, recitation, broadcasting, reproduction on microfilms or in any other physical way, and transmission or information storage and retrieval, electronic adaptation, computer software, or by similar or dissimilar methodology now known or hereafter developed.
The use of general descriptive names, registered names, trademarks, service marks, etc. in this publication does not imply, even in the absence of a specific statement, that such names are exempt from the relevant protective laws and regulations and therefore free for general use.
The publisher, the authors and the editors are safe to assume that the advice and information in this book are believed to be true and accurate at the date of publication. Neither the publisher nor the authors or the editors give a warranty, express or implied, with respect to the material contained herein or for any errors or omissions that may have been made. The publisher remains neutral with regard to jurisdictional claims in published maps and institutional affiliations.

Printed on acid-free paper

This Springer imprint is published by Springer Nature
The registered company is Springer International Publishing AG
The registered company address is: Gewerbestrasse 11, 6330 Cham, Switzerland

Preface

This book presents the fabrication of a glucose biosensor by modification of the surface of a glassy carbon electrode (GCE) using optimized carbon nanotubes (CNTs). The chemical vapor deposition (CVD) method was utilized to grow vertically aligned carbon nanotubes (VACNTs) with various aspect ratios. Field emission scanning electron microscopy (FESEM) images, coupled with Raman spectroscopy results, highlighted the high aspect ratio and uniformity of the high-crystalline carbon nanotubes. Transmission electron microscopy (TEM) images of the CNTs which had been grown confirmed the successful synthesis of a multiwall carbon nanotube (MWCNTs) due to the larger outer diameter of the CNTs. Furthermore, to increase the graphitic ratio of the synthesized CNTs, sequential experimental strategies, based on response surface methodology (RSM), were employed to investigate the crystallinity model of CNTs. Further to that, glucose oxidase (GOx) was immobilized on an optimized multiwall carbon nanotube/gelatin (MWCNTs/Gl) composite, using the entrapment technique to achieve the enzyme-catalyzed oxidation of glucose at anodic potentials, which was then drop-casted onto the GCE. Cyclic voltammetry (CV) results, coupled with the chronoamperometric response obtained from a modified GCE, indicated that a GOx/MWCNTs/Gl/GC electrode can be utilized as a glucose biosensor with a high direct electron transfer rate (8.42 s^{-1}) between GOx and MWCNTs/Gl within a wide linearity range (8.9 mM) of glucose. The recorded detection limit of the fabricated biosensor was 0.59 mM by keeping its initial stability of 75.4% after 25 days. The performance of the fabricated biosensor as a glucose-based electronic tongue was also investigated by designing an electric circuit which was attached to the electrochemical cell. The resistivity alteration of GOx/MWCNTs/Gl/GCE was recorded in the electrochemical cell, after each drop of glucose, by measuring the output

resistivity recorded by the electric circuit. The oscilloscope results clearly showed that, by adding glucose to the circuit design, the output oscillation frequency changed and the square-wave frequency reached a new stable value. These results indicated that the modified GCE, with GOx/MWCNTs/Gl, showed potential as an application in the determination of glucose in human serum samples, as well as a voltammetric-based electronic tongue for diagnose glucose.

Boston, USA Amin TermehYousefi
April 2017

Acknowledgements

First and foremost, I would like to thank my family: especially my parents Mehdi and Afsar for their constant warm support throughout my entire life; and my siblings Amir, Sara, Omid, and Haleh for being my rivals and motivating me. Moreover, I would like to thank my niece Arousha for being one of the main reasons of my life.

This book would not have been possible without the efforts and support of people at the following: the Chemical Energy Conversions and Applications iKoza Research Laboratory at the University of Technology, Malaysia; the Centre of Nanoscience and Nanotechnology at the University of Technology, MARA; the Nanotechnology and Catalysis Research Centre at the University of Malaya; and the Department of Human Intelligence Systems, Graduate School of Life Science and Systems Engineering, Kyushu Institute of Technology, Japan.

Contents

1 Introduction 1
1.1 Nanotechnology in Medical Science 1
1.2 Carbon Nanotubes 2
1.2.1 Synthesis of Carbon Nanotubes 3
1.2.2 Carbon Nanotubes: Surface Modification 3
1.2.3 Optimization of the Growth Condition: Response Surface Methodology 4
1.2.4 Purification of Carbon Nanotubes 4
1.2.5 Functionalization of Carbon Nanotubes 4
1.3 Chemically Modified Electrodes 5
1.4 Glucose Biosensors 5
1.5 Application of Carbon Nanotubes in the Glucose Biosensor 6
1.6 World Demand of the Electrochemical Glucose Biosensor 6
1.7 Aim and Objectives of the Book 7
1.8 Research Scope 7
1.9 Significance of Research on Electrochemical Glucose Biosensors 8
1.10 Organization of the Book 8
References 9

2 Background of the Study 13
2.1 Structures of Carbon Nanotubes 13
2.2 Generation of Carbon Nanotubes 14
2.2.1 The Arc Discharge Method 14
2.2.2 The Laser Vaporization Method 14
2.2.3 The Chemical Vapor Deposition Method 15
2.3 Fabrication of Glucose Biosensor: The First, Second, and Third Generation 19
2.3.1 Carbon Nanotube-Based Biosensors 20
2.3.2 Functionalization of Carbon Nanotubes 20

2.3.3 Functionalized Carbon Nanotubes to Enhance Electron Transfer Mechanism in Glucose Biosensor 21
2.4 Carbon Nanotube-Based Composites in Glucose Biosensors 25
2.5 Functionalization of Carbon Nanotubes for Other Applications 25
2.5.1 Thermal Applications of Carbon Nanotubes 26
2.5.2 Medical Applications of Carbon Nanotubes 28
2.5.3 Antimicrobial Activity of Carbon Nanotubes. 29
2.5.4 Drug Delivery Applications of Carbon Nanotubes. 30
2.5.5 Electro-optical Properties of Carbon Nanotubes 30
2.5.6 Mechanical Properties of Carbon Nanotubes 30
2.5.7 Gas Sensors Based on Carbon Nanotubes 31
References. 31

3 Experimental Procedures and Materials 39
3.1 Introduction 39
3.2 Materials. 39
3.3 Synthesis of Multilayer Carbon Nanotubes from Camphor Oil by Chemical Vapor Deposition Method 41
3.4 Synthesis of Well-Crystalline Carbon Nanotubes Via Neutralized Cooling Technique by Carbon Vapor Deposition Method 42
3.5 Synthesis of Highly Oriented Vertically Aligned Carbon Nanotubes Via Chemical Vapor Deposition Method. 42
3.6 Synthesis of Selective Aspect Ratio Vertically Aligned Carbon Nanotubes Via Carbon Vapor Deposition Method 43
3.7 Optimization of Highly Oriented Vertically Aligned Carbon Nanotubes' Growth Conditions Using Response Surface Methodology: Design of Experimental Matrix and Experimental Procedure 43
3.8 Characterization of Synthesized Carbon Nanotubes 46
3.8.1 Raman Spectroscopy: Measurement Conditions. 47
3.8.2 Thermogravimetric Analysis: Measurement Conditions 47
3.8.3 Field Emission Scanning Electron Microscopy: Measurement Conditions 49
3.8.4 High Resolution Transmission Electron Microscopy: Measurement Conditions 49
3.8.5 Fourier Transform Infrared Spectroscopy: Measurement Conditions 51
3.9 Chemically Modified Electrodes 52
3.9.1 Pretreatment of the Electrodes 52
3.9.2 Preparation of Phosphate Buffer 53
3.9.3 Preparation of Serum Samples and Real Sample Analysis 53

3.9.4 Fabrication of Chemically Modified Electrodes 53
3.10 Fabrication of Glucose Biosensor Based on Vertically Aligned Carbon Nanotubes Composite: GOx/MWCNTs/Gl/GCE 54
3.10.1 Synthesis, Purification, and Optimization of Multi-walled Carbon Nanotubes 54
3.10.2 Fabrication of GOx/MWCNTs/Gl/GCE 54
3.11 Electrochemical Measurements of Modified Electrodes 55
3.11.1 Electrochemical Setup 55
3.11.2 Cyclic Voltammetry 56
3.11.3 Chronoamperometric Response 57
3.12 Integration of Electronic Tongue Based on Frequency Response of GOx/MWCNTs/Gl/GCE Biosensor 57
3.12.1 Square Wave Frequency Measurements of the Electrical Circuit Attached to the Modified Electrodes 58
References 59

4 Results and Discussions 63
4.1 Fast Synthesis of Multilayer Multi-walled Carbon Nanotubes from Camphor Oil 63
4.2 Synthesis of Well-Crystalline Carbon Nanotubes Via Neutralized Cooling Method 66
4.3 Highly Oriented Vertically Aligned Carbon Nanotubes Via Carbon Vapor Deposition Method 69
4.4 Synthesis of Selective Aspect Ratio Vertically Aligned Carbon Nanotubes Via Carbon Vapor Deposition Method 74
4.5 Optimization of the Growth Condition Using Response Surface Methodology 76
4.5.1 Crystallinity Model: I_G/I_D-Single-Response Optimization 76
4.5.2 Effect of Deposition Temperature and Concentration of Camphor Oil on Carbon Nanotubes' Crystallinity 80
4.6 Constant Glucose Biosensor Based on Vertically Aligned Carbon Nanotubes Composites 81
4.6.1 Raman Spectroscopy 81
4.6.2 Field Emission Scanning Electron Microscopy 82
4.6.3 Direct Electron Transfer of GOx/MWCNTs/Gl/GCE 83
4.6.4 Biocatalytic Activity of GOx/MWCNTs/Gl/GC Electrode 84
4.6.5 Amperometric Determination of Glucose on GOx/MWCNTs/Gl/GC Electrode 86
4.6.6 Reproducibility and Stability of the GOx/MWCNTs/Gl/GC Electrode 86

4.6.7 Determination of Glucose in Human Blood Serum and Analytical Recovery of Glucose . . . 87
4.7 Brain-Like Taste Bud Circuit Using the GOx/MWCNTs/Gl/GCE Glucose Biosensor . . . 87
4.7.1 Electrical Circuit of a Taste Bud Inspired Network: Single Membrane . . . 88
References . . . 90

5 Conclusion . . . 93
5.1 Introduction . . . 93
5.2 Morphology Optimization of Synthesized Carbon Nanotubes . . . 93
5.3 Fast Synthesizing of the Multilayer Carbon Nanotubes . . . 94
5.4 Well-Crystalline Multi-walled Carbon Nanotubes . . . 94
5.5 Highly Oriented Carbon Nanotubes . . . 94
5.6 Selective Aspect Ratio of Carbon Nanotubes . . . 94
5.7 Vectorial Crystal Growth of Oriented Vertically Aligned Carbon Nanotubes . . . 95
5.8 Constant Glucose Biosensor Based on Vertically Aligned Carbon Nanotubes Composites . . . 95
5.9 Brain-Like Taste Bud Circuit Using the GOx/MWCNTs/Gl/GCE Glucose Biosensor . . . 96
5.10 Research Contribution . . . 96
5.11 Recommendations and Future Work . . . 97

Index . . . 99

Acronyms

CE	Counter electrode
CMEs	Chemically modified electrodes
CNT	Carbon Nanotube
CVD	Chemical vapor deposition
DC	Direct current
DWCNTs	Double-walled carbon nanotubes
E	Potential
FAD	Flavin adenine dinucleotide
FESEM	Field emission scanning electron microscopy
FTIR	Fourier transform infrared spectroscopy
GCE	Glassy carbon electrode
Gl	Gelatin
GOx	Glucose oxidase
HRTEM	High resolution transmission electron microscopy
I	Current
LED	Light emitting diode
MWCNTs	Multi-walled carbon nanotubes
PBS	Phosphate buffered saline
R	Resistance
RE	Reference electrode
RSD	Relative standard deviation
SWCNTs	Single-walled carbon nanotubes
TGA	Thermogravimetric analysis
VACNTs	Vertically aligned carbon nanotubes
WE	Working electrode

Chapter 1
Introduction

Abstract Glucose monitoring is one of the main targets of biosensing studies, as 5% of the populations of developed countries are suffering from diabetes. Therefore, an accurate monitoring of the blood glucose level seems to play a major role in the diagnosis and management of *diabetes mellitus*. Carbon nanotube (CNT) is one of the most promising materials widely used in this area due to its electrical properties. Beside glucose monitoring for diabetes, the biosensors array for the electronic tongue has also become an important area of research. Generally, an electronic tongue is a single or multisensory device dedicated to the automated analysis of complex composition samples and recognizes their characteristic taste properties. This chapter introduces the synthesis method, optimization approach, properties, and electrochemical applications of the CNTs-based glucose biosensor. Furthermore, the significance of the electrochemical glucose biosensor in both medical application and glucose-based electronic tongue is discussed in detail.

1.1 Nanotechnology in Medical Science

Recently, nanotechnology became an area of interest in physics, chemistry, and material science. Many chemical and electrochemical methods rely on nanomaterials, especially nanostructures [1]. Nanostructures differ from bulk materials due to their small size and unique structure that exhibits perfect physical, chemical, and electronic properties [2]. They can be used to construct novel materials to improve electrochemical devices and biosensors [3]. Currently, a large number of nanostructures in different sizes and compositions are being utilized in chemistry and physics.

Vast and diverse types of devices have been employed in engineering, fundamental sciences, and biology [4]. Nanotechnology is very beneficial and useful in medical applications, such as drug development [5], diseases diagnoses [6], cell treatment [7], and biological technologies [8], owing to its roles in the production of stronger, lighter, and purified materials [9]. One of the most valuable applications of nanotechnology is in the development of novel and effective medical treatments

© Springer International Publishing AG 2018

A. TermehYousefi, *Nanocomposite-Based Electronic Tongue*, Springer Series in Materials Science 259, https://doi.org/10.1007/978-3-319-66848-2_1

that addressed the limitations of current molecular diagnostics, provided accurate diagnosis, and lead to the development of personalized treatments [10]. Recent advancements in nanotechnology that combine biosensors with nanomaterials have introduced efficient and simple devices to be used for the measurements of the analytes' concentration and the response-time functions of target biomolecules to the biological cell, drug, or toxic reagents [11]. Researchers have exploited a variety of measurement techniques using miniaturized and portable devices to optimize the conditions, observe, and control biological reactions on micro or nano-surfaces. Electrochemical devices are one of the useful methods in biosensor development, due to their simplicity, low costs, accuracy, and sensitivity toward medical diagnosis [12]. The transducer converts the biological recognition events to useful electrical signals. Easy-to-use and self-medical-testing are major roles of nanotechnology in the context of home-use medical devices via electrochemical approaches and other applicable methods [13].

1.2 Carbon Nanotubes

The electrochemical biosensor converts biological recognition events to useful and understandable electrical signals. Electrochemical biosensors rely on nanomaterials, especially nanostructures [1, 14]. They can be used to construct novel materials to improve biosensors. Generally, nanostructures such as carbon nanomaterials (for example, fullerenes, nanotubes, and graphene) possess excellent electrical properties and conductivity, rendering them suitable for electrochemical sensors [15]. Carbon nanotube is a novel type of nanomaterial that has significantly different properties compared to its counterparts [16].

Rolled graphene sheets are known as CNTs with capped ends, which could be single-walled carbon nanotube (SWCNTs), double-walled carbon nanotube (DWCNTs), or multi-walled carbon nanotubes (MWCNTs) [17]. Based on the rolling axis of the graphene sheets, CNTs are classified into three groups, namely armchair CNTs, zigzag CNTs, and chiral CNTs [18]. The differences that separate these CNTs are the method of turning axis with respect to the hexagonal network of the graphene sheet, as well as the closing cylinder radius. A pair of indices, m and n, shows the chiral vector, where these two integers correspond to the number of unit vectors in two directions in the honeycomb crystal lattice of graphite. For the nanotube in the category of "zigzag", the m value is 0 [19]. When the value of m is equal to n, the nanotube is called "armchair" [20]. All other configurations are created in chiral form [21]. Potential application(s) of CNTs motivated scientists to improve its operation and utilization. CNTs and chemically modified CNTs have the potential for diverse applications, such as nanoelectronics/nanospintronics

components, biosensing, tissue engineering, and drug delivery. CNTs display a perfect combination of excellent electrical properties, resulting in increasing interest in biosensors based on CNTs [22].

1.2.1 Synthesis of Carbon Nanotubes

There are some high temperature techniques to produce CNTs. Although techniques such as arc discharge or laser ablation have been traditionally employed to build CNTs, currently low temperature techniques (<800 °C), such as CVD, have been developed to produce CNTs [23]. Low temperature techniques are capable of accurately controlling the orientation, alignment, length, diameter, purity, and density of CNTs [24]. Despite the significant amount of byproducts from these methods, they manage to produce high quality nanotubes [25]. CVD is touted as the most popular synthesizing method for CNTs, due to its highly suitable architecture for different applications from the length of the nanotubes, the uniform orientation, extra high purity of growing CNTs, and low costs [26]. The containing gas over a supported catalyst is the basis of this method. Although many types of carbon sources were used to grow CNTs, the thermal decomposition reaction of the carbon source restricted their synthesis. Most of the optimization methods of growth parameters rely on empirical experiments [27].

1.2.2 Carbon Nanotubes: Surface Modification

One of the stiffest (Young's modulus) and strongest (yield strength) nanostructures are CNTs, due to C–C bonds. It was concluded that CNTs are suitable for different biological applications, such as electrochemical, optical, and pyroelectric biosensors [28]. Also, CNTs are very predominant in current medical research, especially in disease diagnosis and health screening [29]. Uniformity and purity of dispersed CNTs play an important role in collecting concentration results [30]. Therefore, developing biosensors based on CNTs is classified as a degree of solubilization for pristine CNTs in aqueous solvents, due to the hydrophobic attributes of the side walls of the CNTs, coupled with individual π–π interactions of the tubes [31]. For this purpose, CNTs should be modified by a desired dispersion method to decrease the tube's bundle formation. Surfactant-assisted dispersion, solvent dispersion, biomolecular dispersion, and functionalization of side walls are some of the advance methods for a desirable dispersion [32]. According to the previous results highlighted by researchers, the functionalization method is the most effective approach, due to the active surface of CNTs [33]. Sequential experimental strategies are also an important method to quantify a correlation between effective parameters involved in the growth mechanism and synthesis a condition of CNTs for their respective applications [34].

1.2.3 Optimization of the Growth Condition: Response Surface Methodology

CNTs have been considered for many technological applications, due to their unique electrical and mechanical properties. Recently, interest in growing CNTs with high crystallinity and low defects in a controlled orientation is fast becoming the focus of research activities in producing defect-free CNTs [31]. However, optimizing the performance of a process in its own setup is generally more difficult than building the system itself [35]. Having a set of techniques to determine the optimum condition of the growth process beyond the available surface resources of experiments is being employed as the new strategy to gain a better understanding of synthesizing conditions of low defect CNTs [36]. Two major advantages of these statistical strategies are: (1) the number of essential experiments was decreased by using a few carefully selected points for each parameter—thus, the minimum number of experiments provides information about real systems; and (2) the new method provides a better understanding of the physical behavior of the system by adequately choosing a range for each parameter [37].

1.2.4 Purification of Carbon Nanotubes

The synthesized nanotubes often consist of impurities such as amorphous carbon and metal nanoparticles [38]. The metal nanoparticles are significant when metal catalysts are employed. Amorphous carbon can be easily removed. The high density of defects in amorphous carbon allows it to be oxidized under inert conditions [39]. Carbonaceous and metal impurities need to be removed as well [40]. They possess wide particle size distributions and different amounts of defects or curvature based on their synthesis conditions [41]. Therefore, it is not easy to develop a unified purification method to reproduce high purity CNTs. Acid treatment, gas phase oxidation, microfiltration, and hydrothermal treatment are some of the viable methods to eliminate amorphous carbon and catalyst particles [42].

1.2.5 Functionalization of Carbon Nanotubes

Adding a functional group to CNTs may improve their solubility and processability. The functionalization results in a combination of unique properties in the resulting material [43]. Interaction between the nanotube and other entities such as solvent, polymer, and biopolymer matrices, or other nanotubes can be tailored by means of chemical bonds. Functionalized nanotubes might have different mechanical and electrical properties [44]. Fine-tuning the chemistry and physics of CNTs involves functionalized properties [45]. Functionalized covalent and non-covalent CNTs

should be separated as well. In addition, the functionalization of SWCNTs and MWCNTs should be distinguished as individual and bundle tube [46]. The basis of the covalent functionalization is that the covalent links functional entities onto the nanotube's carbon scaffold, while a non-covalent functionalization relies on supramolecular complexation utilizing a variety of sorption forces like van der Waals' and pi-stacking interaction. In fact, this functionalization is called exohedral derivatizations [47].

1.3 Chemically Modified Electrodes

One route to designing an electrode system is chemically modified electrodes (CMEs) [48]. CMEs have been used in many electrochemical device and system designs, such as chemical sensing energy conversion and storage, molecular electronics, electrochromic displays, and electroorganic synthesis [49]. Generally, experimental measurements and studies in CMEs have some related parameters, where charge transfer reaction is the most significant [50]. Coating conductor or semiconductor electrodes with a specific monomolecular, multimolecular, ionic, or polymeric film of a chemical modifier constitutes CMEs [51]. The difference between CMEs and other electrodes in electrochemistry is a thin film of a selected substance [52]. This substance is bonded to or is coated onto the electrode surface, and applies the desirable properties of the film in a rational chemically designed manner to the electrode. Desirable properties in this case include chemical, electrochemical, optical, electrical, and transport [53].

1.4 Glucose Biosensors

Change of the blood glucose concentrations from being higher or lower than 80–120 mg/dL (4.4–6.6 mM) cause diabetes which is a major cause of death or disabilities to people across the world. It also increases the risks of heart disease, kidney failure, and blindness. These complications can be prevented, or at least decreased, by an accurate personal control of blood glucose levels [54]. Therefore, an accurate monitoring of the blood glucose level seems to play a major role in the diagnosis and management of *diabetes mellitus* [55]. Biosensors are the most common method for blood glucose detection, due to advantages such as simplicity and quickness. Biosensors are specific kinds of CMEs that combine biochemical recognitions with an appropriate electrochemical transducer. The attachment of a biocomponent, such as an enzyme, antigen, antibody, plant, or animal tissue alters the surface of the electrode, functioning as a biological recognition element [56].

1.5 Application of Carbon Nanotubes in the Glucose Biosensor

A major trend in the development and application of biosensors can be observed during the past decade [57]. Biosensors have been used for detecting biological analytes. The main anticipated applications of CNTs are as components in biological devices [58]. Much research has been conducted on the attachment of biological molecules to these nanomaterials [59]. Based on conducted studies and research results, the inner channel of opened nanotubes entraps small proteins by simple adsorption. Small proteins can be attached on the outer surface of CNTs as well [60]. This may happen due to hydrophobic and electrostatic interactions by means of covalent bonding or functionalization of nanotube sides by polymer coating [61]. The speed of electron transfer between the enzymes' active site and the electrochemical transducer is very important in biosensor designs [62]. When the system needs to be miniaturized, extra restrictions may be applied. Small surface area leads to constraints concerning the minimum enzyme loading that can be repeatably immobilized for analytical applications [63]. The metallic character of CNTs shows structure dependent properties enabling them to promote electron transfer reactions at low overpotentials [64]. The ground for unique biochemical sensing systems has been provided by means of this characteristic along with high surface area. Latest advances of well controlled aligned CNT arrays show the way for incorporation of nanotechnology in biosensor design [65].

1.6 World Demand of the Electrochemical Glucose Biosensor

It is reported that 5% of the population of developed countries suffers from diabetes; thus, a tight monitoring of glucose level is urgent for preventing and managing *diabetes mellitus* [66]. Due to constraints in current glucose detection methods, such as low stability and sensitivity, high costs, and complex understanding of the mechanisms, the implementation of an effective approach is essential in designing modern glucose biosensors, such as the electrochemical approach [67]. Electrochemical detecting of glucose mostly owes a wide dynamic detection range and continuous determination of glucose both in diabetic and electronic tongue approaches [68]. CNTs demonstrate better electrochemical reactivity due to the hollow core being suitable for storing enzymes and promoting electron transfer reactions of enzymes, such as glucose oxides [69]. Unfortunately, there are some limitations in the immobilization of enzymes on the electrode's surface, coupled with the poor electron transfer between the enzymes' active site and the electrode from enzyme leaching and the short lifetime of enzyme. Based on our knowledge,

several methods have been developed to increase the biological function, stability, and efficacy of enzyme immobilization in electrochemical method by increasing the surface area of the CNTs [70]. Therefore, the synthesis of optimized CNTs and fabricating CNTs-modified electrodes is extremely attractive in improving the detection range, sensitivity, and the selectivity of the electrochemical glucose biosensor [71].

Beside glucose monitoring for diabetes, the biosensors array for the electronic tongue has also become an important area of research [72]. Generally, an electronic tongue is a single or multisensory device dedicated to the automated analysis of complex composition samples which recognizes their characteristic taste properties [73]. Recently, the number of fabricated electronic tongues has significantly increased due to the increase of the electrochemical detection of biomolecules [74]. However, several possible architectures of electronic tongue were proposed, such as potentiometric, voltammetric, embracing mass, and optical sensors.

1.7 Aim and Objectives of the Book

This book mainly focuses on the synthesis, optimization, and utilization of CNTs composite materials to develop the amperometric glucose biosensor applied in the electronic tongue. Amperometric glucose biosensors are employed as the model system to compare the effects of different components on the performance of the biosensors. The objectives are: (1) to synthesize and optimize VACNTs using the CVD method; (2) to fabricate chemically modified glassy carbon electrodes (GCEs) using an optimized CNTs composite; and (3) to investigate the performance of fabricated nanocomposite-based electrodes in the electrochemical glucose biosensor and electronic tongue.

1.8 Research Scope

The central theme of this book highlights the critical role of optimized MWCNTs to achieve enhanced performance and miniaturization of the modified GCE applied in fabrication of the glucose biosensor and electronic tongue. With the intention of achieving the above-mentioned objective, a series of scopes was carefully designed:

- VACNTs were synthesized by using the CVD method. Camphor oil and ferrocene was used to compose the vaporized CNTs, and different CVD conditions were applied to obtain the best morphology of VACNTs.
- The optimized MWCNTs were mixed with gelatin to produce a MWCNTs/gelatin composite to entrap glucose oxidase and then drop-casted on the surface of the GCE. The modified GCE was examined under the different

conditions to ensure the successful immobilization of glucose oxidase on the modified GCE.

- The modified GCE was used for electrochemical detection of glucose in the buffer solution. The polymeric entrapment and covalent immobilization of enzyme enhances the direct and fast electron transfer in the continuous monitoring of glucose. The glucose biosensor was attached to a brain-like circuit to fabricate an electronic tongue which consisted of two different layers. In the first layer, the alteration of current obtained by glucose detection of biosensor was transduced to a spiking pattern. The spiking pattern was conducted to the second layer via paracrine-like optical transmission, and induced synchronization of neural spiking activity in the second layer.

1.9 Significance of Research on Electrochemical Glucose Biosensors

The development of an authentic, economical, and convenient glucose biosensing system for diabetes diagnosis is essentially important in monitoring and treating diabetes. This study is significant since optimized VACNTs can maximize enzyme immobilization on the surface of the electrode, which can further promote electron transfer rates between the enzymes' active site and the modified electrode, resulting in an amperometric glucose biosensor with high stability and sensitivity.

1.10 Organization of the Book

This Chapter introduces the synthesis, optimization, properties, and electrochemical applications of CNTs-based glucose biosensors. Chapter 2 describes a comprehensive review on the synthesis, characterization, optimization of CNTs and glucose biosensors based on CNTs composites. Chapter 3 describes the materials and methods of synthesis, characterization, optimization of carbon nanotubes, and modification methods of GCEs via CNT/gelatin composites. The fabrication method of glucose biosensors and electronic tongues will also be discussed in this chapter. Chapter 4 describes the results and discussion of all experiments, including the synthesis, characterization, and optimization of CNTs, as well as glucose biosensors utilized in investigation of frequency based electronic tongues by modifying the GCEs. Chapter 5 concludes the experiments conducted during the course of this work.

References

1. Challa SSR Kumar. 2007. *Nanomaterials for medical diagnosis and therapy*. Weinheim: Wiley-VCH.
2. Desheng Kong, Haotian Wang, Judy J. Cha, Mauro Pasta, Kristie J. Koski, Jie Yao, and Yi Cui. 2013. Synthesis of MoS2 and MoSe2 films with vertically aligned layers. *Nano letters* 13 (3): 1341–1347.
3. Hasanzadeh, Mohammad, Nasrin Shadjou, and Miguel de la Guardia. 2015. Iron and iron-oxide magnetic nanoparticles as signal-amplification elements in electrochemical biosensing. *TrAC Trends in Analytical Chemistry* 72: 1–9.
4. Andrianantoandro, Ernesto, Subhayu Basu, David K. Karig, and Ron Weiss. 2006. Synthetic biology: New engineering rules for an emerging discipline. *Molecular Systems Biology* 2 (1).
5. Ochekpe, Nelson A., Patrick O. Olorunfemi, and Ndidi C. Ngwuluka. 2009. Nanotechnology and drug delivery part 2: Nanostructures for drug delivery. *Tropical Journal of Pharmaceutical Research* 8 (3).
6. Giljohann, David A. and Chad A. Mirkin. 2009. Drivers of biodiagnostic development. *Nature* 462 (7272): 461–464.
7. Baca, Helen K., Carlee Ashley, Eric Carnes, Deanna Lopez, Jeb Flemming, Darren Dunphy, Seema Singh, Zhu Chen, Nanguo Liu, and Hongyou Fan. 2006. Cell-directed assembly of lipid-silica nanostructures providing extended cell viability. *Science* 313 (5785): 337–341.
8. Klaus-Joerger, Tanja, Ralph Joerger, Eva Olsson, and Claes-Göran Granqvist. 2001. Bacteria as workers in the living factory: Metal-accumulating bacteria and their potential for materials science. *Trends in Biotechnology* 19 (1): 15–20.
9. Fan, Jinxin, Jianquan Luo, Weijie Song, and Yinhua Wan. 2017. One-step purification of α 1-antitrypsin by regulating polyelectrolyte ligands on mussel-inspired membrane adsorber. *Journal of Membrane Science* 528: 155–162.
10. Ju, Huangxian, Xueji Zhang, and Joseph Wang. 2011. Nanobiosensing for clinical diagnosis. In *NanoBiosensing*, 535–567. Springer.
11. Salata, Oleg V. 2004. Applications of nanoparticles in biology and medicine. *Journal of Nanobiotechnology* 2 (1): 3.
12. Ahuja, Tarushee, and Devendra Kumar. 2009. Recent progress in the development of nano-structured conducting polymers/nanocomposites for sensor applications. *Sensors and Actuators B: Chemical* 136 (1): 275–286.
13. Wang, Joseph. 2006. Electrochemical biosensors: Towards point-of-care cancer diagnostics. *Biosensors & Bioelectronics* 21 (10): 1887–1892.
14. Zhong-Shuai, Wu, Guangmin Zhou, Li-Chang Yin, Wencai Ren, Feng Li, and Hui-Ming Cheng. 2012. Graphene/metal oxide composite electrode materials for energy storage. *Nano Energy* 1 (1): 107–131.
15. Hu, Liangbing, David S. Hecht, and George Gruner. 2010. Carbon nanotube thin films: Fabrication, properties, and applications. *Chemical Reviews* 110 (10): 5790–5844.
16. Chronakis, Ioannis S. 2005. Novel nanocomposites and nanoceramics based on polymer nanofibers using electrospinning process—A review. *Journal of Materials Processing Technology* 167 (2): 283–293.
17. Odom, Teri Wang, Jin-Lin Huang, Philip Kim, and Charles M Lieber. 2000. Structure and electronic properties of carbon nanotubes. *The Journal of Physical Chemistry B* 104 (13): 2794–2809.
18. Valcárcel, M., S. Cárdenas, and B.M. Simonet. 2007. Role of carbon nanotubes in analytical science. *Analytical Chemistry* 79 (13): 4788–4797.
19. Dresselhaus, Mildred S., Gene Dresselhaus, and Peter C. Eklund. 1996. *Science of fullerenes and carbon nanotubes: Their properties and applications*. Academic press.
20. Wilder, Jeroen W.G., Liesbeth C. Venema, Andrew G. Rinzler, Richard E. Smalley, and Cees Dekker. 1998. Electronic structure of atomically resolved carbon nanotubes. *Nature* 391 (6662): 59–62.

21. Odom, Teri Wang, Jin-Lin Huang, Philip Kim, and Charles M Lieber. 1998. Atomic structure and electronic properties of single-walled carbon nanotubes. *Nature* 391 (6662): 62–64.
22. Ma, Peng-Cheng, Naveed A Siddiqui, Gad Marom, and Jang-Kyo Kim. 2010. Dispersion and functionalization of carbon nanotubes for polymer-based nanocomposites: A review. *Composites Part A: Applied Science and Manufacturing* 41 (10): 1345–1367.
23. Prasek, Jan, Jana Drbohlavova, Jana Chomoucka, Jaromir Hubalek, Ondrej Jasek, Vojtech Adam, and Rene Kizek. 2011. Methods for carbon nanotubes synthesis—Review. *Journal of Materials Chemistry* 21 (40): 15872–15884.
24. Kwok, Kinghong, and Wilson K.S. Chiu. 2005. Growth of carbon nanotubes by open-air laser-induced chemical vapor deposition. *Carbon* 43 (2): 437–446.
25. Cheung, Chin Li, Andrea Kurtz, Hongkun Park, and Charles M Lieber. 2002. Diameter-controlled synthesis of carbon nanotubes. *The Journal of Physical Chemistry B* 106 (10): 2429–2433.
26. Kong, Jing, Alan M Cassell, and Hongjie Dai. 1998. Chemical vapor deposition of methane for single-walled carbon nanotubes. *Chemical Physics Letters* 292 (4): 567–574.
27. Lee, Cheol-jin and Jae-eun Yoo. 2002. Mass synthesis method of high purity carbon nanotubes vertically aligned over large-size substrate using thermal chemical vapor deposition. Google Patents.
28. Ciofani, Gianni, Serena Danti, Leonardo Ricotti, Delfo D'Alessandro, Stefania Moscato, Stefano Berrettini, Virgilio Mattoli, and Arianna Menciassi. 2011. Boron nitride nanotubes: Production, properties, biological interactions and potential applications as therapeutic agents in brain diseases. *Current Nanoscience* 7 (1): 94–109.
29. Yousefi, Amin Termeh, Shoichiro Ikeda, Mohammad Rusop Mahmood, and Haleh Termeh Yousefi. 2014. Simulation of nano sensor based on carbon nanostructures in order to form multifunctional delivery platforms. *Advanced Materials Research* 832: 778–782.
30. Liu, Huaping, Ye Feng, Takeshi Tanaka, Yasuko Urabe, and Hiromichi Kataura. 2010. Diameter-selective metal/semiconductor separation of single-wall carbon nanotubes by agarose gel. *The Journal of Physical Chemistry C* 114 (20): 9270–9276.
31. Chen, Jiangyao, Guiying Li, Yong Huang, Haimin Zhang, Huijun Zhao, and Taicheng An. 2012. Optimization synthesis of carbon nanotubes-anatase TiO_2 composite photocatalyst by response surface methodology for photocatalytic degradation of gaseous styrene. *Applied Catalysis, B: Environmental* 123: 69–77.
32. Pan, Bo, and Baoshan Xing. 2008. Adsorption mechanisms of organic chemicals on carbon nanotubes. *Environmental Science and Technology* 42 (24): 9005–9013.
33. Kong, Hao, Chao Gao, and Deyue Yan. 2004. Controlled functionalization of multiwalled carbon nanotubes by in situ atom transfer radical polymerization. *Journal of the American Chemical Society* 126 (2): 412–413.
34. Rycenga, Matthew, Claire M Cobley, Jie Zeng, Weiyang Li, Christine H Moran, Qiang Zhang, Dong Qin, and Younan Xia. 2011. Controlling the synthesis and assembly of silver nanostructures for plasmonic applications. *Chemical Reviews* 111 (6): 3669–3712.
35. Berg, Marc. 2001. Implementing information systems in health care organizations: Myths and challenges. *International Journal of Medical Informatics* 64 (2): 143–156.
36. Fan, Yuwei, Brett R. Goldsmith, and Philip G. Collins. 2005. Identifying and counting point defects in carbon nanotubes. *Nature Materials* 4 (12): 906–911.
37. Bezerra, Marcos Almeida, Ricardo Erthal Santelli, Eliane Padua Oliveira, Leonardo Silveira Villar, and Luciane Amélia Escaleira. Response surface methodology (RSM) as a tool for optimization in analytical chemistry. *Talanta* 76 (5): 965–977.
38. Leonhardt, Albrecht, Silke Hampel, Christian Mueller, Ingolf Moench, Radinka Koseva, Manfred Ritschel, Dieter Elefant, Kati Biedermann, and Bernd Buechner. 2006. Synthesis, properties, and applications of ferromagnetic-filled carbon nanotubes. *Chemical Vapor Deposition* 12 (6): 380–387.
39. Hiura, Hidefumi, Thomas W Ebbesen, and Katsumi Tanigaki. 1995. Opening and purification of carbon nanotubes in high yields. *Advanced Materials* 7 (3): 275–276.

40. Fenglian, Fu, and Qi Wang. 2011. Removal of heavy metal ions from wastewaters: A review. *Journal of Environmental Management* 92 (3): 407–418.
41. Dabbousi, Bashir O., Javier Rodriguez-Viejo, Frederic V. Mikulec, Jason R. Heine, Hedi Mattoussi, Raymond Ober, Klavs F. Jensen, and Moungi G. Bawendi. 1997. (CdSe) ZnS core —shell quantum dots: Synthesis and characterization of a size series of highly luminescent nanocrystallites. *The Journal of Physical Chemistry B* 101 (46): 9463–9475.
42. Liang, Zhou, Liu Jiping, and Li Xiaohe. 2004. Purification of carbon nanotubes. *Chemistry* 2: 96–102.
43. Won-Chun, Oh, Weon-Bae Ko, and Feng-Jun Zhang. 2010. The functionalization and preparation methods of carbon nanotube-polymer composites: A review. *Elastomers and Composites* 45 (2): 80–86.
44. Shim, Moonsub, Nadine Wong Shi Kam, Robert J. Chen, Yiming Li, and Hongjie Dai. 2002. Functionalization of carbon nanotubes for biocompatibility and biomolecular recognition. *Nano Letters* 2 (4): 285–288.
45. Serp, Philippe and José Luís Figueiredo. 2009. *Carbon materials for catalysis*. Wiley.
46. Zhangquan Peng, Allan Hjarbæk Holm, Lasse Tholstrup Nielsen, Steen Uttrup Pedersen, and Kim Daasbjerg. 2008. Covalent sidewall functionalization of carbon nanotubes by a "formation—degradation" approach. *Chemistry of Materials* 20 (19): 6068–6075.
47. Holzinger, Michael, Otto Vostrowsky, Andreas Hirsch, Frank Hennrich, Manfred Kappes, Robert Weiss, and Frank Jellen. 2001. Sidewall functionalization of carbon nanotubes. *Angewandte Chemie International Edition* 40 (21): 4002–4005.
48. Zen, Jyh-Myng, Annamalai Senthil Kumar, and Dong-Mung Tsai. 2003. Recent updates of chemically modified electrodes in analytical chemistry. *Electroanalysis* 15 (13): 1073–1087.
49. Murray, Royce W., Andrew G. Ewing, and Richard A. Durst. 1987. Chemically modified electrodes molecular design for electroanalysis. *Analytical Chemistry* 59 (5): 379A–390A.
50. Barsoukov, Evgenij, and J. Ross Macdonald. 2005. *Impedance spectroscopy: Theory, experiment, and applications*. Wiley.
51. Harikumar P.S., and VN Sivasankara Pillai. 1990. Cochin University of Science and Technology.
52. Li, Yijun, Kunlin Wang, Jinquan Wei, Gu Zhiyi, Zhicheng Wang, Jianbin Luo, and Wu Dehai. 2005. Tensile properties of long aligned double-walled carbon nanotube strands. *Carbon* 43 (1): 31–35.
53. Shanmugam, Ranganathan, Palani Barathi, and Annamalai Senthil Kumar. 2014. *Engineering aspects*.
54. Malhotra, Bansi D., and Asha Chaubey. 2003. Biosensors for clinical diagnostics industry. *Sensors and Actuators B: Chemical* 91 (1): 117–127.
55. Cooper, Jon, and Tony Cass. 2004. *Biosensors*. Oxford University Press.
56. Wang, Joseph. 2001. Glucose biosensors: 40 years of advances and challenges. *Electroanalysis* 13 (12): 983.
57. Shannon, Mark A., Paul W. Bohn, Menachem Elimelech, John G. Georgiadis, Benito J. Marinas, and Anne M. Mayes. 2008. Science and technology for water purification in the coming decades. *Nature* 452 (7185): 301–310.
58. Lin, Yuehe, Lu Fang, Tu Yi, and Zhifeng Ren. 2004. Glucose biosensors based on carbon nanotube nanoelectrode ensembles. *Nano Letters* 4 (2): 191–195.
59. Trojanowicz, Marek. 2006. Analytical applications of carbon nanotubes: A review. *TrAC Trends in Analytical Chemistry* 25 (5): 480–489.
60. Ji, Qingmin, Suk Bon Yoon, Jonathan P. Hill, Ajayan Vinu, Jong-Sung Yu, and Katsuhiko Ariga. 2009. Layer-by-layer films of dual-pore carbon capsules with designable selectivity of gas adsorption. *Journal of the American Chemical Society* 131 (12): 4220–4221.
61. Gruner, G. 2006. Carbon nanotube transistors for biosensing applications. *Analytical and Bioanalytical Chemistry* 384 (2): 322–335.
62. Luo, Xi-Liang, Xu Jing-Juan, Jin-Li Wang, and Hong-Yuan Chen. 2005. Electrochemically deposited nanocomposite of chitosan and carbon nanotubes for biosensor application. *Chemical Communications* 16: 2169–2171.

63. Neville, Frances, Michael J.F. Broderick, Tim Gibson, and Paul A. Millner. 2010. Fabrication and activity of silicate nanoparticles and nanosilicate-entrapped enzymes using polyethyleneimine as a biomimetic polymer. *Langmuir* 27 (1): 279–285.
64. Barsan, Madalina M., Ricardo C. Carvalho, Yu Zhong, Xueliang Sun, and Christopher Brett. 2012. Carbon nanotube modified carbon cloth electrodes: Characterisation and application as biosensors. *Electrochimica Acta* 85: 203–209.
65. Zhu, Zhigang, Luis Garcia-Gancedo, Andrew J. Flewitt, Huaqing Xie, Francis Moussy, and William I Milne. 2012. A critical review of glucose biosensors based on carbon nanomaterials: Carbon nanotubes and graphene. *Sensors* 12 (5): 5996–6022.
66. Joshi Shashank, R., A.K. Das, V.J. Vijay, and V. Mohan. 2008. Challenges in diabetes care in India: Sheer numbers, lack of awareness and inadequate control. *Journal of Association of Physicians of India* 56 (6): 443–450.
67. Telediab, Sea. 2005. Glucosim: Educational software for diabetes and simulation of glucose dynamics in blood. *Diabetes Technology & Therapeutics* 7 (2).
68. Barraud, Antoine. 2009. Molecular selective interface for an implantable glucose sensor based on the viscosity variation of a sensitive fluid containing Dextran and Concanavalin A.
69. Md Mahbubur Rahman, AJ Ahammad, Joon-Hyung Jin, Sang Jung Ahn, and Jae-Joon Lee. 2010. A comprehensive review of glucose biosensors based on nanostructured metal-oxides. *Sensors* 10 (5): 4855–4886.
70. Singh, Ravi, Davide Pantarotto, David McCarthy, Olivier Chaloin, Johan Hoebeke, Charalambos D Partidos, Jean-Paul Briand, Maurizio Prato, Alberto Bianco, and Kostas Kostarelos. 2005. Binding and condensation of plasmid DNA onto functionalized carbon nanotubes: Toward the construction of nanotube-based gene delivery vectors. *Journal of the American Chemical Society* 127 (12): 4388–4396.
71. Beitollahi, Hadi, Mohammad Ali Taher, and Nasrin Keshtkar. 2014. Voltammetric determination of L-Dopa in the presence of Tryptophan using a modified carbon nanotubes paste electrode. *Sensor Letters* 12 (1): 183–190.
72. Krajcik, Rasti, Adrian Jung, Andreas Hirsch, Winfried Neuhuber, and Oliver Zolk. 2008. Functionalization of carbon nanotubes enables non-covalent binding and intracellular delivery of small interfering RNA for efficient knock-down of genes. *Biochemical and Biophysical Research Communications* 369 (2): 595–602.
73. Sutcliffe, Alistair. 2003. *Multimedia and virtual reality: Designing multisensory user interfaces*. Psychology Press.
74. Merkoçi, Arben, Martin Pumera, Xavier Llopis, Briza Pérez, Manel del Valle, and Salvador Alegret. 2005. New materials for electrochemical sensing VI: Carbon nanotubes. *TrAC Trends in Analytical Chemistry* 24 (9): 826–838.

Chapter 2
Background of the Study

Abstract CNTs are allotropes of carbon in the nano form of a cylinder. In this chapter, the history of generating CNTs, the applications, and chemical properties of CNTs are reviewed. Also, the different generation of glucose biosensors as well as CNTs-based nanocomposite for electrochemical detection of glucose are highlighted. Generally, nanostructures have great potential to explore as simple and easy blood glucose checking medical tools. Electrochemical based oxidation of the immobilized enzymes (glucose oxidase) on CNTs has opened exciting opportunities for the determination of glucose. According to the previous publication related to the CNTs-based biosensor, CNTs display a perfect combination of electrical properties which enhance the sensitivity and selectivity of the fabricated amperometric glucose biosensors.

2.1 Structures of Carbon Nanotubes

The study reported by Saifuddin [1] highlighted three different possible types of CNTs namely; zigzag carbon nanotubes, chiral carbon nanotubes, and armchair carbon nanotubes. In fact, the method of rounded rolled axis of the graphene sheet's hexagonal network and the diameter of the closed end cylinder. The study presented by Lehman [2] also provides another classification of carbon nanotubes into SWCNTs and MWCNTs. Mostly, SWCNTs are more prone to defects during functionalization compared with MWCNTs. In terms of characterization and evaluation, this is easier with SWCNTs than MWCNTs [3]. SWCNTs are also simply pliable in contrast to MWCNTs which are not easily pliable. SWCNTs show resistivity in the range of 10^{-4}–10^{-3} Ω while the resistivity range of MWCNTs is from 1.8×10^{-5} to 6.1×10^{-5} Ω owing to the absence of defects in the structure. The purity of MWCNTs is higher since many studies highlighted that the purity of a typical MWCNTs depends on its synthesizing method [4].

© Springer International Publishing AG 2018

A. TermehYousefi, *Nanocomposite-Based Electronic Tongue*, Springer Series in Materials Science 259, https://doi.org/10.1007/978-3-319-66848-2_2

2.2 Generation of Carbon Nanotubes

Different morphology of CNTs has been reported based on powder form and Thin film due to their proposed application. Since the discovery of CNTs by Iijima [5], much attention has been attracted to this novel nanostructured material. Different synthesizing methods have been investigated to grow powder/thin film CNTs, including arc discharge [6], laser vaporization [7], and CVD [8]. In this section, some of the popular growing methods of CNTs are discussed in detail [9].

2.2.1 The Arc Discharge Method

Generally, the arc discharge method is one of the most practical synthesizing methods of CNTs for scientific purposes. Arc discharge yields highly graphitized CNTs due to a high temperature synthesizing process [10]. With this method, a direct current (DC) voltage is provided across the two electrodes (graphite) which are immersed in inert gas. When a pure graphite rod is utilized, a quantity of soot fullerenes are deposited inside a chamber, and MWCNTs are localized on the cathode. Ando [11] demonstrated that the growing CNTs followed by the DC arc discharge between a silicon anode and a graphite cathode. Anodic silicon is attached to a graphite rod. Then, the block of the silicon was removed and the DC arc is continuously discharged between the electrodes (approximately 1–2 mm apart). Ando suggested that there is a large amount of a soot carbon was discharged with fullerene. In addition to this result, MWCNTs were investigated as an additional carbon remained at the negative graphite electrode.

2.2.2 The Laser Vaporization Method

This method is also used to grow CNTs especially for synthesizing SWCNTs since the carbon target is ablated by a very high energy extracted from the laser beam. The collected results highlighted by Lebedkin [12] show that SWCNTs were grown by different diameters using laser vaporization of carbon rods which were doped with Co, Ni, and FeS (in an atmosphere of Ar:H_2). The results illustrate that the temperature and the gas pressure in the laser vaporization directly affects the diameter distribution of the grown CNTs. The obtained results were also represented that by the laser vaporization of a FeS: Ni: Co: C target in the Ar:H_2, with large diameters of tubes broadly distributed from $\sim$2 to $\sim$5.6 nm were obtained.

2.2.3 The Chemical Vapor Deposition Method

Nowadays, CVD is the most popular method for synthesizing CNTs, due to its ability to produce different CNTs by varying length of nanotube [13], uniformity of orientation [14], purity [15], and low cost [16]. The main part of this synthesis is to exhaust ahydrocarbon vapor for a period of 15–60 min via a tubular reactor. Inside this reactor [17] is a metal catalyst which can accommodate temperature in the range of 180–400 °C on which SWCNTs or MWCNTs can be grown. These will be extracted after the cooling system has reduced the catalyst to the room temperature. Where liquid hydrocarbons are used as a carbon source, the catalyst will be heated while an inert carrier gas carries the hydrocarbons. Hence, the hydrocarbon vapors are transported to the reaction zone of the CVD. Solid hydrocarbon needs time to become usable as the CNTs precursor in a low temperature zone within the reaction tube. The implication drawn from this synthesis is that hydrocarbon vapor initially decomposes into two elements namely carbon and hydrogen [15]. This decomposition happens when the hydrocarbon vapor touches the hot catalyst nanoparticles. Thus the hydrogen leaves and the carbon dissolves into the particular metal [18]. Figure 2.1 represents the schematic of the horizontal CVD setup described above.

2.2.3.1 Main Parameters on Carbon Nanotubes Produced by Chemical Vapor Deposition Method

It has been found the CNTs morphology grown by CVD depends on the most effective parameters in the synthesizing process. A perfect control of the amount of the flow rate of the carrier inert gas, amount of the catalyst and precursor, the reaction time and its duration, applied temperature, and annealing system allow CVD to produce the interested structure of CNTs. A number of research groups reported that selective and controlled growth of MWCNTs by varying the effective parameters in fabrication process is necessary for their proposed applications [19].

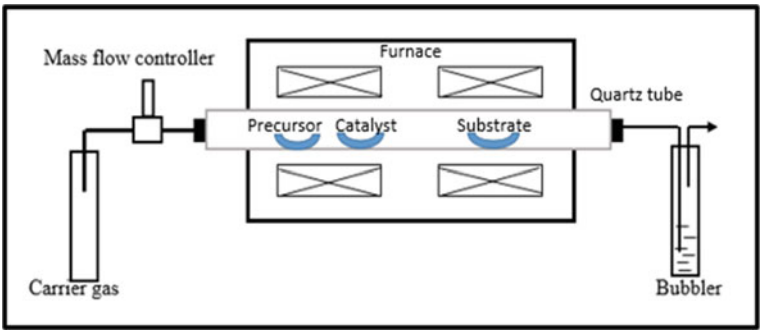

Fig. 2.1 Schematic setup of the horizontal CVD

However, to maintain consistency with the objective of this book, we will consider some key parameters in the following.

2.2.3.2 Effects of Temperature on Carbon Nanotubes Growth

The main aspect of the relationship between temperature and the growth of CNTs is the increase of thermal resistances when the CNTs arrangement growth temperature is decreased [17]. In the study by Cola [20], thermal resistances of silicon-CNT-silver interfaces grown through CVD can accommodate temperatures ranging from 506 to 806 °C where the temperature was measured via the photoacoustic technique. The results of this study showed that CNTs arrangements which offer fine heat interface conductivity could be grown when temperatures are reduced. When the temperatures are reduced, there is a possibility of integration with some sensitive substrates. The measurement of thermal resistance showed that it increased when the CNTs array growth temperature was reduced. In other research on the effect of the temperature in the CVD method, Amama [21] found that the CNTs growth rate (length of CNTs/duration of the process) goes up by four times by increasing the growth temperature. In a meantime, the average diameter of the grown CNTs was doubled with an increase in temperature [22].

2.2.3.3 Effects of Carrier Gas Flow Rate on Carbon Nanotubes Growth

Flow rate of the carrier gas also has an impact on the growth of CNTs and this is shown in the study by Reynolds [23]. The authors conducted research on the synthesis of CNTs as well as their characteristics when used on silicon substrates. The synthesis of CNTs in this study involves the CVD method at a temperature of 900 °C with the aid of methane and hydrogen flow—different flow rates of hydrogen gas were used to optimize the CNTs' yields. Their results illustrated that hydrogen gas at a flow rate of 100 sccm yields a very low quantity of CNTs. However, hydrogen at a flow rate of 200 sccm yields a slightly higher quantity of CNTs but still a limited amount. However, a hydrogen flow rate of 300 sccm yields plentiful CNTs with a smaller outside diameter and shorter branches. From these results it is concluded that the quantity of CNTs increases when the flow rate of hydrogen is increased from 100 to 300 sccm and the density of CNTs is at its peak when the flow rate of hydrogen is in the range of 300–400 sccm.

2.2.3.4 Effects of the Annealing and Vaporization Time on Carbon Nanotubes Growth

The diffusion of the hydrocarbons and the duration of the annealing step have a significant effect on the length and the diameter of grown CNTs. In fact, the aspect

ratio of synthesized SWCNTs or MWCNTs increases by increasing the durations of CVD, especially at longer vaporization and annealing times. This alteration in the diameter or the length of the synthesized CNTs might be due to sintering and the agglomeration of the feedstock. The results reported by Kim [24] show that on top of the reaction temperatures in the CVD method, the aspect ratio of CNTs is directly affected by the application of multiple reaction times. In cases of longer reaction times, both the diameter and length of the grown CNTs will also increase. The results also confirmed that the reaction time adapts to CNTs growth. In other words, the diameter of the grown CNTs is determined by the duration time of tubes in the hottest zone of the CVD reactor. Choi [25] reported that the diameter of a CNT was a function of its growth rate (length of the CNTs/reaction time). Accordingly, the length of CNTs increases with reaction times, clearly showing that the development of the structure of CNTs continues up to the point that the hydrocarbons are depleted.

Controlling annealing time is one of the main factors affecting the quality and yield of CNTs, as highlighted in Park [26]. Based on the obtained results from low deposition temperatures, in samples annealed for 20 min some remaining carbonaceous particles were removed from the CNTs' surface, and the total weight was reduced by $\sim$70%. By increasing the annealing time to 40 min, a major amount of the exciting carbonaceous particles was removed and the weight was reduced to $\sim$35%. The author also pointed out that although the relative population of nanotubes to carbonaceous particles should increase more with increasing annealing time, extended annealing times will result in overburning of nanotubes.

2.2.3.5 Effects of Catalyst on Carbon Nanotubes Growth: Ferrocene

Compared to the numerous methods developed to synthesize CNTs, catalytic CVD has the tendency to produce nanotubes with fewer impurities and nanotubes produced via this method appear to be amenable to large scale low cost processing [27]. According to Liao [28], there are few theories developed about the way CNTs grow from catalyst particles when CVD is conducted. One of the predicted theories described in the above study holds that CVD using catalysts involves the process of decomposition of gases containing carbon such as hydrocarbons or carbon monoxide. This decomposition occurs on one of the sides of a very small catalyst particle followed by the diffusion of carbon atoms via the particle's surface. Eventually, precipitation of CNTs occurs in the second furnace. The research based on this theory found that the size of metal-based catalysts will impact the growth rates of CNTs. For instance, sometimes the carbons have different morphologies but the catalyst particles can be alike in sizes. But in their experiment the researchers found that a catalyst with much larger particles was able to catalyze some long CNTs formation. The most common catalysts used for the CVD method are iron, cobalt, and nickel due to the perfect solubility and excellent diffusion rate of carbon in these metal particles [29, 30]. Some hypotheses state that carbon morphology changes when the temperature used for synthesis is varied [31]. Researchers

perceive that a potential factor in the carbon morphology is the constitution of the catalyst. Kumar [32] reported that iron has a high catalytic effect in hydrocarbon decomposition during the synthesizing process of CNTs. However, using cobalt as a catalyst resulted in well-graphitized CNTs but lower CNTs yield than using iron. On the other hand, the appropriate concentration of catalyst also plays an important role in the desired growth rate of CNTs.

Carbon nanotube mechanistic models described by Neil [33] clearly show both the mechanisms used to illustrate the catalytic growth of CNTs on the substrate. According to the results, in the tip-growth mechanism (Fig. 2.2a), the catalyst is located at the top of a growing nanotube. But in the base-growth mechanism (Fig. 2.1b), the catalyst is located at the bottom of the nanotube. In both mechanisms, the carbon reagent decomposes on the catalyst under the reaction process. The results also demonstrate that the interaction between catalyst and CNTs in the base-growth mechanism is stronger than in the tip-growth mechanism.

According to Asli [34], if a lower quantity of ferrocene is applied, a lower yield of CNTs will be obtained. There will also be lesser bend and multidirected growth. Another observation is that nearby nanotubes do not support each other resulting in random orientation of the CNTs. The study observed that with less than 0.4 g ferrocene, there is no indication of aligned CNTs production. However, when the quantity of ferrocene was multiplied, the CNTs production improved stage by stage. On the CNTs produced by higher amounts of ferrocene, carbonaceous crusts were visible covering the upper part of the CNTs. The authors attribute the presence of carbonaceous crusts to the greater quantity of ferrocene relative to the quantity of carbon supplied and the lack of uniformity in the evaporation of the ferrocene and

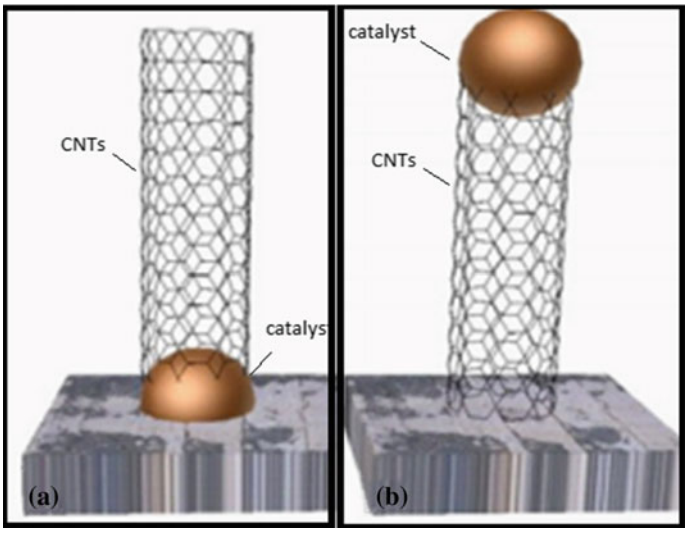

Fig. 2.2 Carbon nanotube mechanistic models: **a** Base-growth mechanism; **b** Tip-growth mechanism [33]

camphor oil during the synthesis. When they experimented using 0.5 g of ferrocene and 5 g of camphor oil, CNTs appeared to have a dense configuration with uniformly shaped vertical columns. This experiment demonstrated the formation of CNTs with the length of 110–113 μm. It also showed a growth process of CNTs in vertical columns providing support for each in order to continue growing in the same direction, at 90° to the template surface. Thus the implication is that lower quantities of catalyst can produce CNTs lower in density. The researchers summarized their findings by stating that CNTs growth can be observed even with a quantity of ferrocene as low as 0.3 g. However, to produce VACNTs, the minimum amount of ferrocene required is 0.4 g [32].

2.3 Fabrication of Glucose Biosensor: The First, Second, and Third Generation

Diagnosis and management of *diabetes mellitus* needs unique investigation and blood monitoring for glucose. Many patients are suffering from sugar related diseases, such as diabetes, which requires them to check their blood glucose levels every day. This makes glucose one of the most common blood analytes for testing. Hence, glucose biosensors account for about 85% (enzymatic biosensors) of the whole biosensors market. This huge demand and potential market size leads the development of new biosensing concepts [35]. Much of the interesting research and novel strategies for glucose detection by biosensors has led scientists to improve and develop cheap and easy-to-use glucose biosensors. Enzyme electrodes, especially electrodes based on GOx, have played a leading role in the move to simpler and easy-to-use methods for monitoring blood sugar [36].

Lower dynamic ranges as well as susceptibility to variations in oxygen concentration in the solution are some of their main disadvantages of the first generation of glucose biosensors. These rely on detection of hydrogen peroxide and the use of natural oxygen cosubstrate [37]. Reactions based on biocatalytic processes involve reduction of the flavin group (FAD) in the enzyme by reaction with glucose to produce the reductive form of the enzyme ($FADH_2$) [38].

The second generation of glucose biosensors rely on detection of the glucose level in the buffer solutions via enzymes which can catalyze the glucose. However, due to the thick layer (protein), enzymes do not transfer the electrons directly to counter electrodes. Different approaches have been investigated for monitoring the existing electrical contact of the redox center of GOx and the last surface of the electrode [39]. Measuring the catalytic current arising from the reoxidation of the mediator is the principal mechanism of the second generation of glucose biosensors [40]. In this regards, several types of electron mediators could be used as electron shuttle in the system [41]. Thanks to the presence of the mediator, greater linear detection range is one of the advantages of the second generation of glucose

biosensors. They are also less susceptible to electroactive interference because of their ability to operate at lower potentials [42].

In the third and latest generation of biosensors the exited electron from the detection process is transferred directly to the electrode from the analyte [43]. Omitting mediators from the system is one of the advantages of these biosensors, making them an excellent selective with low operating potential biosensor [44].

2.3.1 Carbon Nanotube-Based Biosensors

CNTs are one of the best materials for use in different sensing tasks due to their electrical properties and functional possibilities. Beside the aspect ratio of CNTs, chemical functionalized can also be a useful to immerse any chemical species to surface of the CNTs which is improving the solubility and biocompatibility of the CNTs. This can allow the realization of composite electrodes comprising CNTs well dispersed in an desired matrix of polymers [45, 46]

2.3.2 Functionalization of Carbon Nanotubes

The functionalization methods of CNTs include non-covalent and covalent techniques which can improve the interactions of nanotubes with solvents [47]. Covalent functionalization is defined as a linkage of functional entities by changing hybridization from sp^2 to sp^3 which can take place at the terminus of the tubes as well as the on the sidewalls of them [48]. Recent published reports show that many methods can improve the possible application of CNTs using functionalization methods which include: oxidative purification based on carboxylation [49], defect functionalization [50], halogenation [51], hydrogenation [52], addition of radicals [53], addition of nucleophilic carbenes, sidewall functionalization through electrophilic addition [54], cycloadditions [55], and aryl diazonium chemistry [56]. Non-covalent functionalization consists of complexation of supramolecules through various attractive or repulsive adsorption forces, such as π–π stacking interactions and van der Waals [57]. Results investigated by Gorton [58] and Challa [59] clearly demonstrated that functionalized CNTs enhance the electrochemical reactivity of biomolecules and can improve electron-transfers in proteins with embedded deep redox centers. Therefore, a variety of studies were focused on using the remarkable advantages of functionalized CNTs in electrochemical sensing applications such as clinical diagnostics or environmental monitoring. Alcohol, amino acids, cholesterol, lactate, pyruvate, glucose, glutamate, and hydroxybutyrate are some of the important clinical analytes to generate electrochemically detectable products. The focus of this book is the glucose monitoring process which consists of common chemical functionalized methods of CNTs for immobilization of GOx to fabricate electrochemical glucose biosensor based on CNTs.

2.3.3 Functionalized Carbon Nanotubes to Enhance Electron Transfer Mechanism in Glucose Biosensor

Monitoring of blood glucose is conducted routinely in medical practice [60]. In almost all of the developed countries about 5% of population have a diabetic condition. Thus the detection of glucose in patients' body fluids had been a major activity for doctors [61]. Glucose sensors usually make use of GOx in the detection of glucose. GOx is an enzyme where it functions to catalyze the oxidation process of β-D-glucose to D-glucono-1, 5-lactone and oxygen (O_2) used as the electron acceptor. From this process, a new combination hydrogen peroxide (H_2O_2) is produced. Hydrogen peroxide is electrochemically identified on a suitable electrode. In these processes, GOx displays great specification for β-D-glucose compared to 2-deoxy-D-glucose, D-mannose, and D-fructose which are oxidized at a lesser turnover [62]. The conductivity of CNTs as well as their small size of them makes them suitable as nanoelectrodes in the glucose detection process. Many researchers have focused on promoting the electron transfer reactivity of CNTs in biosensors. Table 2.1 shows some of the recent research reports on glucose biosensors based on functionalized CNTs enhanced by the electron transfer method.

Fabrication of a biosensor using Janegitz method can be easily conducted with precision and it has an accurate response for glucose determination as shown in Fig. 2.3. According to the obtained results it can be concluded that determination of glucose using a glucose oxides-carbon nanotube-dihexadecyl hydrogen phosphate-glassy carbon electrode (GOx-CNTs-DHP-GCE) as a detecting electrode of the biosensor had better analytical characteristics than those described by Li [71] and Wu [72].

Pandey [66] had reported similar findings on VACNTs which show better stability of the synthesized glucose biosensor. According to their results, CNTs were electrochemically functionalized with carboxylic (COOH) group acids. The modified electrodes were then dried in the air. Immobilization of GOx, was performed by immersing CNTs in a solution which contained coupling agents EDC (1-ethyl-3-3-dimethylaminopropyl carbodiimide) and Sulfo-NHS (N-hydroxy-sulfo-succinimide) for 3 h at 4 °C. A cyclic voltammogram of GOx functionalized CNTs clearly indicates a pair of symmetrical redox peaks corresponding to the electron transfer reaction of GOx as shown in Fig. 2.4. The results indicate the limit of detection, which was estimated around 14.4 μM with the sensitivity of 410 nA mM^{-1} cm^{-2} by considering the sensor active area of 0.385 cm^2.

Raicopol [64] published a report using another new type of glucose biosensors by using polypyrrole (PPy). In his report, CNTs were uniformly dispersed in deionized water, and then the suspension solution was transferred to a flask containing sulfanilic acid and tert-butyl nitrite. After mixing, an appropriate amount of acetone was added and then CNTs were filtered. In the last step, the CNTs were treated with a diluted NaOH solution and again filtered, washed with water followed by acetone, and dried. The selected amount of GOx was then added to the CNTs solution (functionalized nanotubes were dispersed in bidistilled water), and then pyrrole was added to the GOx-CNTs-$PhSO_3$ mixture, followed by

Table 2.1 Glucose biosensor based on functionalized CNTs improved by immobilizing CNTs

Nanoelectrode nanoensembles	Functionalizing method of CNTs	Immobilizing method	Limit of detection	Sensitivity	Stability (approx)
GOx-CNTs-DHP [63]	Pretreatment sulfuric and nitric acids	Carboxyl coupling reaction using EDC and N-hydroxysuccinimidyl (NHS)	9 μM	Not mentioned	One month
PPY/GOx/SWCNTs-$PhSO_3^-$/PB [64]	Flask fitted with a magnetic stirrer using sulfanilic acid and tert-butyl nitrite	Electropolymerization of GOx in dispersed CNTs	0.01 mM	6 μA mM^{-1} cm^{-2}	Not mentioned
PyBA-CNTs-GOx [65]	Modified using 4-(pyrrol-1-yl) benzoic acid (PyBA)	Embedding by composite film	10.2 mM	Not mentioned	Less than a month
VA-MWCNTs-GOx [66]	Sonication by HNO_3 and H_2SO_4	Immersing method using EDC and Sulfo-NHS	14.4 μM	410 nA mM^{-1} cm^{-2}	Six months
TP/MWCNT/GOx [67]	Sonicating in a mixture of concentrated sulfuric and nitric acids	Electrostatically deposited by stirring MWCNTs and GOx in PBS	Not mentioned	Not mentioned	Not mentioned
GOx/MWCNTs [68]	Carbodiimide coupling reactions	Covalent method	12 mM	20.6 μA mM^{-1} cm^{-2}	One week
CP- GOx-CNT_{EF} [69]	Electrooxidizing method using HNO_3	Physisorption of GOx based on soaking method	10 mM	Not mentioned	Not mentioned
PDDA/GOx/PDDA/CNTs [70]	Sonication by HNO_3 and H_2SO_4	Adsorption by dipping technique	7 μM	15 μA mM^{-1} m^{-2}	Four weeks

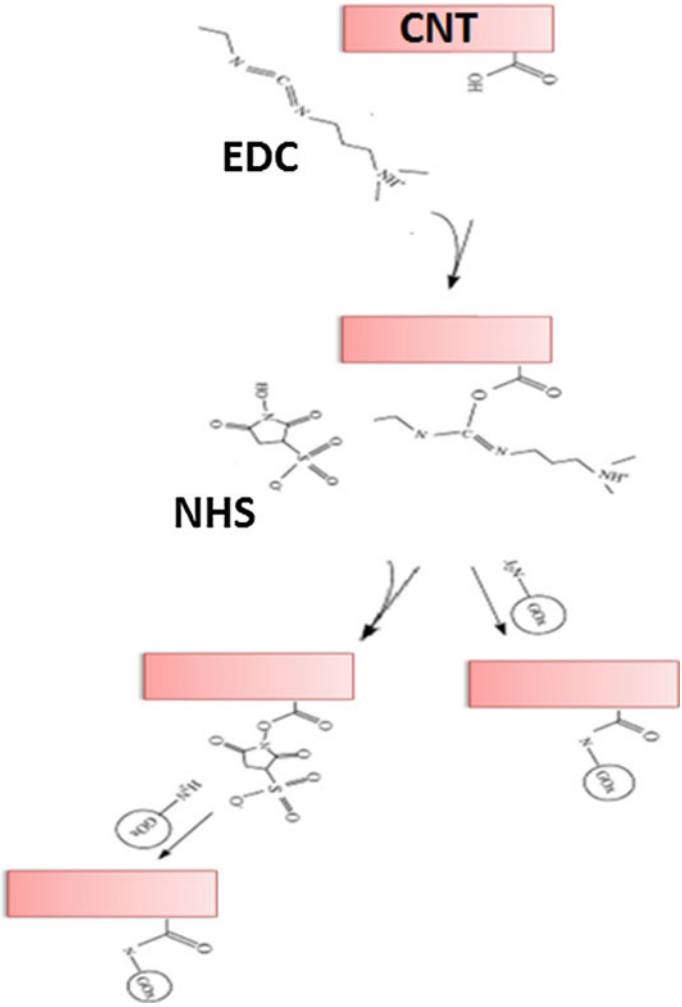

Fig. 2.3 Scheme of the reaction of 1-ethyl-3-3(dimethylaminopropyl) carbodiimide (EDC) and N-hydroxysuccinimidyl (NHS) with CNTs and GOx [73]

electropolymerization in pH 7 and the sample was subjected to overoxidation by cycling the potential in PBS solution as indicated by Fig. 2.5.

Self-assembling of GOx-based biosensors on the surface of CNTs was reported by Liu [70]. In this "flow injection method", the CNTs were firstly functionalized by ultrasonication with H_2SO_4 and HNO_3 and then dried in the vacuum. Then, the functionalized CNTs were immediately dispersed in N,N-dimethylformamide following by dropping on the GCE. The results show that fast current responses and well-defined detection were obtained for different glucose concentrations. The low noise level and high sensitivity allow the detection of micromolar concentrations in

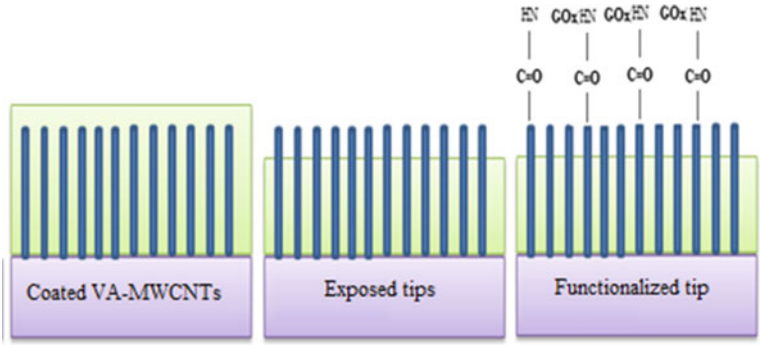

Fig. 2.4 Schematic diagram of the fabrication steps of CNTs nanoelectrode nanoensembles (CNNEs). VA-MWCNTs dipped and coated with poly methyl methacrylate (PMMA). The polished PMMA coated VA-MWCNTs with exposed tips and CNNEs functionalized with GOx [66]

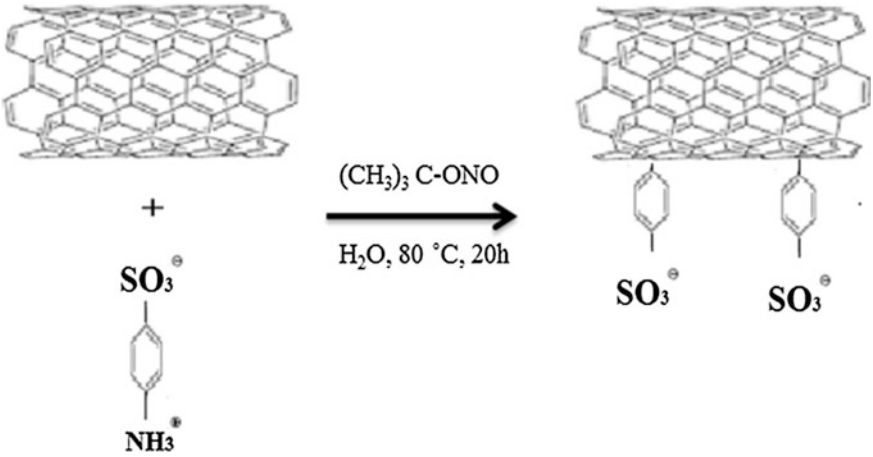

Fig. 2.5 Functionalized single-walled carbon nanotubes (SWCNTs) [64]

the range 15–120 μM. Figure 2.6 shows a schematic of wall-jet flow cell and upper piece of the wall-jet flow cell.

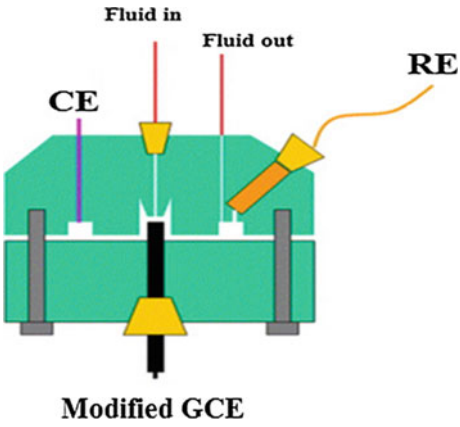

Fig. 2.6 Scheme of homemade wall-jet flow cell [70]

2.4 Carbon Nanotube-Based Composites in Glucose Biosensors

As shown by the previous results in Table 2.1, the incorporation of enzymes with SWCNTs and MWCNTs allows the fabrication of selective and sensitive enzyme-based CNTs biosensors. In this regard, CNTs nanocomposite and some other possible materials such as nanoparticles can be used to enhance selectivity and sensitivity of the fabricated biosensors as shown in Fig. 2.7 [74].

The use of CNTs-nanocomposites is another fabrication method for glucose biosensors that follows the entrapment technique which can be defined by its stability, sensitivity, and detection limit [75]. Table 2.2 summarizes some of the recent fabrication methods of nanocomposite-based CNTs for glucose biosensors.

From the data in Table 2.2 it can be concluded that the CNTs nanocomposite-based biosensors that incorporated nanoparticles are responsible for producing higher sensitivity than the conventional glucose biosensors. Attribution of this can be made to the improved catalyst functions, fine biocompatibility, and the very large surface area produced.

2.5 Functionalization of Carbon Nanotubes for Other Applications

Functionalized CNTs is one of the effective methods of enhancing the solubility of the CNTs which allows researchers to modify the CNTs for their potential applications. The functionalization methods include covalent and non-covalent functionalization which can improve the interactions of nanotubes with polymers or solvents [47]. Covalent functionalization is defined as a linkage of functional

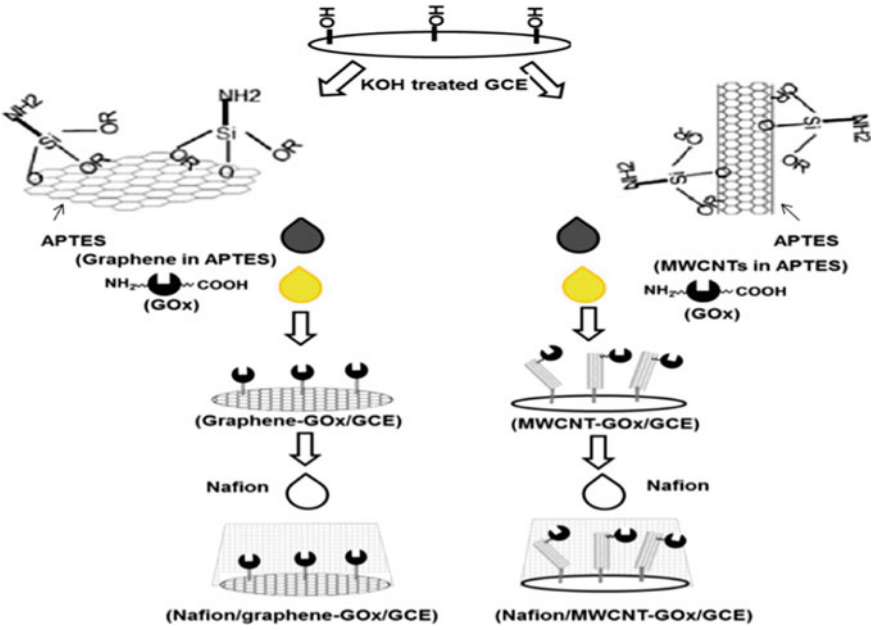

Fig. 2.7 Schematic configuration of graphene versus MWCNTs for electrochemical glucose biosensing [76]

entities by changing hybridization from sp^2 to sp^3 which can be performed at the termini of the tubes as well as on the sidewalls of it [48].

2.5.1 Thermal Applications of Carbon Nanotubes

The history of CNTs and their various applications discussed above lead us to questions about the suitability of using CNTs in those applications. Studies of the physical and chemical properties of CNTs by many researchers are essential in identifying application for which CNTs will be appropriate. Since the discovery of CNTs, this material been applied in various fields for various purposes. One such applications is described by Fabris [89]. The researchers concluded that improvements in thermal interface materials (TIMs) can enhance heat transfer in electronic packages and reduce high temperatures. In their experiment, two types of TIMs were tested based on the addition of CNTs. The first one was mixed with a commercial TIM product and the other one made of only CNTs and silicon oil. After that the materials were tested using an in-house apparatus that allowed for the simultaneous measurement of temperature, pressure, heat flux, and TIM thickness. The results show that CNT-thermal grease mixtures are more compliant, with a small increase in bulk thermal conductivity over the range of tested pressures [90].

Table 2.2 The key parameters in CNTs-based nanocomposites for glucose sensors

Fabrication method	Sensors	Sensitivity $(mmol/L)^{-1}$	Linear range of detection (mmol/L)	Response time (s)	Stability
Nanoparticle decoration, Enzyme adsorption	Nafion/GOx/PtNP/CNT/Graphite [77]	14 μA	0.1–13.5	<5	73% after 22 days
Nanoparticle decoration	CuNP-SWCNT-Nafion/GCE [78]	256 μA	0–0.5	10	Not mentioned
Electro polymerization	PPy-GOx-MWCNT array/Gold [79]	350 nA	2.5–20	Not mentioned	70% after 3 days
Encapsulation	GOx-Nafion-MWCNT/GCE [80]	330 nA	0–0.002	<3	
Electro polymerization	POAP-GOx/FePc MWCNT [81]	735 nA	0.0005–4	<8	120 days
Nanoparticle decoration, Enzyme adsorption	GOx/PtNP-SWCNT-Nafion/GCE [82]	2.11 μA	0.0005–5	3	
Electro polymerization	PPy-GOx-MWCNT/GCE [83]	2.33 nA	0.2–50	15	Not mentioned
Encapsulation, sol-gel process	GOx-SGC/MWCNT/bppg [84]	196 nA	0.2–20	<5	3 weeks
Adsorption	GOx/Au/Pt/CNTs [85]	21 nA	0.4–11.89	5–7	25 days
Electro deposition	Nafion/GOx/Pt/MWNTs [86]	58.9 μA	1–23	5	50 days
Electro deposition	Pd-GOx-Nafion CNTs [87]	Not mentioned	12	3	14 days
Electro deposition, sol-gel	CNT-PtNP-CS-MTOS [88]	4.94 μA	1.2–6	5	30 days

2.5.2 Medical Applications of Carbon Nanotubes

Because of their properties CNTs have found many biomedical applications. Wu [91] found that CNTs have created much interdisciplinary interest due to their unusual structural, mechanical, and electronic properties. The authors of this research first reviewed the covalent surface chemistry for CNT functionalization and then studied the surface chemistry of CNTs for biomedical applications, especially in relation to controlling biomedical functions. The outcome showed that CNTs had exactly the needed chemistry for use in biomedical applications. CNTs are predominant in today's medical research domain and are being thoroughly researched in the areas of efficient drug delivery, biosensing approaches for treatment of disease, and health screening. Growing knowledge of CNTs has revealed the possibility of modifying drug delivery as well as biosensing approaches in various fields of medicine.

The application of CNTs in the field of drug delivery and biosensing has revolutionary potential in medicine. Functionalization of SWCNTs has improve the solubility rate allowing for effective tumor targeting or efficiently drug delivery. It also avoids the threat of SWCNTs displaying cytotoxic behavior and modifying the role of immune cells.

Cancer, a type of disease in which cells in the body or at a certain organ develop and divide in an abnormal way, is one of the main diseases being focused on with regards to the way it reacts to CNT drug delivery. Present cancer therapy mainly includes surgery, radiation therapy, and chemotherapy which normally cause pain, destroy healthy cells, and produce opposing side effects. As drug delivery transporters, CNTs have displayed the capability of targeting certain cancer cells with a lower quantity of drugs than usually applied—which is equally efficient in destroying the cancer cells, does not harm healthy cells, and drastically reduces side effects. Zhang [92] provides vital information and knowledge about the usage of CNTs in cancer treatment.

The study revealed that CNTs have fulfilled three main requirements making them ideal carriers for targeted drug delivery: they themselves have target effects; they have sufficiently strong adsorptive effects for anticancer drugs to ensure they can transport the drugs to the effect-relevant sites; and they can release the drugs from them in the effect-relevant sites [93].

Among the above approaches, Zhang [92] found that functionalization has been the most effective. In addition, functionalization has been shown as capable of decreasing cytotoxicity, improving biocompatibility, and giving opportunity to appendage molecules of drugs, proteins, or genes for the construction of delivery systems.

According to Abdelbary, CNTs are applied in cancer therapy and drug delivery [94]. CNTs have been studied as possible nanocarriers for the delivery of drugs, genes, and proteins. Most of the study on CNTs has centered on their potential as deliverers of anticancer agents. This function is possible due to the needle-like shapes of CNTs which is unique, allowing CNTs to absorb or bond covalently to a

huge range of therapeutic materials and deliver them internally into the aimed cell. This study further discussed the application of CNTs as carriers of anticancer molecules because it is widely known that cancer cells overly express folic acid receptors and some research groups have made nanocarriers with engineered surfaces to which folic acid derivatives can be attached. The research also provided the information that non-spherical nanocarriers have been discovered to stay in the lymph nodes for longer periods of time compared to spherical nanocarriers. CNTs are examples of non-spherical nanocarriers and as such may have potential use for destroying lymph node cancers [95].

The study summarized that the capability of macromolecules to move against biological obstacles and be conveyed into a target cell is especially limited, because of their hydrophilicity and large molecular size. The researchers in this study also added that gene therapy targets to utilize genetic substances to medicate diseased cells by mending the reason of the disease. Due to the reason genetic substances are unable to bypass the biological membrane the application of viral or non-viral vectors to bring the gene and suppress it inside the cell is highly needed. Non-viral vectors are inefficient compared to viral vectors and have a shorter lifespan; nevertheless, these non-viral vectors are safe.

According to the researchers of this paper, previous researchers have established original functionalized SWCNT-DNA multiplexes and found that more DNA manifestation when compared with naked DNA [96]. Commonly, functionalized SWCNTs have been recommended by this study as appropriate non-viral carriers of macromolecules and internalization of those macromolecules within living cells by CNTs has been found to take place via energy-based endocytosis. The finding showed that confocal microscopy and flow cytometry have displayed much bigger fluorescent movement of protein and DNA when conjugated to SWCNTs compared to the naked macromolecules which shows that CNTs are prominent vectors for gene and protein. According to the authors, other researchers have presented a method for gene distribution called “carbon nanotube spearing” [97]. Carbon nanotube spearing consists of a process where plasmid DNA with a fluorescent protein was immobilized onto nickel-embedded CNTs. This was “speared” into Bal 17 B lymphoma cells with the aid of a magnetic field, which makes for a high rate of transfection in the target cells.

2.5.3 Antimicrobial Activity of Carbon Nanotubes

Other than cancer, other research reported therapeutic applications of CNTs where there is a possibility for surface-engineered CNTs to be able to capture pathogenic bacteria in a liquid medium [98]. Therefore, CNTs themselves may have antimicrobial process possibilities since microorganisms may be adsorbed into the engineered surfaces of CNTs. For examples, utilizing *Escherichia coli* as a sample microorganism, it has been discovered that the electronic attributes of SWCNTs might control their antibacterial process. The antibacterial property was a result of

CNT-induced oxidation of the intracellular antioxidant glutathione [99] causing increased oxidative stress on the bacterial cells and eventual death of the bacteria [100].

2.5.4 Drug Delivery Applications of Carbon Nanotubes

The researchers added that functionalized CNTs have the perfect ability to act as carriers for antimicrobial biocomponents such as antifungal amphotericin B [101]. CNTs are able to be covalently attached to amphotericin B in order to bring it into mammalian cells [102]. The study reported the reduction of antifungal toxicity compared to the toxicity of the free drug: 40% of the cells were destroyed by the CNTs-free formulation compared to no cell death by the CNTs formulation [103]. It was also discovered that the antifungal activity was increased using the CNTs [104].

2.5.5 Electro-optical Properties of Carbon Nanotubes

Mansano [105] studied the electro-optical properties of CNTs. According to the published report, this system is based on a new concept of plasma generation: "a planar coil is coupled to an RF system for plasma generation." This was used together with an electrostatic shield for plasma densification, thereby obtaining high-density plasmas. The CNTs were deposited using pure methane plasmas. The researchers used three methods for the surface modification of the sample.

According to their study, the electro-optical effects depend strongly on the preparation of the substrate as well as the deposition parameters of the CNTs. Their CNTs were highly aligned showing singular properties that could be a platform for many exciting applications.

2.5.6 Mechanical Properties of Carbon Nanotubes

Treacy [106] indicates that CNTs are predicted have appealing mechanical properties especially the high stiffness and axial strength. These two properties are due to their seamless cylindrical graphitic structure. So far it has not been possible to directly measure the mechanical properties of CNTs because of their tiny dimensions. In this study, the researchers approximated the Young's modulus of isolated nanotubes by measuring (in a transmission electron microscope) the amplitude of their intrinsic thermal vibrations. They found that CNTs have remarkably high Young's moduli, in the TPa range. Their high stiffness, together with their low

density, shows that CNTs may be useful as nanoscale fibers in strong, lightweight, composite substances.

2.5.7 Gas Sensors Based on Carbon Nanotubes

Wang [107] reported that CNTs are from the group of fullerene structures. The results defined SWCNTs as a one atom thick layer of graphite rolled up into a seamless cylinder with a diameter of several nanometers, and length on the order of 1–100 μm. The study also reported that, thermally, CNTs have high stability in both vacuum and air. The authors' description of electrical properties shows that CNTs can be either metallic (conductors) or semiconducting, depending upon the tube diameter and the chirality—which is the direction in which the graphite sheet is rolled to form the tube [108]. The chirality is usually represented by an integer pair (n, m). Nanotubes with $n - m = 3j$ (j being a nonzero integer) are metallic (conductors) while all the others are semiconducting [109]. The dielectric property of CNTs is highly anisotropic due to their nearly one-dimensional structures, which may enable nanotubes to carry high currents with negligible heating effect [110].

References

1. Saifuddin, N., A.Z. Raziah, and A.R. Junizah. 2012. Carbon nanotubes: A review on structure and their interaction with proteins. *Journal of Chemistry 2013*.
2. Lehman, John H., Mauricio Terrones, Elisabeth Mansfield, Katherine E. Hurst, and Vincent Meunier. 2011. Evaluating the characteristics of multiwall carbon nanotubes. *Carbon 49* (8): 2581–2602.
3. Hirsch, Andreas, and Otto Vostrowsky. 2005. Functionalization of carbon nanotubes. In *Functional molecular nanostructures*, 193–237. Berlin: Springer.
4. Avouris, Phaedon. 2002. Molecular electronics with carbon nanotubes. *Accounts of Chemical Research 35* (12): 1026–1034; Pop, Eric, David A. Mann, Kenneth E. Goodson, and Hongjie Dai. 2007. Electrical and thermal transport in metallic single-wall carbon nanotubes on insulating substrates. *Journal of Applied Physics 101* (9): 093710.
5. Iijima, Sumio. 1991. Helical microtubules of graphitic carbon. *Nature* 354 (6348): 56–58.
6. Gamaly, Eugene G., and Thomas W. Ebbesen. 1995. Mechanism of carbon nanotube formation in the arc discharge. *Physical Review B 52* (3): 2083.
7. Rinzler, A.G., Jie Liu, H. Dai, P. Nikolaev, C.B. Huffman, F.J. Rodriguez-Macias, P.J. Boul, An Huai Lu, Dominique Heymann, and D.T. Colbert. 1998. Large-scale purification of single-wall carbon nanotubes: Process, product, and characterization. *Applied Physics A: Materials Science & Processing 67* (1): 29–37.
8. Kong, Jing, Alan M. Cassell, and Hongjie Dai. 1998. Chemical vapor deposition of methane for single-walled carbon nanotubes. *Chemical Physics Letters 292* (4): 567–574.
9. Keidar, Michael, and Anthony M. Waas. 2004. On the conditions of carbon nanotube growth in the arc discharge. *Nanotechnology 15* (11): 1571.
10. Ando, Yoshinori, Xinluo Zhao, Toshiki Sugai, and Mukul Kumar. 2004. Growing carbon nanotubes. *Materials Today* 7 (10): 22–29.

11. Ando, Yoshinori, and Sumio Iijima. 1993. Preparation of carbon nanotubes by arc-discharge evaporation. *Japanese Journal of Applied Physics Part 2 Letters* 32: L107–L107.
12. Harris, Peter J.F. 2001. *Carbon nanotubes and related structures: New materials for the twenty-first century*. Cambridge University Press.
13. Wang, Xueshen, Qunqing Li, Jing Xie, Zhong Jin, Jinyong Wang, Yan Li, Kaili Jiang, and Shoushan Fan. 2009. Fabrication of ultralong and electrically uniform single-walled carbon nanotubes on clean substrates. *Nano Letters* 9 (9): 3137–3141.
14. Ming, Su, Bo Zheng, and Jie Liu. 2000. A scalable CVD method for the synthesis of single-walled carbon nanotubes with high catalyst productivity. *Chemical Physics Letters* 322 (5): 321–326.
15. Andrews, Rodney, David Jacques, Dali Qian, and Terry Rantell. 2002. Multiwall carbon nanotubes: Synthesis and application. *Accounts of Chemical Research* 35 (12): 1008–1017.
16. Nessim, Gilbert D. 2010. Properties, synthesis, and growth mechanisms of carbon nanotubes with special focus on thermal chemical vapor deposition. *Nanoscale 2* (8): 1306–1323.
17. Vlassiouk, Ivan, Murari Regmi, Pasquale Fulvio, Sheng Dai, Panos Datskos, Gyula Eres, and Sergei Smirnov. 2011. Role of hydrogen in chemical vapor deposition growth of large single-crystal graphene. *ACS Nano* 5 (7): 6069–6076.
18. Li, Yiming, David Mann, Marco Rolandi, Woong Kim, Ant Ural, Steven Hung, Ali Javey, Jien Cao, Dunwei Wang, and Erhan Yenilmez. 2004. Preferential growth of semiconducting single-walled carbon nanotubes by a plasma enhanced CVD method. *Nano Letters* 4 (2): 317–321.
19. Cola, Baratunde A., Placidus B. Amama, Xianfan Xu, and Timothy S. Fisher. 2008. Effects of growth temperature on carbon nanotube array thermal interfaces. *Journal of Heat Transfer 130* (11): 114503.
20. Amama, Placidus B., Baratunde A. Cola, Timothy D. Sands, Xianfan Xu, and Timothy S. Fisher. 2007. Dendrimer-assisted controlled growth of carbon nanotubes for enhanced thermal interface conductance. *Nanotechnology 18* (38): 385303.
21. Danafar, Firoozeh, A. Fakhru'l-Razi, Mohd Amran Mohd Salleh, and Dayang Radiah Awang Biak. 2009. Fluidized bed catalytic chemical vapor deposition synthesis of carbon nanotubes—A review. *Chemical Engineering Journal 155* (1): 37–48.
22. Reynolds, Carolyn, Binh Duong, and Supapan Seraphin. 2010. Effects of hydrogen flow rate on carbon nanotube growth. *Journal of Undergraduate Research in Physics*. http://www.jurp.org/2010/ms115_082710.pdf.
23. Kim, Ki-Eun, Kang-Jin Kim, Woo Sung Jung, Seung Yong Bae, Jeunghee Park, Junghyun Choi, and Jaebum Choo. 2005. Investigation on the temperature-dependent growth rate of carbon nanotubes using chemical vapor deposition of ferrocene and acetylene. *Chemical Physics Letters 401* (4): 459–464.
24. Choi, Young Chul, Young Min Shin, Young Hee Lee, Byung Soo Lee, Gyeong-Su Park, Won Bong Choi, Nae Sung Lee, and Jong Min Kim. 2000. Controlling the diameter, growth rate, and density of vertically aligned carbon nanotubes synthesized by microwave plasma-enhanced chemical vapor deposition. *Applied Physics Letters 76* (17), 2367–2369.
25. Park, Young Soo, Young Chul Choi, Keun Soo Kim, Dong-Chul Chung, Dong Jae Bae, Kay Hyeok An, Seong Chu Lim, Xiao Yan Zhu, and Young Hee Lee. 2001. High yield purification of multiwalled carbon nanotubes by selective oxidation during thermal annealing. *Carbon 39* (5): 655–661.
26. Zheng, B., Y. Li, and J. Liu. 2006. CVD synthesis and purification of single-walled carbon nanotubes on aerogel-supported catalyst. *Applied Physics A 74* (3): 345–348; Cantoro, Mirco, Stephan Hofmann, Simone Pisana, Vittorio Scardaci, Atlus Parvez, Caterina Ducati, Andrea C Ferrari, Arthur M Blackburn, Kai-You Wang, and John Robertson. 2006. Catalytic chemical vapor deposition of single-wall carbon nanotubes at low temperatures. *Nano Letters 6* (6): 1107–1112.
27. Liao, X.Z., A. Serquis, Q.X. Jia, D.E. Peterson, Y.T. Zhu, and H.F. Xu. 2003. Effect of catalyst composition on carbon nanotube growth. *Applied Physics Letters* 82 (16): 2694–2696.

28. Che, G., B.B. Lakshmi, C.R. Martin, E.R. Fisher, and Rodney S. Ruoff. 1998. Chemical vapor deposition based synthesis of carbon nanotubes and nanofibers using a template method. *Chemistry of Materials 10* (1): 260–267.
29. Colomer, J.-F., C. Stephan, Serge Lefrant, Gustaaf Van Tendeloo, Isabelle Willems, Z. Konya, Antonio Fonseca, Ch Laurent, and Janos B. Nagy. 2000. Large-scale synthesis of single-wall carbon nanotubes by catalytic chemical vapor deposition (CCVD) method. *Chemical Physics Letters 317* (1): 83–89.
30. Zhao, Bin, Don N. Futaba, Satoshi Yasuda, Megumi Akoshima, Takeo Yamada, and Kenji Hata. 2008. Exploring advantages of diverse carbon nanotube forests with tailored structures synthesized by supergrowth from engineered catalysts. *ACS Nano 3* (1): 108–114.
31. Kumar, Mukul, and Yoshinori Ando. 2010. Chemical vapor deposition of carbon nanotubes: A review on growth mechanism and mass production. *Journal of Nanoscience and Nanotechnology* 10 (6): 3739–3758.
32. Coville, Neil J., Sabelo D. Mhlanga, Edward N. Nxumalo, and Ahmed Shaikjee. 2011. A review of shaped carbon nanomaterials. *South African Journal of Science 107* (3–4): 01–15.
33. Asli, Noor Asnida, Muhammad Salleh Shamsudin, Suriani Abu Bakar, Mohamad Rusop Mahmood, and Saifollah Abdullah. 2013. Effect of the ratio of catalyst to carbon source on the growth of vertically aligned carbon nanotubes on nanostructured porous silicon templates. *International Journal of Industrial Chemistry 4* (1): 1–7.
34. Wang, Joseph. 2008. Electrochemical glucose biosensors. *Chemical Reviews* 108 (2): 814–825.
35. Yoo, Eun-Hyung, and Soo-Youn Lee. 2010. Glucose biosensors: An overview of use in clinical practice. *Sensors 10* (5): 4558–4576; Castillo, J., Szilveszter Gáspár, Suzanne Leth, M. Niculescu, Alessia Mortari, Ibolya Bontidean, V. Soukharev, S.A. Dorneanu, A.D. Ryabov, and Elisabeth Csöregi. 2004. Biosensors for life quality: Design, development and applications. *Sensors and Actuators B: Chemical 102* (2): 179–194.
36. Zhang, M.N., and L.Q. Mao. 2005. Enzyme-based amperometric biosensors for continuous and on-line monitoring of cerebral extracellular microdialysate. *Frontiers in Bioscience 10*: 345–352; Karyakin, Arkady A., Olga V. Gitelmacher, and Elena E. Karyakina. 1995. Prussian blue-based first-generation biosensor. A sensitive amperometric electrode for glucose. *Analytical Chemistry 67* (14): 2419–2423.
37. Gilmartin, Markas A.T., and John P. Hart. 1995. Sensing with chemically and biologically modified carbon electrodes. A review. *Analyst 120* (4): 1029–1045.
38. Montornesa, Josep M., Mark S. Vreekeb, and Ioanis Katakisa. 2008. Glucose biosensors. *Bioelectrochemistry: Fundamentals, Experimental Techniques and Applications 199*.
39. Chen, Chao, Qingji Xie, Dawei Yang, Hualing Xiao, Fu Yingchun, Yueming Tan, and Shouzhuo Yao. 2013. Recent advances in electrochemical glucose biosensors: A review. *RSC Advances* 3 (14): 4473–4491.
40. Scheller, Frieder W., Fred Lisdat, and Ulla Wollenberger. 2005. Application of electrically contacted enzymes for biosensors. *Bioelectronics: From Theory to Applications*, 99–126.
41. Chaubey, Asha, and B.D. Malhotra. 2002. Mediated biosensors. *Biosensors & Bioelectronics* 17 (6): 441–456.
42. Karyakin, Arkady A., Olga V. Gitelmacher, and Elena E. Karyakina. 1994. A high-sensitive glucose amperometric biosensor based on Prussian Blue modified electrodes. *Analytical Letters 27* (15): 2861–2869.
43. Ghindilis, Andrey L., Plamen Atanasov, and Ebtisam Wilkins. 1997. Enzyme-catalyzed direct electron transfer: Fundamentals and analytical applications. *Electroanalysis 9* (9): 661–674.
44. Habermüller, Katja, Marcus Mosbach, and Wolfgang Schuhmann. 2000. Electron-transfer mechanisms in amperometric biosensors. *Fresenius' Journal of Analytical Chemistry* 366 (6–7): 560–568.
45. Lin, Yuehe, Lu Fang, Tu Yi, and Zhifeng Ren. 2004. Glucose biosensors based on carbon nanotube nanoelectrode ensembles. *Nano Letters* 4 (2): 191–195.

46. Salimi, Abdollah, Ensiyeh Sharifi, Abdollah Noorbakhsh, and Saied Soltanian. 2007. Immobilization of glucose oxidase on electrodeposited nickel oxide nanoparticles: Direct electron transfer and electrocatalytic activity. *Biosensors & Bioelectronics* 22 (12): 3146–3153.
47. Balasubramanian, Kannan, and Marko Burghard. 2006. Biosensors based on carbon nanotubes. *Analytical and Bioanalytical Chemistry* 385 (3): 452–468.
48. Hanna Varghese, Saino, Remya Nair, Baiju G. Nair, T. Hanajiri, T. Maekawa, Y. Yoshida, and D. Sakthi Kumar. 2010. Sensors based on carbon nanotubes and their applications: A review. *Current Nanoscience 6* (4): 331–346.
49. Washe, Alemayehu P., Santiago Macho, Gastón A. Crespo, and F. Xavier Rius. 2010. Potentiometric online detection of aromatic hydrocarbons in aqueous phase using carbon nanotube-based sensors. *Analytical Chemistry 82* (19): 8106–8112.
50. Zhao, Qiang, Zhenhai Gan, and Qiankun Zhuang. 2002. Electrochemical sensors based on carbon nanotubes. *Electroanalysis* 14 (23): 1609–1613.
51. Lin, Yuehe, Wassana Yantasee, and Joseph Wang. 2005. Carbon nanotubes (CNTs) for the development of electrochemical biosensors. *Frontiers in Bioscience* 10 (492–505): 582.
52. Peng, Xiaohui, and Stanislaus S. Wong. 2009. Functional covalent chemistry of carbon nanotube surfaces. *Advanced Materials 21* (6): 625–642.
53. Wen, Dongsheng, and Yulong Ding. 2004. Effective thermal conductivity of aqueous suspensions of carbon nanotubes (carbon nanotube nanofluids). *Journal of Thermophysics and Heat Transfer* 18 (4): 481–485.
54. Wang, Chenchen, Gang Zhou, Haitao Liu, Wu Jian, Yong Qiu, Bing-Lin Gu, and Wenhui Duan. 2006. Chemical functionalization of carbon nanotubes by carboxyl groups on Stone-Wales defects: A density functional theory study. *The Journal of Physical Chemistry B* 110 (21): 10266–10271.
55. Barthos, R., D. Méhn, A. Demortier, N. Pierard, Y. Morciaux, G. Demortier, A. Fonseca, and J.B. Nagy. 2005. Functionalization of single-walled carbon nanotubes by using alkyl-halides. *Carbon* 43 (2): 321–325.
56. Borisenko, V.E., S.V. Gaponenko, and V.S. Gurin. 1997. *Physics, chemistry and application of nanostructures*. World Scientific.
57. Umek, Polona, Jin Won Seo, Klara Hernadi, Ales Mrzel, Peter Pechy, Dragan D. Mihailovic, and László Forró. 2003. Addition of carbon radicals generated from organic peroxides to single wall carbon nanotubes. *Chemistry of Materials 15* (25): 4751–4755.
58. Bettinger, Holger F. 2006. Addition of carbenes to the sidewalls of single-walled carbon nanotubes. *Chemistry-A European Journal 12* (16): 4372–4379.
59. Tagmatarchis, Nikos, Vasilios Georgakilas, Maurizio Prato, and Hisanori Shinohara. 2002. Sidewall functionalization of single-walled carbon nanotubes through electrophilic addition. *Chemical Communications* 18: 2010–2011.
60. Brunetti, Fulvio G., M. Antonia Herrero, Juan de M. Munoz, Silvia Giordani, Angel Díaz-Ortiz, Salvatore Filippone, Giorgio Ruaro, Moreno Meneghetti, Maurizio Prato, and Ester Vázquez. 2007. Reversible microwave-assisted cycloaddition of aziridines to carbon nanotubes. *Journal of the American Chemical Society 129* (47): 14580–14581.
61. Bahr, Jeffrey L., Jiping Yang, Dmitry V. Kosynkin, Michael J. Bronikowski, Richard E. Smalley, and James M. Tour. 2001. Functionalization of carbon nanotubes by electrochemical reduction of aryl diazonium salts: A bucky paper electrode. *Journal of the American Chemical Society 123* (27): 6536–6542; Petrov, Petar, Fabrice Stassin, Christophe Pagnoulle, and Robert Jérôme. 2003. Noncovalent functionalization of multi-walled carbon nanotubes by pyrene containing polymers. *Chemical Communications* (23): 2904–2905.
62. Gorton, L., E. Csöregi, E. Dominguez, J. Emneus, G. Jönsson-Pettersson, G. Marko-Varga, and B. Persson. 1991. Selective detection in flow analysis based on the combination of immobilized enzymes and chemically modified electrodes. *Analytica Chimica Acta* 250: 203–248.
63. Challa, Ashok. 2004. *Trench structure for semiconductor devices*. Google Patents.

64. Wang, S.G., Qing Zhang, Ruili Wang, S.F. Yoon, J. Ahn, D.J. Yang, J.Z. Tian, J.Q. Li, and Q. Zhou. 2003. Multi-walled carbon nanotubes for the immobilization of enzyme in glucose biosensors. *Electrochemistry Communications 5* (9): 800–803.
65. Gluckman, Peter D., and Mark A. Hanson. 2004. Living with the past: Evolution, development, and patterns of disease. *Science 305* (5691): 1733–1736.
66. Sotiropoulou, Sofia, and Nikolas A. Chaniotakis. 2003. Carbon nanotube array-based biosensor. *Analytical and Bioanalytical Chemistry 375* (1), 103–105.
67. Janegitz, Bruno C., Rasa Pauliukaite, Mariana E. Ghica, Christopher M.A. Brett, and Orlando Fatibello-Filho. 2011. Direct electron transfer of glucose oxidase at glassy carbon electrode modified with functionalized carbon nanotubes within a dihexadecylphosphate film. *Sensors and Actuators B: Chemical 158* (1): 411–417.
68. Pandey, Archana, Abhishek Prasad, Jason Moscatello, and Yoke Khin Yap. 2009. *Presented at the MRS Proceedings*, 2009 (unpublished).
69. Barbara Kowalewska and Katarzyna Jakubow, presented at the Meeting Abstracts, 2014 (unpublished).
70. Raicopol, Matei, Alina Prună, Celina Damian, and Luisa Pilan. 2013. Functionalized single-walled carbon nanotubes/polypyrrole composites for amperometric glucose biosensors. *Nanoscale Research Letters* 8 (1): 1–8.
71. Moumene, Mouna, Dominic Rochefort, and Mohamed Mohamedi. 2013. Electrochemical functionalization as a promising avenue for glucose oxidase immobilization at carbon nanotubes: Enhanced direct electron transfer process. *International Journal of Electrochemical Science 8* (2).
72. Zhao, Hua-Zhang, Juan-Juan Sun, Juan Song, and Qin-Zheng Yang. 2010. Direct electron transfer and conformational change of glucose oxidase on carbon nanotube-based electrodes. *Carbon* 48 (5): 1508–1514.
73. Chen, Yan-Shi, Jin-Hua Huang, and Chia-Chih Chuang. 2009. Glucose biosensor based on multiwalled carbon nanotubes grown directly on Si. *Carbon* 47 (13): 3106–3112.
74. Liu, Guodong, and Yuehe Lin. 2006. Amperometric glucose biosensor based on self-assembling glucose oxidase on carbon nanotubes. *Electrochemistry Communications* 8 (2): 251–256.
75. Ahuja, Tarushee, and Devendra Kumar. 2009. Recent progress in the development of nano-structured conducting polymers/nanocomposites for sensor applications. *Sensors and Actuators B: Chemical* 136 (1): 275–286.
76. Janegitz, Bruno C., Rasa Pauliukaite, Mariana E. Ghica, Christopher Brett, and Orlando Fatibello-Filho. 2011. Direct electron transfer of glucose oxidase at glassy carbon electrode modified with functionalized carbon nanotubes within a dihexadecylphosphate film. *Sensors and Actuators B: Chemical 158* (1): 411–417.
77. Li, Fenghua, Jixia Song, Fei Li, Xiaodan Wang, Qixian Zhang, Dongxue Han, Ari Ivaska, and Li Niu. 2009. Direct electrochemistry of glucose oxidase and biosensing for glucose based on carbon nanotubes@ SnO_2-Au composite. *Biosensors & Bioelectronics* 25 (4): 883–888.
78. Wu, Yunhua, and Shengshui Hu. 2007. Direct electrochemistry of glucose oxidase in a colloid Au–dihexadecylphosphate composite film and its application to develop a glucose biosensor. *Bioelectrochemistry* 70 (2): 335–341.
79. Moumene, Mouna, Dominic Rochefort, and Mohamed Mohamedi. 2013. Electrochemical functionalization as a promising avenue for glucose oxidase immobilization at carbon nanotubes: Enhanced direct electron transfer process. *International Journal of Electrochemical Science* 8: 2009–2022.
80. Atta, Nada F., Ahmed Galal, and Shimaa M. Ali. 2011. *Nanobiosensor for health care*.
81. Zheng, Dan, Sandeep Kumar Vashist, Michal Marcin Dykas, Surajit Saha, Khalid Al-Rubeaan, Edmond Lam, John H.T. Luong, and Fwu-Shan Sheu. 2013. Graphene versus multi-walled carbon nanotubes for electrochemical glucose biosensing. *Materials 6* (3): 1011–1027.

82. Kang, Xin Huang, Zhi Bin Mai, Xiao Yong Zou, Pei Xiang Cai, and Jin Yuan Mo. 2007. A novel sensitive non-enzymatic glucose sensor. *Chinese Chemical Letters 18* (2): 189–191.
83. Zeng, Zhiyuan, Xiaozhu Zhou, Xiao Huang, Zhijuan Wang, Yanli Yang, Qichun Zhang, Freddy Boey, and Hua Zhang. 2010. Electrochemical deposition of Pt nanoparticles on carbon nanotube patterns for glucose detection. *Analyst* 135 (7): 1726–1730.
84. Hrapovic, Sabahudin, Yali Liu, Keith B. Male, and John H.T. Luong. 2004. Electrochemical biosensing platforms using platinum nanoparticles and carbon nanotubes. *Analytical chemistry 76* (4): 1083–1088.
85. Ye, Jian-Shan, Ying Wen, Wei De Zhang, Hui Fang Cui, Guo Qin Xu, and Fwu-Shan Sheu. 2005. Electrochemical biosensing platforms using phthalocyanine-functionalized carbon nanotube electrode. *Electroanalysis 17* (1): 89–96.
86. Gao, Mei, Liming Dai, and Gordon G. Wallace. 2003. Biosensors based on aligned carbon nanotubes coated with inherently conducting polymers. *Electroanalysis 15* (13): 1089–1094.
87. Chopra, Nitin, Vasilis G. Gavalas, Leonidas G. Bachas, Bruce J. Hinds, and Leonidas G. Bachas. 2007. Functional one-dimensional nanomaterials: applications in nanoscale biosensors. *Analytical Letters 40* (11): 2067–2096.
88. Salimi, Abdollah, Richard G. Compton, and Rahman Hallaj. 2004. Glucose biosensor prepared by glucose oxidase encapsulated sol-gel and carbon-nanotube-modified basal plane pyrolytic graphite electrode. *Analytical Biochemistry 333* (1): 49–56.
89. Wang, Joseph, and Mustafa Musameh. 2005. Carbon-nanotubes doped polypyrrole glucose biosensor. *Analytica Chimica Acta* 539 (1): 209–213.
90. Lim, San Hua, Ji Wei, Jianyi Lin, Qiutian Li, and Jin KuaYou. 2005. A glucose biosensor based on electrodeposition of palladium nanoparticles and glucose oxidase onto Nafion-solubilized carbon nanotube electrode. *Biosensors and Bioelectronics 20* (11): 2341–2346.
91. Chu, Xiaochen, Wu Bohua, Chunhui Xiao, Xiaohua Zhang, and Jinhua Chen. 2010. A new amperometric glucose biosensor based on platinum nanoparticles/polymerized ionic liquid-carbon nanotubes nanocomposites. *Electrochimica Acta* 55 (8): 2848–2852.
92. Li, Jingjing, Ruo Yuan, Yaqin Chai, and Xin Che. 2010. Fabrication of a novel glucose biosensor based on Pt nanoparticles-decorated iron oxide-multiwall carbon nanotubes magnetic composite. *Journal of Molecular Catalysis. B, Enzymatic* 66 (1): 8–14.
93. Kang, Xinhuang, Zhibin Mai, Xiaoyong Zou, Peixiang Cai, and Jinyuan Mo. 2008. Glucose biosensors based on platinum nanoparticles-deposited carbon nanotubes in sol–gel chitosan/silica hybrid. *Talanta* 74 (4): 879–886.
94. Fabris, Drazen, Michael Rosshirt, Christopher Cardenas, Patrick Wilhite, Toshishige Yamada, and Cary Y. Yang. 2011. Application of carbon nanotubes to thermal interface materials. *Journal of Electronic Packaging 133* (2): 020902.
95. Wilhite, Patrick, Toshishige Yamada, and Cary Y. Yang. *Application of carbon nanotubes to thermal interface materials*.
96. Premkumar, Thathan, and Kurt E. Geckeler. 2010. 4 DNA and carbon-based nanomaterials. *Materials Science of DNA 77*; Albertazzi, Lorenzo, Michela Serresi, Alberto Albanese, and Fabio Beltram. 2010. Dendrimer internalization and intracellular trafficking in living cells. *Molecular Pharmaceutics 7* (3): 680–688.
97. Cai, Dong, Jennifer M. Mataraza, Zheng-Hong Qin, Zhongping Huang, Jianyu Huang, Thomas C. Chiles, David Carnahan, Kris Kempa, and Zhifeng Ren. 2005. Highly efficient molecular delivery into mammalian cells using carbon nanotube spearing. *Nature Methods 2* (6): 449–454.
98. Liu, Shaobin, Li Wei, Lin Hao, Ning Fang, Matthew Wook Chang, Rong Xu, Yanhui Yang, and Yuan Chen. 2009. Sharper and faster "nano darts" kill more bacteria: a study of antibacterial activity of individually dispersed pristine single-walled carbon nanotube. *Acs Nano 3* (12): 3891–3902.
99. Tiraferri, Alberto, Chad D. Vecitis, and Menachem Elimelech. 2011. Covalent binding of single-walled carbon nanotubes to polyamide membranes for antimicrobial surface properties. *ACS Applied Materials & Interfaces 3* (8): 2869–2877.

100. Aslan, Seyma, Codruta Zoican Loebick, Seoktae Kang, Menachem Elimelech, Lisa D. Pfefferle, and Paul R. Van Tassel. 2010. Antimicrobial biomaterials based on carbon nanotubes dispersed in poly (lactic-co-glycolic acid). *Nanoscale 2* (9): 1789–1794.
101. Wei, Wu, Sébastien Wieckowski, Giorgia Pastorin, Monica Benincasa, Cédric Klumpp, Jean-Paul Briand, Renato Gennaro, Maurizio Prato, and Alberto Bianco. 2005. Targeted delivery of amphotericin B to cells by using functionalized carbon nanotubes. *Angewandte Chemie International Edition* 44 (39): 6358–6362.
102. Prato, Maurizio, Kostas Kostarelos, and Alberto Bianco. 2007. Functionalized carbon nanotubes in drug design and discovery. *Accounts of Chemical Research* 41 (1): 60–68.
103. Foldvari, Marianna, and Mukasa Bagonluri. 2008. Carbon nanotubes as functional excipients for nanomedicines: II. Drug delivery and biocompatibility issues. *Nanomedicine: Nanotechnology, Biology and Medicine* 4 (3): 183–200.
104. Kang, Seoktae, Mathieu Pinault, Lisa D. Pfefferle, and Menachem Elimelech. 2007. Single-walled carbon nanotubes exhibit strong antimicrobial activity. *Langmuir 23* (17): 8670–8673.
105. Mansano, Ronaldo D., and Ana Paula Mousinho. 2011. Electro-optical properties of carbon nanotubes obtained by high density plasma chemical vapor deposition. *Materials Sciences and Applications 2* (05): 381.
106. Treacy, M.M.J., T.W. Ebbesen, and J.M. Gibson. 1996. *Exceptionally high Young's modulus observed for individual carbon nanotubes*.
107. Wang, Yun, and John T.W. Yeow. 2009. A review of carbon nanotubes-based gas sensors. *Journal of Sensors 2009*.
108. Baughman, Ray H., Anvar A. Zakhidov, and Walt A. de Heer. 2002. Carbon nanotubes–the route toward applications. *Science 297* (5582): 787–792.
109. Dresselhaus, Mildred S., Gene Dresselhaus, P.C. Eklund, and A.M. Rao. 2000. *Carbon nanotubes.* Springer.
110. Sinha, Niraj, Jiazhi Ma, and John T.W. Yeow. 2006. Carbon nanotube-based sensors. *Journal of Nanoscience and Nanotechnology* 6 (3): 573–590.

Chapter 3
Experimental Procedures and Materials

Abstract In this chapter, the main experimental steps used for synthesis, optimization, characterization, applications of CNTs, and preparation of CNTs-based nanocomposites electrode by drop-casting technique, and electrochemical measurements are discussed in detail. Furthermore, the equipment used to characterize grown CNTs as well as amperometric glucose biosensors are discussed. The mechanism of CNTs growth and glucose detection is also schematically illustrated. All the discussed methods are reproducible within the given experimental limitations.

3.1 Introduction

Figure 3.1 is a flowchart of the experimental procedures for the detection of glucose by modifying the surface of the electrode. All these experimental steps are different from each other and in each case standard procedures were adopted for collecting the results. Many variable factors and parameters such as concentration of analyte, current density, pH, calcination temperature, sample purity, surface uniformity of GCE, and the nature of surface modification by agitation were adjusted to get accurate results. Maximum care was taken in conducting the experiments and collecting data and wherever necessary duplicate experiments were conducted to confirm the results of particular experiments.

3.2 Materials

Agron grade chemicals with high purity [1] were used as listed in Table 3.1. Deionized (DI) water (18.2 MΩ cm at 25 °C) was used for preparing all solutions and to clean all materials and glassware [2].

© Springer International Publishing AG 2018

A. TermehYousefi, *Nanocomposite-Based Electronic Tongue*, Springer Series in Materials Science 259, https://doi.org/10.1007/978-3-319-66848-2_3

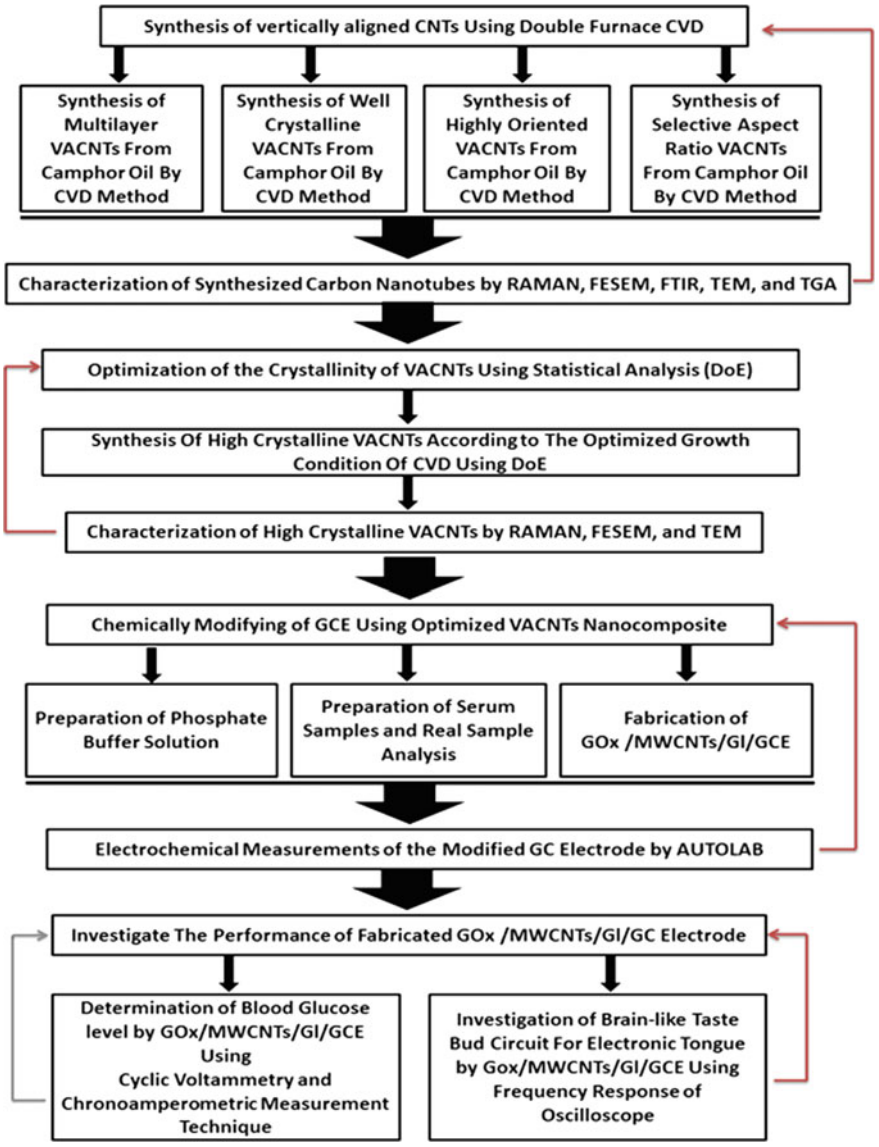
Synthesis of vertically aligned CNTs Using Double Furnace CVD
Synthesis of Multilayer VACNTs From Camphor Oil By CVD Method
Synthesis of Well Crystalline VACNTs From Camphor Oil By CVD Method
Synthesis of Highly Oriented VACNTs From Camphor Oil By CVD Method
Synthesis of Selective Aspect Ratio VACNTs From Camphor Oil By CVD Method
Characterization of Synthesized Carbon Nanotubes by RAMAN, FESEM, FTIR, TEM, and TGA
Optimization of the Crystallinity of VACNTs Using Statistical Analysis (DoE)
Synthesis Of High Crystalline VACNTs According to The Optimized Growth Condition Of CVD Using DoE
Characterization of High Crystalline VACNTs by RAMAN, FESEM, and TEM
Chemically Modifying of GCE Using Optimized VACNTs Nanocomposite
Preparation of Phosphate Buffer Solution
Preparation of Serum Samples and Real Sample Analysis
Fabrication of GOx /MWCNTs/GI/GCE
Electrochemical Measurements of the Modified GC Electrode by AUTOLAB
Investigate The Performance of Fabricated GOx /MWCNTs/GI/GC Electrode
Determination of Blood Glucose level by GOx/MWCNTs/GI/GCE Using Cyclic Voltammetry and Chronoamperometric Measurement Technique
Investigation of Brain-like Taste Bud Circuit For Electronic Tongue by Gox/MWCNTs/GI/GCE Using Frequency Response of Oscilloscope

Fig. 3.1 Flowchart of the experimental procedures for detection of glucose

Table 3.1 List of chemical compounds used

Chemical compounds	Molecular formula	Brand	Purity (%)
Alumina powder	Al_2O_3	Sigma Aldrich	≥ 99.9
Ascorbic acid	$C_6H_8O_6$	Sigma Aldrich	≥ 99.9
Camphor oil	$C_{10}H_{16}O$	Sigma Aldrich	≥ 96.0
Cysteine	$C_3H_7NO_2S$	Sigma Aldrich	>98.0
Disodium phosphate	Na_2HPO_4	Fluka	≥ 97.5
Ferrocene	$C_{10}H_{10}Fe$	Sigma Aldrich	>98.0
Glucose	$C_6H_{12}O_6$	Sigma Aldrich	≥ 99.5
Hydrochloric acid	HCl	Sigma Aldrich	>37.0
Lactose	$C_{12}H_{22}O_{11}$	Sigma Aldrich	≥ 97.0
Monosodium phosphate	NaH_2PO_4	Fluka	≥ 98.0
Nitric acid	HNO_3	Fluka	>89.0
Oxalic acid	$H_2C_2O_4$	Sigma Aldrich	≥ 99.9
Potassium chloride	KCl	Sigma Aldrich	>97.5
Potassium ferricyanide	$C_6N_6FeK_4$	Sigma Aldrich	≥ 98.0
Potassium ferricyanide	$C_6N_6FeK_3$	Sigma Aldrich	≥ 98.0
Sucrose	$C_{12}H_{22}O_{11}$	Sigma Aldrich	>99.0
Sulfuric acid	H_2SO_4	Fluka	>88.0
Trisodium phosphate	Na_3PO_4	Fluka	≥ 99.0

3.3 Synthesis of Multilayer Carbon Nanotubes from Camphor Oil by Chemical Vapor Deposition Method

The experimental setup was based on horizontal electronic furnaces used to cover the quartz tube during CNTs fabrication [3]. A mass flow controller was used to adjust the velocity of the argon gas by means of syringe pump into the substrate [4]. 12 mL camphor oil as a precursor was mixed with 0.06 mg ferrocene, and then introduced to the inlet of the horizontal quartz tube of the CVD fitted by the first furnace to release the vaporized CNTs. The reaction temperature was increased to 180 °C [5], and maintained for 30 min to ensure that the camphor oil and ferrocene were completely pyrolyzed. Ferrocene decomposes to form the iron catalyst necessary for the experiment, while camphor acts as a carbon source (feedstock) of the substrate in the second furnace. The CVD experiments commenced when the deposition temperature of the second furnace reached the optimal temperature (between 750 and 850 °C). The exhaust argon gas in the quartz tube induced movement of the amorphous vaporized carbon into the second furnace, thereby allowing CNTs growth on the surface of the proposed substrate [6]. To identify the relation between the flow rate of the argon gas and CNTs diameter on the silicon substrate (25 mm × 20 mm sized) at the second furnace, three different argon flow rates were employed while the pressure of the reactor (horizontal quartz tube) was

fixed at 1 bar. Argon gas was injected into the inlet of the quartz tube at a maximum velocity of 600 sccm. After 10 min, the velocity was gradually decreased to 400 sccm as its medium range of the argon flow rate. Then, after 20 min, the argon flow rate was decreased to 200 sccm until complete consumption of the carbon source. After 1 h of reaction time, the reactor was cooled down slowly to room temperature in argon ambient space after the synthesis [7].

3.4 Synthesis of Well-Crystalline Carbon Nanotubes Via Neutralized Cooling Technique by Carbon Vapor Deposition Method

Approximately 0.05 g of ferrocene was used to produce Fe catalyst particles for seeding nanotube growth in the presence of 10 mL camphor oil in a horizontal electronic furnace [8]. The furnaces were equipped with a quartz tube (35 mm outer diameter) that acted as a reactor for CNTs production. Several parameters, such as the deposition temperature, feedstock acceleration, and total reaction time were adjusted to refine the growth process of VACNTs [9]. The entire CVD was based on vaporization and deposition [10]. In the first step, ferrocene was used to prepare the catalyst by heating the internal surface of the first furnace up to the optimal temperature, followed by feeding in gas of vaporized camphor oil and ferrocene. In the second step, at 800 °C, decomposed carbon sources were deposited onto the silicon substrate (20 mm × 30 mm sized) to produce perpendicular nanostructures of carbon. Subsequently, the argon gas was changed to oxygen to neutralize formation of disorders, and the CVD was cooled down for 5 min, exposed to oxygen gas with a 500 sccm flow rate. The neutralized cooling method was concluded by the removal of synthesized CNTs from the quartz tube at 400 °C [11].

3.5 Synthesis of Highly Oriented Vertically Aligned Carbon Nanotubes Via Chemical Vapor Deposition Method

Typical experiments were performed on horizontal quartz tube, 25 mm in diameter and 1200 mm in length using a two-stage furnace to optimize the vaporization and deposition step. Silicon substrate (20 mm × 30 mm sized) with 15 Ω cm resistivity has been oxidized using 2% hydrofluoric acid in an ultrasonic water bath for 5 min [12]. Different ferrocene amounts were used to produce Fe catalyst particle seeds for nanotubes growth in the presence of 13 mL camphor oil in the horizontal electronic furnaces equipped with a quartz tube. The entire CVD process was based on two frequentative steps, namely vaporization and deposition process. In the first step, ferrocene was used to prepare the catalyst by heating the internal surface of the

first furnace up to the optimum temperature (between 750 and 850 °C), followed by feeding in the argon gas. During the second step, the vaporized camphor oil and ferrocene was deposited on the silicon substrate to obtain the perpendicular nanostructures of carbon. The CVD was then cooled down to room temperature while the argon gas was still flowing, and the samples were removed for the characterization [13].

3.6 Synthesis of Selective Aspect Ratio Vertically Aligned Carbon Nanotubes Via Carbon Vapor Deposition Method

The CVD method based on the horizontal quartz tube was used to optimize the growth process of the synthesis condition based on annealing step [14]. Horizontal quartz tubes, 25 mm in diameter and 1200 mm in length, were used to perform the reaction consisting of the two-stage furnace; 20 mm × 30 mm sized silicon substrate was used as CNTs' platform. Approximately 0.05 g of ferrocene was used to produce Fe catalyst particles to seed nanotubes grown in the presence of 13 mL camphor oil as its precursor. The flow rate of argon gas was controlled using a mass flow controller to adjust the velocity of the argon gas by means of a syringe pump to the feedstock of the second furnace. Different temperatures (750–950 °C) were applied to the second furnace during the growth process to optimize the growth condition, while the temperature of the first furnace was fixed at 180 °C to decompose the precursor. When the growth process was completed, argon gas was exhausted into the tube [15]. Oxygen gas was used to pull out the amorphous carbons from the reactor to decrease the defects of the CNTs during the cooling process [16].

3.7 Optimization of Highly Oriented Vertically Aligned Carbon Nanotubes' Growth Conditions Using Response Surface Methodology: Design of Experimental Matrix and Experimental Procedure

A complete description of any process of chemical reaction behavior requires either a quadratic or higher order polynomial model. Hence, full quadratic models were established by using the method of least squares, which includes all linear and interaction terms in calculating the predicted response. The quadratic model is usually sufficient for industrial applications [17]. For *n*-factors, the full quadratic model is shown in (3.1) [18]:

$$Y = b_o + \sum b_i X_i + \sum b_{ij} X_i X_j \quad (i, j = 1, 2, 3, \ldots, k) \tag{3.1}$$

where Y is the predicted response or dependent variable, X_i and X_j are the independent variables, while b_i and b_{ij} are constants [19]. In this case, the number of independent factors is four, and therefore, $k = 4$: (3.1) becomes (3.2) [20]:

$$\begin{aligned} Yu = {} & \beta_o + \beta_1 X_1 + \beta_2 X_2 + \beta_3 X_3 + \beta_4 X_4 + \beta_{12} X_1 X_2 + \beta_{13} X_1 X_3 + \beta_{14} X_1 X_4 \\ & + \beta_{24} X_2 X_4 + \beta_{34} X_3 X_4 + \beta_{11} X_{12} + \beta_{22} X_{22} + \beta_{33} X_{32} + \beta_{44} X_{42} \end{aligned} \tag{3.2}$$

where Y is the predicted response, and X_1, X_2, X_3, and X_4 are the coded form of the input variables for deposition time, vaporization time, deposition temperature, and concentration of precursor, respectively. The term β_o is the intercept term; β_1, β_2, β_3, and β_4 are the linear terms; β_{11}, β_{22}, β_{33}, and β_{44} are the squared terms; β_{12}, β_{13}, β_{23}, β_{14}, β_{24}, and β_{34} are the interaction terms between the four variables [21]. The deposition temperature, deposition time, annealing temperature, and concentration of precursor were selected as the influencing factors [22]. The selections of these variables with their defined experimental ranges were carefully done by screening experiment designs that consists of trials run at the extreme lower and upper level of the variable based on literature [23]. Furthermore, prior studies on the morphology of the CNTs grown by CVD method (Sects. 3.3–3.6), provided alternative information to focus on the correct variables and ranges for statistical experiment designs. The lowest and the highest levels of variables were coded as −1 and +1, respectively, and are given in Table 3.2, including axial star points of ($-\alpha$ and $+\alpha$), where α is the distance of the axial points from the center, making the design rotatable.

Where $\mp\alpha$, star point value; −1, low value; +1, high value; 0, center value. The suggested α value by software was calculated using (3.3) [24].

$$\alpha = (F)\,{}^1\!/_4 \tag{3.3}$$

where F is the number of points in the cube section of the design ($F = 2^k$), and k is the number of factors. Since we have four factors, α is suggested to be 2 by the software, but to avoid unexpected natural errors such as negative time or negative concentration in the design plan, the star points were circumscribed based on $\alpha = 0.5$ (non-rotatable). Therefore, the total number of experimental combinations

Table 3.2 Independent variables and their coded and actual values

Independent variable	Symbol	Coded levels				
		$-\alpha$	−1	0.00	+1	$+\alpha$
Deposition temperature (°C)	X_1	787.50	750	825	900	862.5
Vaporization time (min)	X_2	26.25	15	37.5	60	48.75
Annealing time (min)	X_3	22.50	15	30	45	37.5
Concentration of camphor oil (mL)	X_4	10	5	15	25	20

should be conducted based on similar concept of central composite rotatable design (CCRD) [25] by applying (3.4):

$$\text{Total number of experimental} = 2^k + 2k + n_o \tag{3.4}$$

where k is the number of independent variables, and n_o is the number of experiments repeated at the center point. In our case, $n_o = 6$ and $k = 4$, making the total number of runs 30. A matrix of 30 experiments with four factors was generated using the software package, "Design of Expert version 6.0.6". The six-center points were used to determine the experimental error and the reproducibility of the data. Table 3.3 tabulates the complete design matrix of the experiments, performed together with the results obtained. The responses obtained by Raman spectroscopy were used to develop an empirical model for the crystallinity of the CNTs [26]. In order to estimate the degree of crystallinity of synthesized CNTs, the ratio between the intensity of the G peak (at around 1600 cm^{-1}) and the D peak (at around 1300 cm^{-1}) observed by Raman spectroscopy was investigated [27]. The highest peak intensity ratio of G to D peaks (I_G/I_D), demonstrates the presence of CNTs with a very high degree of crystallinity and a low percentage of amorphous carbon [28]. Crystalline graphitic sheets of CNTs lead to a sharper G peak which is highly dependent on the optimized grown condition of the CNTs. Deposition temperature, vaporization and annealing time, and concentration of camphor oil are considered the most effective parameters on disordered structure of CNTs. Therefore, by optimization of the selected parameters and decreasing the imperfections of CNTs structure, the Raman signal strength for G peak gets stronger due to the detraction of the amorphous carbon in the CNTs structure.

After executing the experimental design, interpretations and analyses of the experimental data were determined using Analysis of Variance (ANOVA) at a 95% level of significance. The total number of required experiments was 30 runs to screen the effect of the parameters on CNTs: 24 predict runs, and 6 consolidation runs to confirm the results. Typical experiments were performed in a horizontal quartz tube with a 35 mm outer diameter using a two-stage furnace. In each run, 0.06 g of ferrocene was used to produce Fe catalyst particles for seeding nanotube growth in the presence of camphor oil as a precursor with various concentration based on the plan of experiments. Explanatory variables were adjusted to refine the growth process of VACNTs. Flow rate of the argon gas was adjusted at 500 sccm to pump the feedstock to the second furnace. As shown in Table 3.3, the deposition temperature of the growth process was within 750–900 °C, limited from 15 min to 1 h. The concentration of precursor was confined within a range of 5–25 mL. The annealing process was also done within 15–45 min, and subsequently, the carrier gas was changed to oxygen in the post-annealing step with flow rate of 500 sccm to neutralize formation of disorders. Then, the CVD was cooled down for 5 min. The CVD process was completed by the removal of grown CNTs from the quartz tube at 400 °C in order to neutralize the intrinsic disorders constructed by the mobile surface contaminants on the structure of CNTs [29].

Table 3.3 Central composite design matrix and experimental results

	X_1	X_2	X_3	X_4	Y
Run	Deposition temperature (° C)	Vaporization time (min)	Annealing time (min)	Concentration of camphor oil (mL)	I_G/I_D
1	750	60	45	5	1.09
2	900	60	15	5	1.096
3	750	15	45	5	1.133
4	900	15	15	5	1.15
5	900	15	45	5	1.115
6	750	15	15	5	1.05
7	825	37.5	30	10	1.25
8	825	26.25	30	15	1.19
9	825	37.5	22.5	15	1.22
10	825	37.5	30	15	1.21
11	825	37.5	30	15	1.21
12	862.5	37.5	30	15	1.2
13	825	37.5	30	15	1.2
14	825	37.5	37.5	15	1.185
15	825	48.75	30	15	1.185
16	787.5	37.5	30	15	1.155
17	825	37.5	30	15	1.21
18	825	37.5	30	15	1.21
19	825	37.5	30	15	1.16
20	825	37.5	30	20	1.185
21	900	15	45	25	1.065
22	750	15	45	25	1.015
23	750	15	15	25	1.152
24	750	60	15	25	1.03
25	750	60	45	25	1.043
26	900	60	15	25	1.085
27	900	15	15	25	1.125
28	900	60	45	25	1.105
29	750	60	45	5	1.09
30	900	60	15	5	1.096

3.8 Characterization of Synthesized Carbon Nanotubes

The successful chemical synthesis of nanostructures can be judged by the yield and the homogeneity of the product, and also confirming the performance of the product by using analytical and spectroscopic techniques [30]. The characterization of CNTs is an important part in the determination of shape, size, phase purity, chemical composition, functional group, and electrochemical behavior [31]. In the

present work, the as-synthesized CNTs were structurally characterized by different analytical and spectroscopic techniques such as Raman spectroscopy, thermogravimetric analysis (TGA), field emission scanning electron microscopy (FESEM), energy-dispersive X-ray spectroscopy, high resolution transmission electron microscopy (HRTEM), and Fourier transform infrared spectroscopy (FTIR).

3.8.1 Raman Spectroscopy: Measurement Conditions

Raman spectroscopy is a spectroscopic method to obtain rotational, vibrational, and other low frequency manners in nanoscale structures [32]. Raman scattering releases monochromatic light, usually from a visible laser, near, or near the ultraviolet range [33]. During characterization by Raman, the visible light of the laser interacts with molecular vibrations, phonons, or other excitations that yield from the energy of the laser photons being shifted up or down. The laser beam illuminates the sample and the alteration and shift in energy gives information about the vibrational modes in the nanostructures [34].

Raman spectroscopy can give much information on synthesized CNTs such as crystalline size, clustering of the sp^2 phase, the mass density, the optical energy gap, defects and other crystal disorder, edge structure, and diameter of the CNTs [35]. Typically, Raman scattering is caused by an inelastic scattering light and the mechanism is based on: (1) an electron is excited from the valence energy band to the conduction energy band by absorbing a photon; (2) the excited electron is scattered by emitting (or absorbing) phonons; and (3) the electron relaxes to the valence band by emitting a photon [36]. To obtain the crystallinity of CNTs and significant information on structural disorders of synthesized CNTs, the samples were evaluated by advanced Raman spectroscopy to measure the intensity of the scattered light as a function of frequency downshift [37]. Figure 3.2 shows a Renishaw Raman Microscope with a spectral resolution limit of $<1\ cm^{-1}$ in the visible region.

3.8.2 Thermogravimetric Analysis: Measurement Conditions

TGA is an analytical technique where the properties of materials are studied as they change with temperature [38]. It is widely used to evaluate heat resistance and to determine the quantity of components, weight loss, and thermal effects during the conversion of precursors to final metal oxides in the heat treatment process [39]. A Mettler Toledo (SDTA-85 1e) thermogravimetric analyzer is shown in Fig. 3.3.

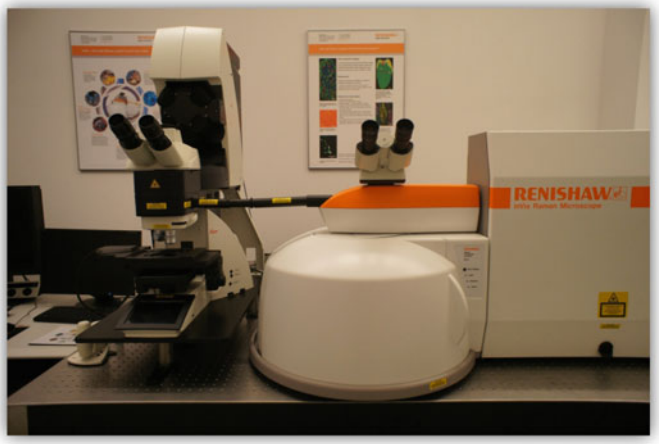

Fig. 3.2 Raman spectroscopy (Renishaw InVia)

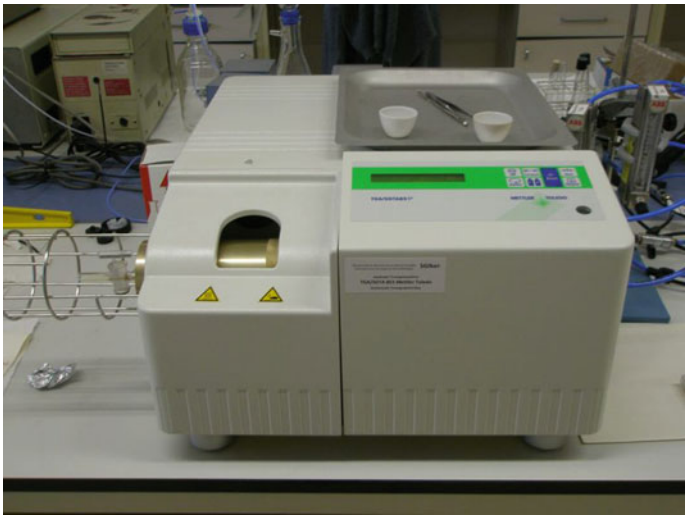

Fig. 3.3 Thermogravimetric analyzer [Mettler Toledo (SDTA-85 1e)]

TGA is one of the most versatile and well known methods for measurement of thermal effect in R&D and quality control environments [40]. TGA measures the weight of a substance subjected to a temperature program [41]. The analyzer used in this study offered the latest balance technology and automatic weight calibration. With such thermobalance, small weight losses can be measured and to identify a weight step, the weight change should be at least twice as large as the peak-to-peak noise, about 2 μg [28].

To investigate the thermal stability of the synthesized CNTs, the measurement was done using TGA. About 10–50 mg of sample was put into an open alumina crucible of 100 µl for the measurements [42]. The TGA temperature program was run dynamically from ambient to 548 K at a heating rate of 10 K min^{-1} under nitrogen gas with flow rate of 50 mL min^{-1}. It was cooled to room temperature before being heated again under argon gas from ambient to 873 K at a heating rate of 2 K min^{-1} with argon gas at the same flow rate [43].

3.8.3 *Field Emission Scanning Electron Microscopy: Measurement Conditions*

One of the most versatile analytical methods for screening the morphological and topological properties of nanostructures is FESEM [44]. Compared to the previous optical techniques, an electron microscope provides several advantages, such as high magnification, large depth of focus on the sample, excellent resolution, and fast sample preparation [45]. An electron gun generates an electron on a surface of the sample and produces several low energy secondary electrons. The surface topography of the sample obtained the intensity of these secondary electrons and the image of the surface of the sample gain by measuring secondary electron intensity as a function of the position of the scanning primary electron beam [46] (Fig. 3.4).

In the present study, an HT7700 transmission electron microscope was used to study the morphology of the synthesized CNTs [47]. The detailed parameters of the measurement were as follows:

Accelerating voltage	5 kV
Vacuum mode	High vacuum
Working distance	8–10 mm
Spot size	2.5–3 µm
Type of detector	Large field detector (LFD)
Cone	X-ray

3.8.4 *High Resolution Transmission Electron Microscopy: Measurement Conditions*

HRTEM is one of the most promising tools used for the determination of shapes of nanostructures [48]. The HRTEM technique is manly based on the analysis of transmitted or forward-scattered beams [49]. An electron beam interaction with a solid specimen results in a number of elastic or inelastic scattering phenomena.

Fig. 3.4 Field emission scanning electron microscope (ZEISS Supra 40VP)

Such a beam is passed through a series of lenses—among which the objective lens mainly determines the image resolution—to obtain the magnified image [50]. The transmission electron microscope used is as shown in Fig. 3.5. In this technique, the ray of electrons is produced by a current heating a pin-shaped cathode. The electrons are vacuumed up by a high voltage at the anode. The accelerating voltage is between 50 and 150 kV. The higher it is, shorter are the electron waves and higher is the power of resolution [51].

The accelerated beam of electrons passes a drill hole at the bottom of the anode —in a way that is analogous to that of a ray of light in a light microscope [52]. The beam is first focused by a condenser and then passes through the object, where it is partially deflected. The degree of deflection depends on the electron density of the object. The greater the mass of the atoms, the greater the degree of deflection. After passing the object the scattered electrons are collected by an objective lens [53]. Therefore, an image is formed that has subsequently been enlarged by an additional lens system. The formed image is then made visible on a fluorescent screen or it is documented on photographic material.

Fig. 3.5 Transmission electron microscope (HT7700, Hitachi High-Tech)

3.8.5 *Fourier Transform Infrared Spectroscopy: Measurement Conditions*

FTIR is an analytical method used to screen organic and inorganic materials [54]. This technique involves the absorption of various infrared light wavelengths by the nanostructures. Infrared absorption bands monitor specific molecular components and nanostructures [55]. FTIR spectrometers gain infrared spectra by first collecting an interferogram of the interested sample signal with an interferometer, that screens all of infrared frequencies simultaneously [56]. FTIR spectroscopy is a chemical analytical technique which measures the IR intensity versus wavelength (wave number) of light. Based upon the wave number, IR light can be categorized as far IR (4–400 cm^{-1}), mid IR (400–4000 cm^{-1}) and near IR (4000–14,000 cm^{-1}). IR spectroscopy detects the vibration characteristics of chemical functional groups in a sample. When IR light interacts with the matter, chemical bonds will stretch, contract, and bend [57]. As a result, a chemical functional group tends to adsorb IR radiation in a specific wave number range, regardless of the structure of the rest of the molecule. Figure 3.6 shows the FTIR spectroscopic instrument. Therefore, FTIR spectroscopy can result in a positive identification (qualitative analysis) of every different kind of material.

The FTIR spectrum was recorded in the transmittance mode using a Bruker-optic spectrometer IFS 66v/s equipped with vacuum using the KBr pellets technique and working with a resolution of 4 cm^{-1} in the middle range. Before analysis, air evacuation was done under vacuum (5 mbar) for 15 min. All the spectra recorded a 32 scan data accumulation in a range 400–4000 cm^{-1} [58].

Fig. 3.6 Fourier transform infrared spectrometer (Bruker, IFS 66v/s)

3.9 Chemically Modified Electrodes

Clearly, the best strategy for successful enzyme-based glucose biosensor fabrication is to devise a configuration by which electrons can directly transfer from the redox center of the enzyme to the GCE (working electrode) [56]. The similarity in length scales between CNTs and redox enzymes suggest the presence of interactions that are favorable for the biosensor electrode. The strategy of physical adsorption or covalent immobilization of enzyme onto the surface of immobilized CNTs may well represent an exciting pathway for direct electrical communication between electrodes and the active site of redox-active enzymes [59].

3.9.1 Pretreatment of the Electrodes

Glassy carbon is a unique material often used for electrodes. In most cases the general cleaning procedure will give satisfactory results. However, a variety of subsequent surface pretreatments have been reported to optimize electrode behavior in specific instances. Automatic polishing machines are useful if large numbers of electrodes have to be polished on a regular basis, however, manual polishing is more usual in a research or teaching lab.

3.9.2 Preparation of Phosphate Buffer

PBS solutions of 0.1 M for different pH values were prepared from phosphoric acid (H_3PO_4) and its salts (NaH_2PO_4, Na_2HPO_4, and Na_3PO_4). Phosphate buffer solutions containing potassium chloride at a concentration of 0.1 M as the carrier electrolyte to stabilize the pH range of pH 2 to pH 12 were used in the test solutions [60]. The following solutions were used for different pH ranges:

- pH 2 to pH 4: from a solution of phosphoric acid and monosodium phosphate (NaH_2PO_4).
- pH 5 to pH 9: from a solution of monosodium phosphate (NaH_2PO_4) and disodium hydrogen phosphate (Na_2HPO_4).
- pH 10 to pH 12: from a solution of disodium hydrogen phosphate (Na_2HPO_4) and trisodium phosphate (Na_3PO_4).

3.9.3 Preparation of Serum Samples and Real Sample Analysis

For determination of glucose in human blood serum, the serum sample was collected from the University of Malaya hospital. Around 50 μL of serum sample was transferred to the cell containing 10 mL of 0.1 M NaOH solution [61]. The response of the modified sensor into mentioned solution was investigated by cyclic voltammetric measurement at a scan rate of 50 mV s^{-1}. For the purpose of proving its practical applications, the modified electrode was used to determine the content of *D*-Penicillamine (*D*-PA) in the tablet using differential pulse voltammetry. A standard addition method was adopted to estimate the accuracy and the measurement.

3.9.4 Fabrication of Chemically Modified Electrodes

Pretreatment or cleaning of the electrode surface prior to modification is one of the important steps in the fabrication process and in electrochemical studies [62]. Before the fabrication of the modified electrode, the GCE was polished with 0.05 μm alumina powder on chamois leather. Then it was sonicated in absolute ethanol and deionized water, respectively.

3.10 Fabrication of Glucose Biosensor Based on Vertically Aligned Carbon Nanotubes Composite: GOx/MWCNTs/Gl/GCE

3.10.1 Synthesis, Purification, and Optimization of Multi-walled Carbon Nanotubes

The experimental setup of growing MWCNTs is based on horizontal electronic furnaces covering the quartz tube during CNTs fabrication. Camphor oil, as a precursor, was mixed with ferrocene and introduced to the inlet of the quartz tube fitted by the first furnace to release the vaporized CNTs. The reaction temperature was increased to 180 °C, and maintained for 30 min to ensure that the precursor and catalysts were completely pyrolyzed. Ferrocene decomposes to form the iron catalyst necessary for the experiment, while camphor acts as a carbon source (feedstock) of the substrate in the second furnace. The CVD experiments began when the deposition temperature of the second furnace was optimal (825 °C). The exhaust argon gas in the quartz tube induced the movement of the amorphous vaporized carbon into the second furnace via a mass flow controller, thereby allowing CNTs growth on the surface of the proposed substrate. After 1 h of reaction, a conventional cooling method was employed to slowly cool the reactor to room temperature in an argon environment. The MWCNTs were purified based on the literature by heating in the air at 600 °C for 100 min, and soaked in 6 M of hydrochloric acid (HCl) solution for 1 day, followed by centrifuging. The precipitate obtained by centrifuging was washed with deionized water and well dried under air. The MWCNTs were chemically functionalized by MWCNTs, according to the literature. MWCNTs were then briefly heated in air at 600 °C for 2 h, and then soaked in 6 M HCl solution for 24 h and centrifuged. The precipitate was rinsed with deionized water and dried under air. A mixture of sulfuric acid and nitric acid (3:1 v/v) was used to chemically functionalize MWCNTs via ultrasonic agitation for 8 h [63].

3.10.2 Fabrication of GOx/MWCNTs/Gl/GCE

MWCNTs/gelatin composites were prepared by dispersing 1 mg of synthesized MWCNTs in 1 mL of 3% gelatin solution by 25 min ultrasonication, and subsequently the GOx was added to the MWCNTs/gelatin composite at a 1:1 volume ratio. The bare GCE was polished on chamois leather with 0.02 μm alumina powder, and sonicated in deionized water and absolute ethanol, respectively. Then 3 μL of MWCNTs/gelatin/GOx was drop casted onto a 3 mm glassy GCE, while the modified GC electrode was well dried at 4 °C for 12 h.

3.11 Electrochemical Measurements of Modified Electrodes

3.11.1 Electrochemical Setup

The electrochemical measurements were performed using a three-electrode system, including working electrode (WE), reference electrode (RE), and counter (auxiliary) electrode (CE) (Fig. 3.7). They are immersed in a solution containing an analyte and a background electrolyte. The electrochemical information about the analyte in this study was extracted from the current flowing through the WE at a potential.

During the data collection, the potential (E) of the WE is monitored with respect to constant potential of RE. The RE contains a chemical system of constant composition and known potential. Typically the Ag|AgCl|KCl_{3M} system is selected as the RE because it is used for its reproducibility, reliability, and convenience. In an electrochemical workstation, the voltage changes ensure that almost no current flows through the RE.

This protects the RE from the negative effects of large currents which can cause changes in the composition and thus in the potential of RE. The presence of the CE also minimizes the amount of uncompensated ohmic drop ($\Delta E_{ohmic} = IR$) between the WE and RE which is proportional to the resistance (R) and current (I) flowing through between the WE and RE. Figure 3.8 shows the experimental setup

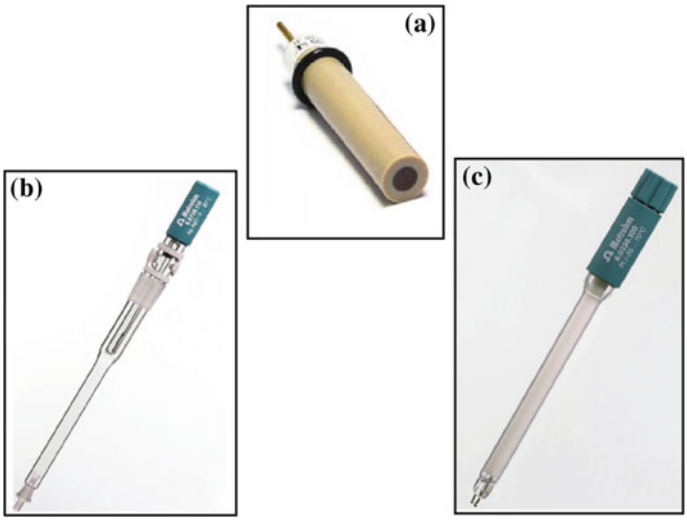

Fig. 3.7 Three-electrode system: **a** working electrode (GCE), **b** reference electrode (Ag|AgCl|KCl_{3M}), and **c** counter electrode (Pt wire)

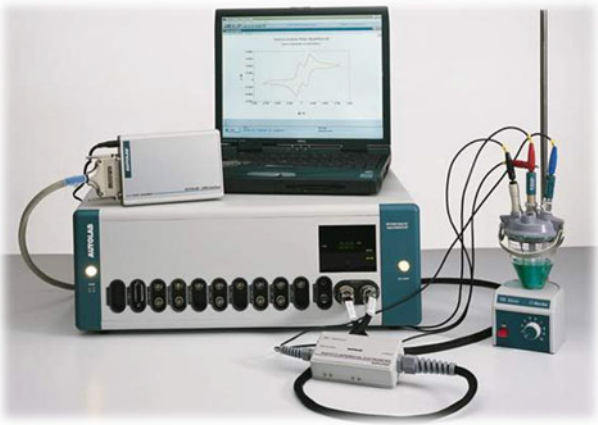

Fig. 3.8 Electrochemical setup with a three-electrode system (Autolab, Metrohm)

(Autolab) that was used for cyclic voltammetry, amperometry, and impedance analysis. The Potentiostat/Galvanostat (Autolab; Netherlands) device coupled with a Pentium IV personal computer which is installed with the General Purpose Electrochemical System (GPES) software to provide the potential and monitor the currents of the electrodes.

3.11.2 Cyclic Voltammetry

Cyclic voltammetric studies were performed by scanning the potential of the WE in a cyclic manner by applying a potential in one direction and switching it in reverse direction. The current flow can be measured through the WE. The plot of the current vs. potential is called as a cyclic voltammogram. The cyclic voltammogram was recorded in stationary solutions that contain an excess of ions of a background electrolyte over the analyte in order to suppress the migration as a mode of the analyte transport to the electrode surface. Under such conditions, the analyte was transported by diffusion to the electrode surface which simplifies the mathematical description of the cyclic voltammograms.

To study the electrochemical behavior of fabricated electrodes, the cyclic voltammetric response of analyte was investigated by successively adding various concentrations of analyte into the background electrolyte. The sensitivity of electrochemical sensors was obtained by linear dynamic range and limit of detection. The reproducibility and storage stability of the modified electrode were examined by the relative standard deviation (RSD).

3.11.3 Chronoamperometric Response

Electrochemical technique in which is stepped the potential of the WE is named. In chronoamperometry, current from faradaic processes occurring at the electrode is monitored as a function of time. The ratio of the peak oxidation current versus the peak current reduction identifies limited information about the electrolyzed species. The electron transfer causes faradaic current. Chronoamperometry is mostly investigated using a three-electrode system since the current is integrated over relatively longer time intervals. Chronoamperometry gives a better signal to noise ratio in comparison to other amperometric technique.

3.12 Integration of Electronic Tongue Based on Frequency Response of GOx/MWCNTs/Gl/GCE Biosensor

The performance of the modified GCE with GOx/MWCNTs/Gl was investigated in the form of an electronic tongue to diagnose sweetness. The proposed electronic tongue, namely the artificial taste bud, consisted of neuron-like circuits attached to the amperometric glucose biosensor. The design of the circuit was based on signal transmission from Type II to Type III cells of the taste bud network, as shown in Fig. 3.9. In fact, Type II cells are responsible for detecting tastes via specific receptors; Type III cells processes the investigated signals from Type II cells by making synaptic contacts with taste nerve terminals. Type III cells are regarded as the output of cells that relay the identity and intensity of chemical stimuli to the brain via taste nerves. According to the glucose detection method reported in Sect. 3.11, GOx/MWCNTs/Gl/GCE is capable of electrocatalyzing the glucose oxidation by taking potassium ferricyanide as a mediator in nitrogen saturated solutions. It can be observed that the sweetness of the buffer solution can be chemically sensed via the integrated brain-like taste bud circuit through the generation of pulse frequency signals. According to the design of the taste bud network

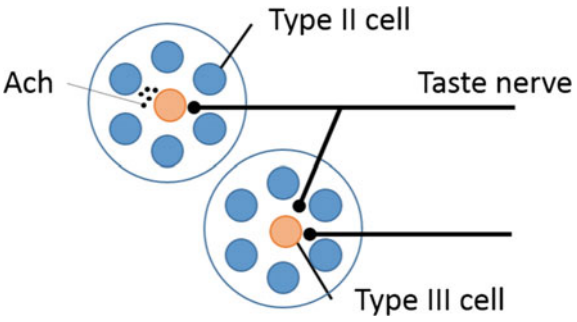

Fig. 3.9 Schematic diagram of taste bud cell network

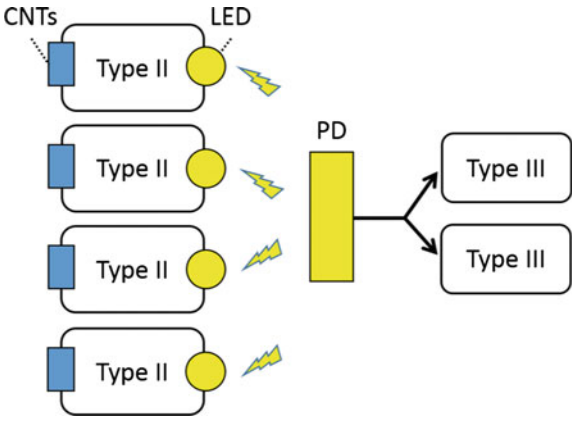

Fig. 3.10 Process of the created signals by the first layer: schematic diagram of a taste bud network inspired by mouse taste bud

shown in Fig. 3.9, pulse signals could be sent as a continuous form of information processing to the pattern recognition system. The circuit design of the taste bud network, namely the pulse generator circuit, is also provided with an infrared light emitting diode (LED) to procreate signals in the first layer and infrared-based photodiode in the second layer to identity and process the created signals via the first layer, as shown in Fig. 3.10. Four different Type II cells with different electrochemical properties generate repetitive pulses in the first layer. The output frequency of the pulse increases with increased concentration of glucose [64].

A pair of electrical circuits in the second layer receives a sum of pulse train derived by the first layer. The sum of many independent spike trains has an exponential form of distribution of interpulse intervals. Those pulse trains potentially induce synchronization in a pair of electrical circuits in the second layer in the manner shown in Fig. 3.11.

3.12.1 Square Wave Frequency Measurements of the Electrical Circuit Attached to the Modified Electrodes

To monitor the output frequency of the fabricated circuit attached to the GOx/MWCNTs/Gl/GCE biosensor, an oscilloscope (OS-5020G) was used to observe the change of an electrical signal as a function of time. Oscilloscope (OS-5020G) can also analyze the amplitude, rise time, time interval, and distortion. The oscilloscope has been adjusted for the output oscillation frequency changes by the GOx/MWCNTs/Gl/GCE biosensor in the form of a continuous shape on the screen. Hence, the alteration of glucose concentration in the system changes the output oscillation frequency and the square wave frequency stabilizes into a new

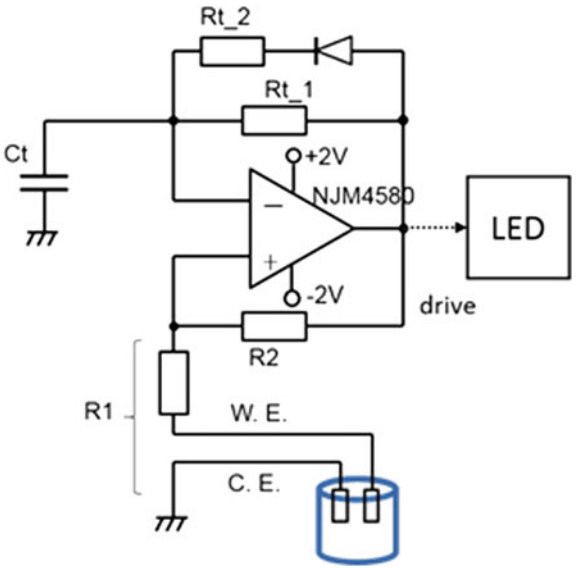

Fig. 3.11 Schematic picture of a taste bud network inspired by mouse taste bud; pulse generator circuit design provided by infrared LED in first layer and infrared based photodiode in the second layer

value. A storage oscilloscope allows single events to be captured by the instrument and displayed for a relatively long time, allowing the observation of events too fast to be directly perceptible.

References

1. Treacy, M.M.J., T.W. Ebbesen, and J.M. Gibson. 1996. Exceptionally high Young's modulus observed for individual carbon nanotubes. *Nature.*
2. Yun, Wang, and John T.W. Yeow. 2009. A review of carbon nanotubes-based gas sensors. *Journal of Sensors*.
3. Baughman, Ray H., Anvar A. Zakhidov, and Walt A. de Heer. 2002. Carbon nanotubes—The route toward applications. *Science* 297 (5582): 787–792.
4. Mildred, S., Dresselhaus, Gene Dresselhaus, P.C. Eklund, and A.M. Rao. 2000. *Carbon nanotubes*. Berlin: Springer.
5. Ming, Su, Bo Zheng, and Jie Liu. 2000. A scalable CVD method for the synthesis of single-walled carbon nanotubes with high catalyst productivity. *Chemical Physics Letters* 322 (5): 321–326.
6. Sinha, Niraj, Jiazhi Ma, and John T.W. Yeow. 2006. Carbon nanotube-based sensors. *Journal of Nanoscience and Nanotechnology* 6 (3): 573–590.
7. Wisconsin v. Yoder. In US (Supreme Court, 1972), vol. 406, 205.
8. De Jong, J.T.M., J. Den Das, Ulrich Bathmann, M.H.C. Stoll, Gerhard Kattner, R.F. Nolting, and H.J.W. De Baar. 1998. Dissolved iron at subnanomolar levels in the Southern Ocean as determined by ship-board analysis. *Analytica Chimica Acta* 377 (2): 113–124.
9. Ogawa, M.F., Y. Natsume, T. Hirayama, and H. Sakata. 1990. Preparation and electrical properties of undoped zinc oxide films by CVD. *Journal of Materials Science Letters* 9 (11): 1351–1353.

10. Jin, Zhong, Haibin Chu, Jinyong Wang, Jinxing Hong, Wenchang Tan, and Yan Li. 2007. Ultralow feeding gas flow guiding growth of large-scale horizontally aligned single-walled carbon nanotube arrays. *Nano Letters* 7 (7): 2073–2079.
11. Govindaraj, A., and C.N.R. Rao. 2006. Synthesis, growth mechanism and processing of carbon nanotubes. *Carbon nanotechnology*, 15–51 (Amsterdam: Elsevier).
12. Miguel A. Correa-Duarte, Nicholas Wagner, José Rojas-Chapana, Christian Morsczeck, Michael Thie, and Michael Giersig. 2004. Fabrication and biocompatibility of carbon nanotube-based 3D networks as scaffolds for cell seeding and growth. *Nano Letters* 4 (11): 2233–2236.
13. Navarro, R.M., M.A. Pena, and J.L.G. Fierro. 2007. Hydrogen production reactions from carbon feedstocks: fossil fuels and biomass. *Chemical Reviews* 107 (10): 3952–3991.
14. Hui, Rob, Zhenwei Wang, Olivera Kesler, Lars Rose, Jasna Jankovic, Sing Yick, Radenka Maric, and Dave Ghosh. 2007. Thermal plasma spraying for SOFCs: Applications, potential advantages, and challenges. *Journal of Power Sources* 170 (2): 308–323.
15. Cao, Yingli, Aimin Liu, Honghao Li, Yiting Liu, Fen Qiao, Hu Zengquan, and Yongcang Sang. 2011. Fabrication of silicon wafer with ultra low reflectance by chemical etching method. *Applied Surface Science* 257 (17): 7411–7414.
16. Xiang, Rong, Erik Einarsson, Jun Okawa, Yuhei Miyauchi, and Shigeo Maruyama. 2009. Acetylene-accelerated alcohol catalytic chemical vapor deposition growth of vertically aligned single-walled carbon nanotubes. *The Journal of Physical Chemistry C* 113 (18): 7511–7515.
17. Sreejarani K. Pillai, Suprakas Sinha Ray, and Mathew Moodley. 2008. Purification of multi-walled carbon nanotubes. *Journal of nanoscience and nanotechnology* 8 (12): 6187–6207.
18. Zhao, Xin, Xiangli Kong, Yanyan Hua, Bin Feng, and Zongbao Kent Zhao. 2008. Medium optimization for lipid production through co-fermentation of glucose and xylose by the oleaginous yeast Lipomyces starkeyi. *European Journal of Lipid Science and Technology* 110 (5): 405–412.
19. Shaibu, A.B., and Byung Rae Cho. 2009. Another view of dual response surface modeling and optimization in robust parameter design. *The International Journal of Advanced Manufacturing Technology* 41 (7): 631–641.
20. Bagheri, Samira, Donya Ramimoghadam, Amin TermehYousefi, and Sharifah Bee Abd Hamid. 2015. Effects of synthetic explanatory variable on saturation magnetization of colloidal nanomagnetite slurry. *International Journal of Hydrogen Energy* 40 (46): 16178–16183.
21. Ryckaert, Jean-Paul, Giovanni Ciccotti, and Herman J.C. Berendsen. 1977. Numerical integration of the cartesian equations of motion of a system with constraints: Molecular dynamics of n-alkanes. *Journal of Computational Physics* 23 (3): 327–341.
22. Gilbert D. Nessim. 2010. Properties, synthesis, and growth mechanisms of carbon nanotubes with special focus on thermal chemical vapor deposition. *Nanoscale* 2 (8): 1306–1323.
23. Fawzi M. Elfghi, and N.A.S. Amin. 2013. Optimization of hydrodesulfurization activity in the hydrotreating process: Canonical analysis and the combined application of factorial design and response surface methodology. *Reaction Kinetics, Mechanisms and Catalysis* 108 (2): 371–390; Kukovecz, A., D, Mehn, E. Nemes-Nagy, R. Szabo, and I. Kiricsi. 2005. Optimization of CCVD synthesis conditions for single-wall carbon nanotubes by statistical design of experiments (DoE). *Carbon* 43 (14): 2842–2849.
24. Mason, Robert L., Richard F. Gunst, and James L. Hess. 2003. *Statistical design and analysis of experiments: With applications to engineering and science*. New York: Wiley.
25. Saban, Tanyildizi, M., Dursun Özer, and Murat Elibol. 2005. Optimization of α-amylase production by Bacillus sp. using response surface methodology. *Process Biochemistry* 40 (7): 2291–2296.
26. Aslan, N. 2008. Application of response surface methodology and central composite rotatable design for modeling and optimization of a multi-gravity separator for chromite concentration. *Powder Technology* 185 (1): 80–86.

27. Rao, A.M., E. Richter, Shunji Bandow, Bruce Chase, P.C. Eklund, K.A. Williams, S. Fang, K.R. Subbaswamy, M. Menon, and A. Thess. 1997. Diameter-selective Raman scattering from vibrational modes in carbon nanotubes. *Science*. 275 (5297): 187–191.
28. Murphy, H., P. Papakonstantinou, and T.I.T. Okpalugo. 2006. Raman study of multiwalled carbon nanotubes functionalized with oxygen groups. *Journal of Vacuum Science & Technology B: Microelectronics and Nanometer Structures Processing, Measurement, and Phenomena* 24 (2): 715–720.
29. McKee, Gregg S.B., and Kenneth S. Vecchio. 2006. Thermogravimetric analysis of synthesis variation effects on CVD generated multiwalled carbon nanotubes. The Journal of Physical Chemistry B 110 (3): 1179–1186.
30. Hajime, Takano, Jeremy R. Kenseth, Sze-Shun Wong, Janese C. O'Brie, and Marc D. Porter. 1999. Chemical and biochemical analysis using scanning force microscopy. *Chemical Reviews* 99 (10): 2845–2890.
31. Pandolfo, A.G., and A.F. Hollenkamp. 2006. Carbon properties and their role in supercapacitors. *Journal of Power Sources* 157 (1): 11–27.
32. Daniel H. Murgida, and Peter Hildebrandt. 2008. Disentangling interfacial redox processes of proteins by SERR spectroscopy. *Chemical Society Reviews* 37 (5): 937–945.
33. Derek Albert, Long, and D.A. Long. 1977. *Raman spectroscopy*. New York: McGraw-Hill.
34. Norman B. Colthup, Lawrence H. Daly, and Stephen E. Wiberley. 1990. *Introduction to infrared and Raman spectroscopy*. Amsterdam: Elsevier.
35. Mildred S. Dresselhaus, Gene Dresselhaus, P.C. Eklund, and A.M. Rao. 2000. *Carbon nanotubes*. Berlin: Springer.
36. Kotani, Akio, and Shik Shin. 2001. Resonant inelastic x-ray scattering spectra for electrons in solids. *Reviews of Modern Physics* 73 (1): 203.
37. Mildred S. Dresselhaus, Gene Dresselhaus, and Peter C. Eklund. 1996. *Science of fullerenes and carbon nanotubes: Their properties and applications*. Cambridge: Academic press.
38. Bandyopadhyay, S., G.K. Paul, R. Roy, S.K. Sen, and Suchitra Sen. 2002. Study of structural and electrical properties of grain-boundary modified ZnO films prepared by sol-gel technique. *Materials Chemistry and Physics* 74 (1): 83–91.
39. Doyle, C.D. 1961. Kinetic analysis of thermogravimetric data. *Journal of Applied Polymer Science* 5 (15): 285–292.
40. Don, Clark, and Alexander Pysik. 2002. The analysis of pharmaceutical substances and formulated products by vibrational spectroscopy. In *Handbook of Vibrational Spectroscopy*.
41. Harwalkar, V.R., and C.Y. Ma. 1996. Thermal analysis: Principles and applications. *Food proteins: Properties and characterization* 405.
42. Ge, Cuicui, Fang Lao, Wei Li, Yufeng Li, Chunying Chen, Yang Qiu, Xueying Mao, Bai Li, Zhifang Chai, and Yuliang Zhao. 2008. Quantitative analysis of metal impurities in carbon nanotubes: Efficacy of different pretreatment protocols for ICPMS spectroscopy. *Analytical Chemistry* 80 (24): 9426–9434.
43. Louis S.K. Pang, John D. Saxby, and S. Peter Chatfield. 1993. Thermogravimetric analysis of carbon nanotubes and nanoparticles. *The Journal of Physical Chemistry* 97 (27): 6941–6942.
44. Min, Ouyang, Jin-Lin Huang, and Charles M. Lieber. 2002. Scanning tunneling microscopy studies of the one-dimensional electronic properties of single-walled carbon nanotubes. *Annual review of physical chemistry* 53 (1): 201–220.
45. José Miguel, Aguilera, and David W. Stanley. 1999. *Microstructural principles of food processing and engineering*. Berlin: Springer Science & Business Media.
46. Jean-Marc Bonard, Kenneth A Dean, Bernard F Coll, and Christian Klinke. 2002. Field emission of individual carbon nanotubes in the scanning electron microscope. *Physical Review Letters* 89 (19): 197602; Seiler, H. 1983. Secondary electron emission in the scanning electron microscope. *Journal of Applied Physics* 54 (11): R1–R18.
47. Mehdi, Shanbedi, Saeed Zeinali Heris, Ahmad Amiri, and Hossein Eshghi. 2015. Synthesis of water-soluble Fe-decorated multi-walled carbon nanotubes: A study on thermo-physical properties of ferromagnetic nanofluid. *Journal of the Taiwan Institute of Chemical Engineers*.

48. Wang, Z.L. 2000. *Transmission electron microscopy of shape-controlled nanocrystals and their assemblies*. ACS Publications.
49. van de Locht, Renée. 2014. On the nanostructure of biogenic and bio-inspired calcium carbonate as studied by electron microscopy techniques. Diss. University of York.
50. Joseph I. Goldstein, Dale E. Newbury, Patrick Echlin, David C. Joy, Charles Fiori, and Eric Lifshi. 1981. *Scanning electron microscopy and X-ray microanalysis. A text for biologists, materials scientists, and geologists*. Plenum Publishing Corporation.
51. Machavaram V Kartikeyan, Edith Borie, and Manfred Thumm. 2013. *Gyrotrons: High-power microwave and millimeter wave technology*. Berlin: Springer Science & Business Media.
52. Makovicky, Milota, et al. 1980. Mineralogical, radiographic and uranium leaching studies on the uranium ore from Kvanefjeld, Ilímaussaq Complex, South Greenland.
53. Reimer, Ludwig, and Helmut Kohl. 2008. *Transmission electron microscopy: Physics of image formation*. Berlin: Springer.
54. Tkachenko, Alexander G., Huan Xie, Donna Coleman, Wilhelm Glomm, Joseph Ryan, Miles F. Anderson, Stefan Franzen, and Daniel L. Feldheim. 2003. Multifunctional gold nanoparticle—Peptide complexes for nuclear targeting. *Journal of the American Chemical Society* 125 (16): 4700–4701.
55. Stewart, Matthew E., Christopher R. Anderton, Lucas B. Thompson, Joana Maria, Stephen K. Gray, John A. Rogers, and Ralph G. Nuzzo. Nanostructured plasmonic sensors. *Chemical Reviews* 108 (2): 494–521.
56. Plunkett, Susan E., James L. Chao, Thomas J. Tague, and Richard A. Palmer. Time-resolved step-scan FT-IR spectroscopy of the photodynamics of carbonmonoxymyoglobin. *Applied Spectroscopy* 49 (6): 702–708.
57. Griffiths, Peter R., and James A. De Haseth. 2007. *Fourier transform infrared spectrometry*. New York: Wiley; Saito, T., K. Matsushige, and K. Tanaka. Chemical treatment and modification of multi-walled carbon nanotubes. *Physica B: Condensed Matter* 323 (1): 280–283.
58. Sung, S.L., S.H. Tsai, C.H. Tseng, F.K. Chiang, X.W. Liu, and H.C. Shih. 1999. Well-aligned carbon nitride nanotubes synthesized in anodic alumina by electron cyclotron resonance chemical vapor deposition. *Applied Physics Letters* 74 (2): 197–199.
59. Lyons, Michael E. 2008. Carbon nanotube based modified electrode biosensors. Part 1. Electrochemical studies of the flavin group redox kinetics at SWCNT/glucose oxidase composite modified electrodes.
60. White, L.O., R. Edwards, H.A. Holt, A.M. Lovering, R.G. Finch, and D.S. Reeves. 1988. The in-vitro degradation at 37 C of vancomycin in serum, CAPD fluid and phosphate-buffered saline. *Journal of Antimicrobial Chemotherapy* 22 (5): 739–745.
61. Peng, Ru, Wenjing Zhang, Qin Ran, Cong Liang, Li Jing, Siqiu Ye, and Yuezhong Xian. 2011. Magnetically switchable bioelectrocatalytic system based on ferrocene grafted iron oxide nanoparticles. *Langmuir* 27 (6): 2910–2916.
62. Nishizawa, M., Y. Miwa, T. Matsue, and I. Uchida. 1993. Surface pretreatment for electrochemical fabrication of ultrathin patterned conducting polymers. *Journal of the Electrochemical Society* 140 (6): 1650–1655.
63. TermehYousefi, Amin, Samira Bagheri, Nahrizul Adib Kadri, Mohamad Rusop Mahmood, and Shoichiro Ikeda. 2015. Constant glucose biosensor based on vertically aligned carbon nanotube composites. *International Journal of Electrochemical Science* 10: 4183–4192.
64. TermehYousefi, Amin, Katsumi Tateno, Samira Bagheri, and Hirofumi Tanaka. 2017. Development of frequency based taste receptors using bioinspired glucose nanobiosensor. *Scientific Reports* 7.

Chapter 4
Results and Discussions

Abstract This chapter indicates that the vertically aligned MWCNTs were successfully synthesized on a silicon substrate via the CVD method with different morphological properties. The crystallinity of synthesized MWCNTs was also optimized using statistical analysis to control the growth condition and defect amount of CNTs. In line with the previous chapter, the optimized MWCNT was used to obtain the MWCNT/GL matrix to improve the direct electron transfer processes between GOx and modified GCE through hydrophobic-hydrophobic interactions in forming stable dispersions of MWCNTs. The GCE modified by GOx/MWCNTs/Gl was used for glucose detection approaches based on the electrochemical method. Furthermore, the GOx/MWCNTs/Gl/GCE was employed to fabricate an electronic tongue for sweetness diagnoses by recording frequency response of the glucose biosensor. The frequency results recorded by oscilloscope indicate that, by adding different glucose concentrations to electrochemical cells connected to the circuit, the output oscillation frequency changes.

4.1 Fast Synthesis of Multilayer Multi-walled Carbon Nanotubes from Camphor Oil

A multilayer CNT from camphor oil has been synthesized as mentioned in Sect. 3.3. Figure 4.1 shows that VACNTs with high uniformity and nearly identical diameters were fabricated. FESEM images confirm that well-aligned CNTs with three different diameters were synthesized. As the flow rate of argon gas decreases, the CNTs gradually thicken [1]. The duration of carrier gas feeding and its flow rate in the reaction zone are key parameters controlling the CNTs' diameter. The growth rates of the active ends of the CNTs vary proportionally to the flow rate of argon gas until complete consumption of the carbon source. Alteration of the argon flow velocity during deposition and limited argon flow rate control the growth conditions of the CNTs [2, 3].

Considering the influx of vaporized CNTs to the silicon substrate at the second furnace, the diameter distribution of synthesized CNTs increases as the flow rate of

© Springer International Publishing AG 2018

A. TermehYousefi, *Nanocomposite-Based Electronic Tongue*, Springer Series in Materials Science 259, https://doi.org/10.1007/978-3-319-66848-2_4

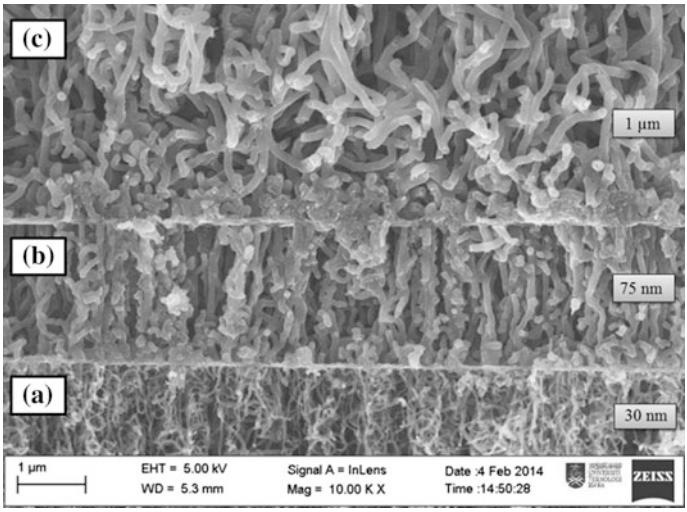

Fig. 4.1 FESEM images of the fast synthesized multilayer CNTs in relation to the applied flow rate of the argon gas: **a** 600 sccm, **b** 400 sccm, and **c** 200 sccm

the argon gas decreased in the reactor. The quantity of carbons covalently attached to the active end of the tube increases with decreasing flow rates of argon gas [4]. Various diameters of CNTs are evident during structural transition of the feedstock around the substrate. During the first stage of the experiment (synthesizing of the first layer of multilayer MWCNTs on silicon substrate), the average diameter of the tubes is approximately 30 nm, and high uniformity is observed. Reducing the flow rate of argon gas during deposition process, the diameters of the tubes change and produce a central layer with uniformity that is identical to that in the first layer, with an average diameter of 75 nm. The minimum flow rate of argon gas generates the last layer of multilayer CNTs with different geometry to the previous layers and an average diameter to up to 1 µm; this final layer is obtained by terminating the carbon source [5].

FESEM images indicate that variations in argon flow rate could systematically change the diameter distribution of the CNTs. It can be proposed that at any given flow rate of argon, an optimal diameter exists for the CNTs. Varying the carrier gas flow rate during the growth process can be employed to control the growth of CNTs.

The FTIR spectrum (400–4000 cm^{-1}) of the fabricated CNTs is shown in Fig. 4.2, and the related peaks are summarized in Table 4.1. The spectra were recorded using pressed disks of pure solid powders combined with KBr. Only a small C–C stretch and a peak at 1532–1560 cm^{-1} were observed, which indicates the presence of a carbon double bond (C=C); this finding confirms the hexagonal structure of the CNTs. Figure 4.3 shows the Raman spectra of the CNTs.

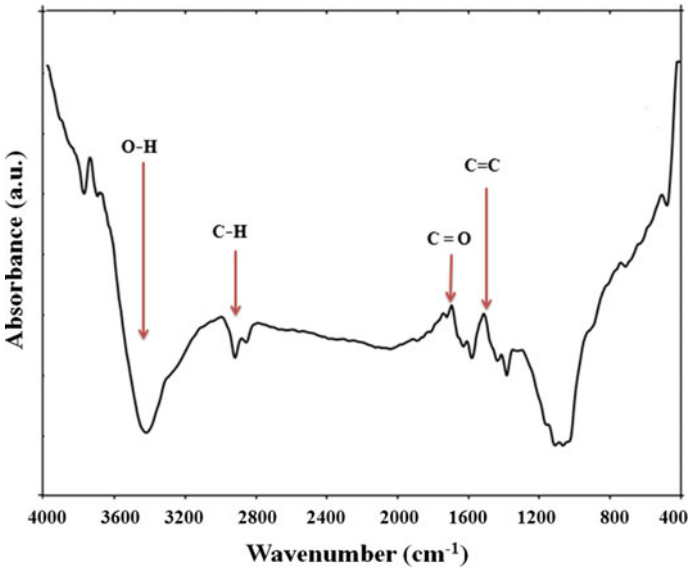

Fig. 4.2 FTIR spectrum of the fast synthesized multilayer carbon nanotubes

Table 4.1 FTIR spectroscopy absorption bands of multilayer carbon nanotubes

Frequency (cm^{-1})	Possible assignment
3424	H-bonded OH groups
2928	C–H bending, stretching
1699	C=O stretching
1540	C=C stretching

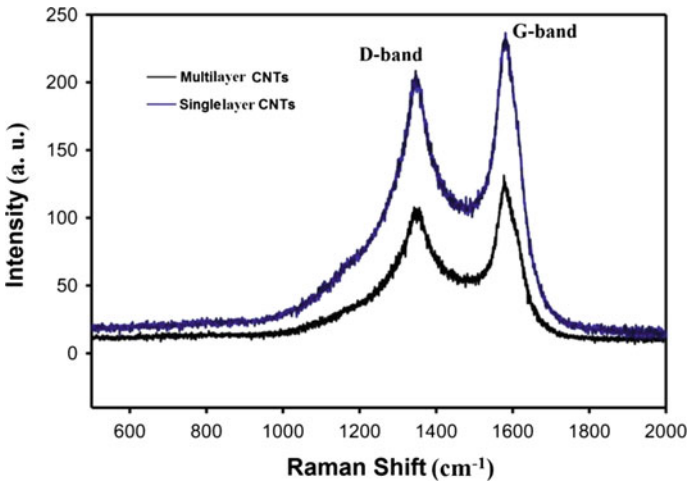

Fig. 4.3 Raman spectra of the fast synthesized multilayer carbon nanotubes

The Raman results have been compared with the grown CNTs in a unique argon flow rate to ensure the effect of the transitive argon gas flow on the growth process (Fig. 4.3). Accordingly, two main peaks are found at 1348 and 1577 cm^{-1}; these peaks correspond to the *D* and *G* bands, respectively [6]. The I_G/I_D ratio suggests that the crystallinity of the synthesized CNTs under varying argon flow rates is identical to those grown under a fixed argon flow rate. The I_G/I_D ratio for both types of CNTs is approximately 1.12. As such, the crystalline quality of the CNTs shows no major variation despite changes in argon flow rate [7].

According to the results, well-aligned CNTs with three different diameters (30 nm, 75 nm, 1 μm) have been synthesized by employing different argon flow rates. FESEM images show that varying the argon flow rate could systematically change the diameter distribution of the CNTs. Reducing the argon flow rate during the deposition process changes the diameter of the tubes, thereby producing a central layer of CNTs with the same uniformity as that in the first layer. The minimum argon flow rate generates the last layer of the CNTs structure with the same geometry as the previous layers and high average diameter. FTIR spectrum indicates the presence of carbon double bonds (C=C), which confirms the integrity of the hexagonal structure of the CNTs. The obtained Raman spectra indicate that the crystallinity of the CNTs structure exhibits no major variation despite changes in argon flow rate.

4.2 Synthesis of Well-Crystalline Carbon Nanotubes Via Neutralized Cooling Method

Well-crystalline CNTs via the neutralized cooling method was synthesized. In fact, changing the argon gas to oxygen gas during the cooling process improved the purity of the synthesized CNTs by neutralizing the formation of disorders such as amorphous carbon. While in the conventional cooling system (using argon gas as an inert gas), the amount of the amorphous carbon is not changed. Furthermore, the minimum applied temperature provided for the neutralized cooling method (to remove the sample from the quartz tube to neutralize the formation of amorphous carbons on surface of CNTs) was 400 °C which also minimizes the formation of impurities on the surface of the synthesized CNTs [8]. Figure 4.4 shows the Raman spectra of well-aligned CNTs optimized by the neutralized cooling method. Generally, peak intensities ranging from approximately 1300 to 1350 cm^{-1}, and approximately 1580 to 1600 cm^{-1} are represented by the disordered *D* line and graphitic G line, respectively [9, 10]. The *D* peaks for CNTs growth using neutralized and conventional cooling systems were $\sim$1354.60 and $\sim$1346.35 cm^{-1}, respectively, whereas the *G* peaks were at $\sim$1588.40 cm^{-1} and $\sim$1577.10 cm^{-1}, respectively. The I_G/I_D ratio that reflects the crystallinity ratio and quality of the synthesized CNTs was calculated both in the neutralized cooling method and conventional cooling method at 1.28 and 1.19, respectively. The obtained results

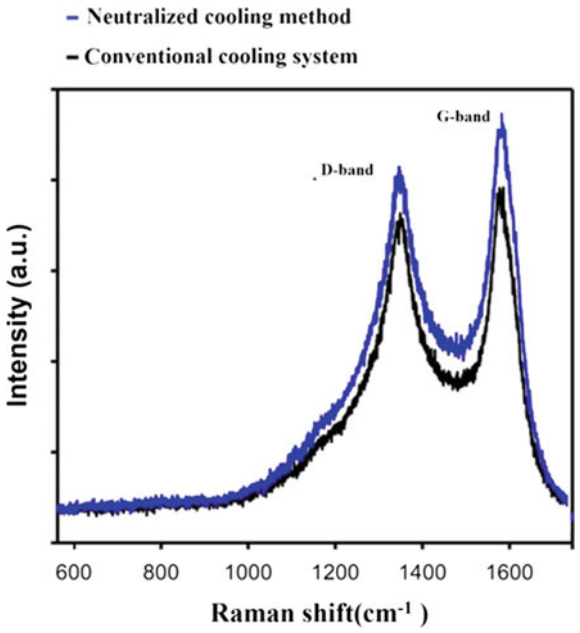

Fig. 4.4 Raman spectra of applying different cooling system to the CVD

clearly show that the graphitic size ratio of the synthesized CNTs will increase by using the neutralized cooling method in CVD process.

Based on the absence of the radial breathing mode in the Raman shifts (which usually appears below 300 cm^{-1}), the grown CNTs were likely to contain more than a single wall [11]. The results also showed similar Raman shifts occurring in both samples; however, the intensity of the *G* band of the CNTs grown by the neutralized cooling method (removing the CNT samples from CVD at 400 °C to neutralize the formation of amorphous carbon) is higher than that of the conventional cooling technique (removing the CNTs sample from CVD at room temperature), which would result in a higher I_G/I_D value. Obtaining a higher crystallinity ratio in the neutralized cooling method suggests that the crystalline quality of the CNTs' structure changes according to the variation in the cooling method. Reproducibility of the experiments and the accuracy of the Raman spectra were verified using replicates of the experiments employing similar growth mechanisms.

The improvement of I_G/I_D might not be related to the applied temperature in the cooling step, because such effects on the structure of CNTs could only be observed at considerably higher temperatures (>1500 °C), at which the crystallinity of carbon is altered [12]. Therefore, the obtained Raman results could be explained by two different hypotheses. First, the formation of defects in solids after modification is known to be related to the cooling process, as high temperatures would energetically preclude the formation of defects. Therefore, the neutralized cooling method will minimize the defects of the structure and the impurities in CNTs, which in turn yields and organizes more crystalline CNTs. Furthermore, CNT samples' contact

with air at 400 °C could lead to burning contaminations, leading to the removal of nanostructures with low crystallinity, and the survival of structures with high crystallinity [8]. Second, removing the CNTs sample at high temperatures leads to have alteration in argon feeding gas. Furthermore, the neutralization of the cooling process was hastened by replacing argon with oxygen, which also minimizes the defects of the CNTs, where oxygen covalently bonds with carbon atoms, and the remaining highly mobile carbons cannot be stabilized or bind with adsorbates to form small, physisorbed clusters of CNTs or amorphous carbon [8, 13]. The FESEM images obtained from CNTs at two different cooling rates (neutralized cooling method and conventional cooling method) are shown in Fig. 4.5. The well-aligned CNTs are formed from the conventional cooling method (Fig. 4.5a), with 87.5 nm diameter, and the neutralized cooling method (Fig. 4.5b) resulted in a diameter of 67.8 nm combined with the substrate. Modifying the diffusion of carrier gas in the cooling step enable the synthesis of more uniform and smaller diameter CNTs compared with the conventional cooling rate [3]. However, CNT arrays could surprisingly be peeled off the silicon substrate following the neutralized cooling method, while retaining their vertical and parallel orientations. A thin layer of CNTs, which was apparent to the naked eye, could be removed from the black and the shiny gray substrate. However, the FESEM results could not provide a comprehensive insight into the arrangement of graphene layers of the CNTs, but it is confirmed that the neutralized cooling method has no effect on the aspect ratio of CNTs.

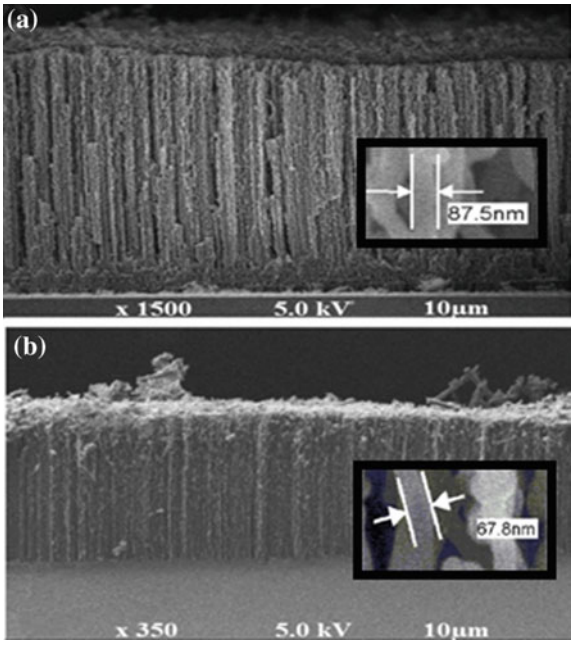

Fig. 4.5 FESEM images of synthesized CNTs by applying conventional cooling rate (**a**) and neutralized cooling method (**b**)

4.3 Highly Oriented Vertically Aligned Carbon Nanotubes Via Carbon Vapor Deposition Method

Highly oriented VACNTs were synthesized as mentioned in Sect. 3.5. As shown in Fig. 4.6, the FESEM results contain the well-aligned CNTs with high uniformity and aspect ratio, which corresponds to the gradual thickening alteration of the CNTs based on the similar orders of feedstock. The inset images in Fig. 4.6 clearly indicate that CNTs are grown in a vertical direction while keeping their initial diameter. This growth condition suggests that the surface area of synthesized VACNTs improves by increasing the length of CNTs. It is well known that CVD produces MWCNTs at low temperatures, while at high temperatures, it favors the growth of SWCNTs [14]. This might be due to the formation energy of SWCNTs, which is higher than MWCNTs. Based on the diameter of the grown CNTs measured by FESEM images, the synthesized CNTs are mostly MWCNTs since MWCNTs needs lower formation energy [2] and are easier to grow (compare with SWCNTs).

The effect of the CVD duration on the morphology of VACNTs was also studied as shown in Fig. 4.7. The diameter of CNTs increases with the CVD durations, especially with increasing deposition time, possibly due to sintering and agglomeration of the feedstock [15]. Furthermore, the lengths of the CNTs are controlled by the duration of the deposition time for the purpose of obtaining the desired morphology in the context of the proposed application. CNTs grown after 5 min reaction time are not vertical since the hydrocarbons have not had enough chance to create the cylindrical structure of CNTs while after 15 min reaction time, CNTs are

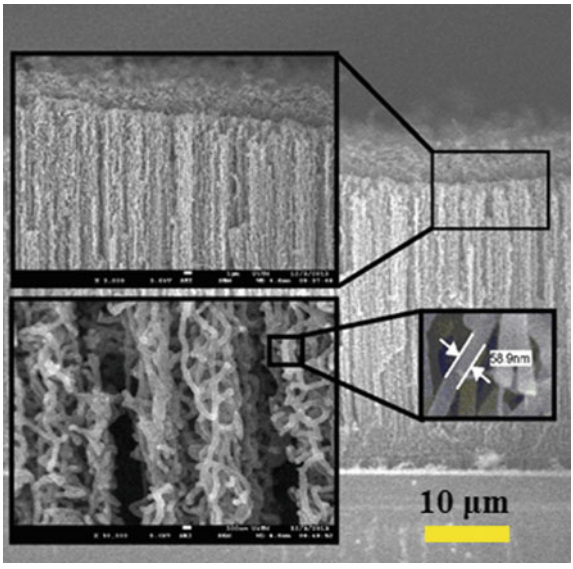

Fig. 4.6 FESEM images of well-aligned CNTs with high uniformity and aspect ratio

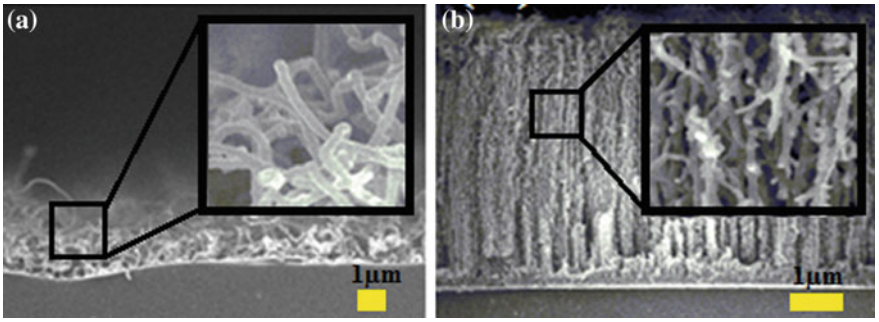

Fig. 4.7 The length of the CNTs controlled by the duration of the deposition time; synthesized CNTs based on 5 min (**a**) and 15 min (**b**) deposition time

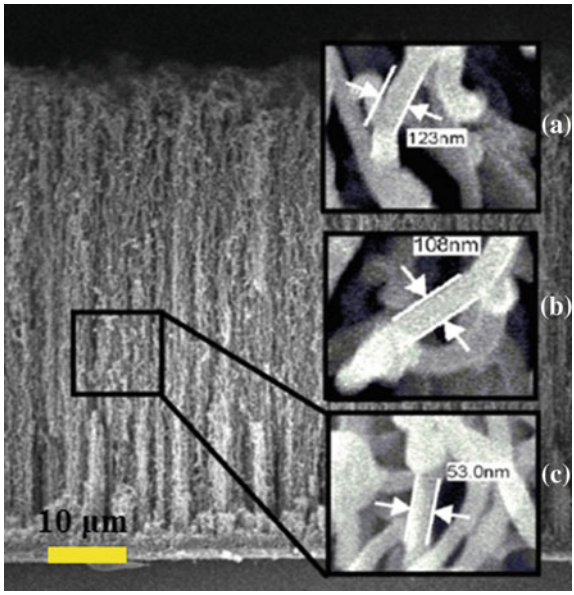

Fig. 4.8 FESEM images of CNTs with different diameters. The catalyst amount is **a** 0.1 g, **b** 0.2 g, and **c** 0.5 g in the presence of 13 mL camphor oil

starting to grow in an oriented direction. These findings also confirm that the aspect ratio and surface area of synthesized VACNTs are highly dependent on the reaction time in the CVD method.

Figure 4.8 shows the relation between the diameter of aligned CNTs and the concentration of ferrocene. As the concentration of ferrocene increases (0.5 mg), the uniformity of VACNTs increases rapidly while the diameter of VACNTs decreases. However, at lower ferrocene concentrations (0.1 mg), a lower growth rate occurs, which is due to the lack of sufficient Fe clusters to catalyze the growth of aligned CNTs [16]. Therefore, the diameters of aligned CNTs fabricated at higher ferrocene concentrations are smaller than those fabricated at higher concentrations [17].

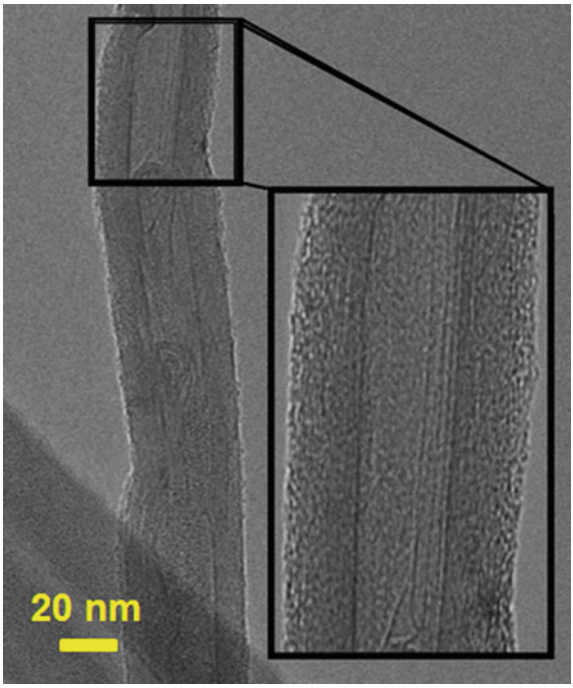

Fig. 4.9 HRTEM images of synthesized CNTs via the CVD method with 0.5 g catalyst in the presence of 13 mL camphor oil

Figure 4.9 demonstrates the HRTEM images of grown VACNTs. As can be seen, the hollow nanostructure confirms MWCNTs growth, but due to presence of defects and amorphous carbon on the surface of the CNTs, the number of the walls are still not clear. However, the external diameter of the CNTs indicates the synthesizing of MWCNTs.

Figure 4.10 presents the effect of the different flow rates of argon gas on the synthesis and characterization of CNTs on silicon substrates by CVD at 900 °C using argon gas. The crystallinity of the CNTs is directly influenced by the diffusion of the feedstock to the second furnace of the CVD process. The increase in the argon flow rate caused structural damage to the synthesized MWCNTs which can be attributed to sluggish activity of ferrocene particles, which were unable to decompose the increased carbon contents into CNTs. Therefore, the amount of amorphous carbon increases with the higher argon flow rates which increase the amount of the amorphous carbon in the synthesized VACNTs.

The plot of crystallinity, length, and tube diameter is shown in Fig. 4.11. According to the observed results, the concentration of ferrocene has a direct effect on the diameter of the grown VACNTs. Hence, at lower ferrocene concentration (less than 0.5 g), CNTs prefer to extend their graphitic structure horizontally producing higher diameters. Also, with lower ferrocene amounts in camphor oil (less than 0.5 g ferrocene in 13 mL camphor oil), the length of the VACNTs decreases slightly due to insufficient vaporized hydrocarbon complex with ferrocene. In contrast, increasing

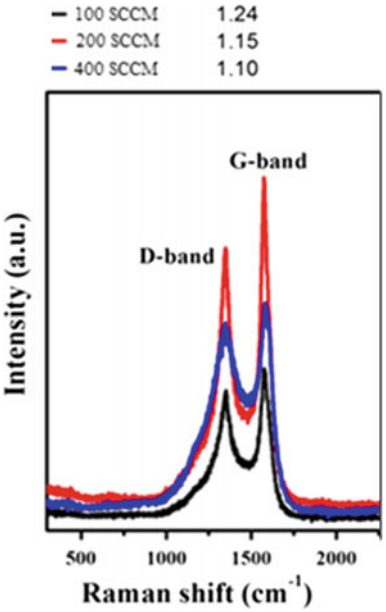

Fig. 4.10 Raman spectra of CNTs based on different argon flow rates

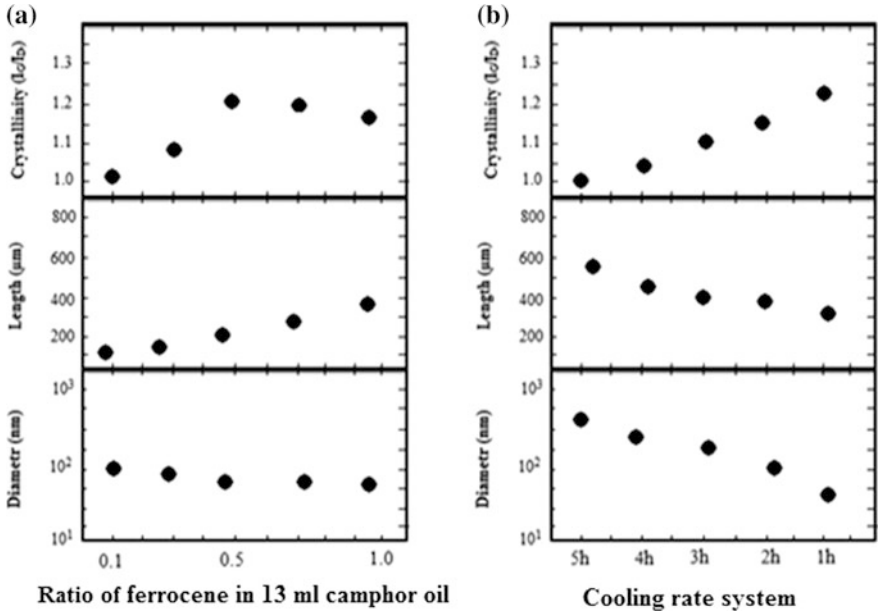

Fig. 4.11 Plot of crystallinity, length, and tube diameter: **a** the ratio of the ferrocene in 13 mL camphor oil (mg/ml), and **b** the cooling rate system (h)

the amount of ferrocene (more than 0.5 g), improves the crystallinity of the grown VACNTs until the optimization ratio of 0.6 g. However, the crystallinity of the VACNTs will decrease at maximum level (1 g ferrocene in 13 mL camphor oil). Diameter and length of the CNTs are regularly following the cooling rate system. At the normal cooling rate (cooling CVD within 5 min), the CNTs grow their cylindrical structure and the growth continues until the CVD cooling completes. By limiting the cooling time of the CVD, both length and diameter of the synthesized VACNTs will also be restricted. In contrast, applying a higher cooling rate (cooling CVD within 1 h or less), the crystallinity of the synthesized VACNTs is at its higher level which is due to the prevention of amorphous carbon formation.

It is well-known that amorphous carbon burns in air at temperatures lower than CNTs. Therefore, TGA is an effective tool to detect the combustion temperature of MWCNT samples after the CVD processes. Qualitative information on purity of CNTs could be obtained from TGA based on the extent of non-oxidizable residue at high temperature and on the difference between the burn temperature of amorphous carbon and that of the CNTs. Figure 4.12 shows the TGA curves for a high-oriented VACNTs array synthesized in an optimized condition of ferrocene/camphor oil ratio and cooling process as described above. Initially, the temperature was set from room temperature to 1000 °C for TGA with the heating rate of 5 °C/min. W_W is the first stage weight loss owing to H_2O absorbed in CNTs. Wc is the second stage weight loss, attributed to the oxidation of carbon. Therefore, these results clearly indicate an improvement of thermal stability with more resistance against oxidation, resulting from reconstruction toward more order in the nanotube structure. TGA can also quantify purity by measuring the mass loss from CNTs from thermal

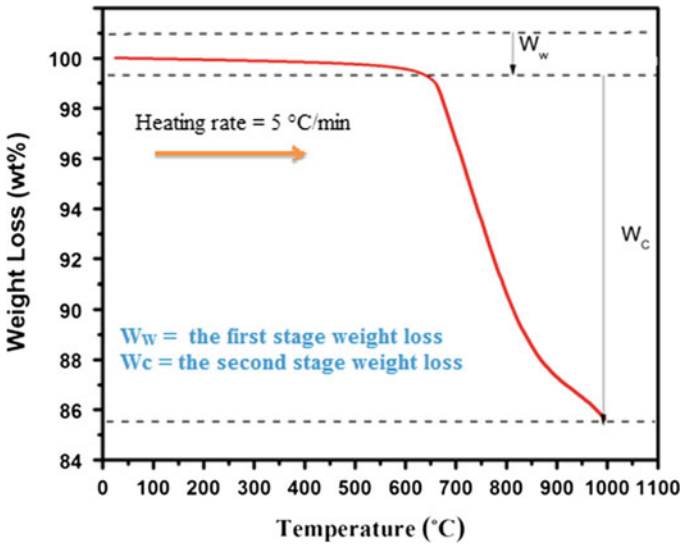

Fig. 4.12 TGA curve (in the air) of the high-oriented VACNTs via CVD

desorption of adsorbed amorphous carbon, which, in the air, typically desorbs at 400 °C, while the carbon atoms from CNTs are typically stable up to 500 °C [18]. According to the TGA results, it is clear that after saturation, the total weight losses of the optimized CNTs from CVD process are higher than 400 °C, which suggests the high stability of grown CNTs by optimized condition.

4.4 Synthesis of Selective Aspect Ratio Vertically Aligned Carbon Nanotubes Via Carbon Vapor Deposition Method

Selective aspect ratio VACNTs were successfully synthesized as mentioned in Sect. 3.6. Annealing temperature, diffusion of hydrocarbon during the annealing process, and its duration also have a direct effect on the growth rate and crystallinity of the grown CNTs [19]. Figure 4.13 shows the effect of the annealing temperature on the crystallinity of the grown CNTs. According to the Raman results, at higher annealing temperatures the crystallinity of the synthesized CNTs also increases.

In contrast with the obtained crystallinity results, according to the FESEM images shown in Fig. 4.14, by applying the annealing temperature higher 800–850 °C, the deposition direction of the hydrocarbons will be altered, and CNTs will start to grow within a fragile structure. The fragile CNTs is not a desirable platform for electrochemical applications, due to the fact that the biocomponents insulating the surface of the electrode disrupt the electron-playing capacity of the electrochemical devices [20, 21].

In fact, by increasing the deposition temperature from 750 to 850 °C, the active amount of deposited CNTs was also enhanced due to increasing of the active amount of CNTs, and the length of the CNTs also increased. But at annealing temperatures higher than the optimum range (above 800–850 °C), the orientation of CNTs also changed due to vertical development of the graphitic sheets.

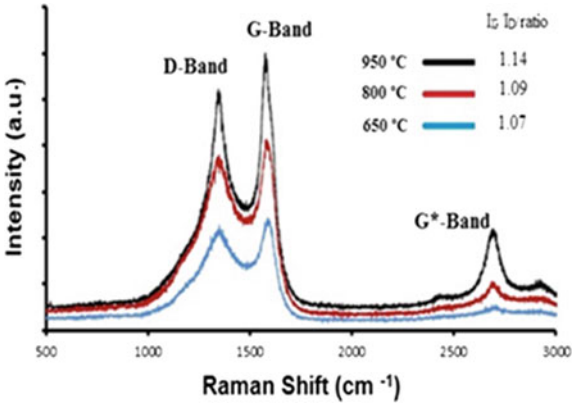

Fig. 4.13 Raman spectroscopy results of synthesized CNTs in different annealing temperature

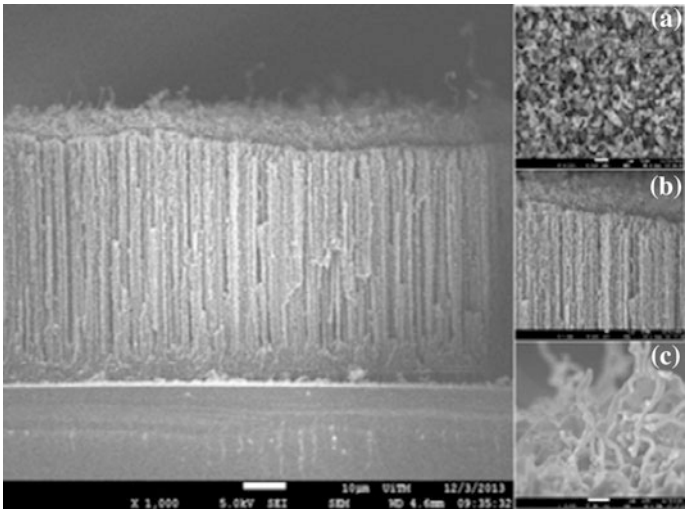

Fig. 4.14 FESEM images of synthesized CNTs in different growth temperatures: **a** high growth temperature (950 °C); **b** optimized growth temperature (800 °C); and **c** low growth temperature (650 °C)

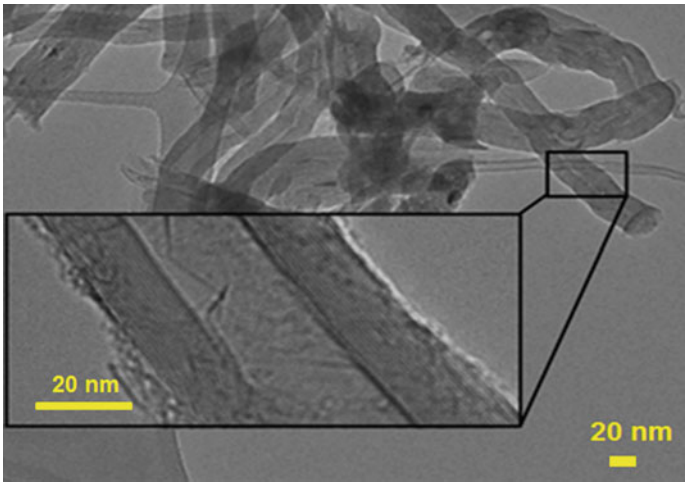

Fig. 4.15 HRTEM images of synthesized CNTs at the optimized annealing temperature (800 °C)

Figure 4.15 demonstrates the HRTEM images of grown CNTs which confirm the successful synthesis of MWCNTs. The HRTEM image clearly confirms that the synthesized nanostructure is made up of CNTs due to higher outer diameter of the CNTs as well as the inside hollow [22].

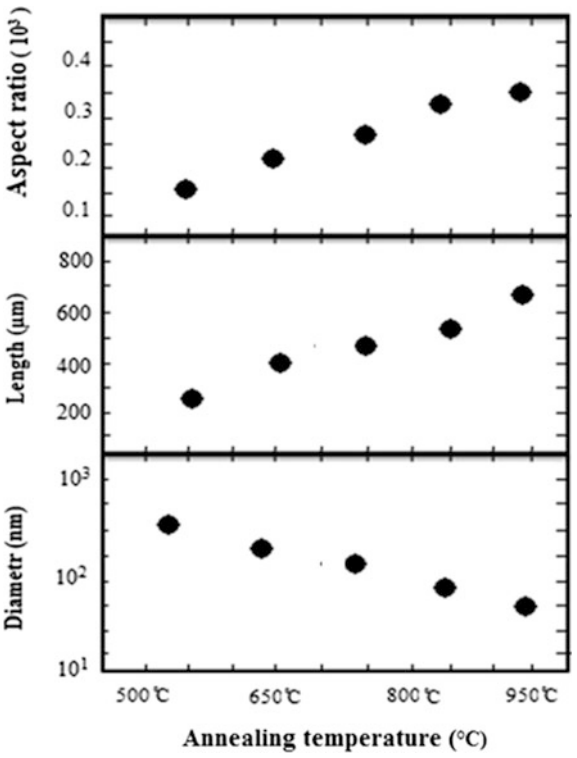

Fig. 4.16 Aspect ratio, length, and nanotube diameter of synthesized CNTs as a function of growth temperature in optimized time

Figure 4.16 shows the relation of the growth process and aspect ratio of aligned CNTs at various annealing temperatures. As seen from Fig. 4.16, the diameters of aligned CNTs formed at a higher annealing temperature are smaller than that growth at a lower annealing temperature. The surfaces of the aligned CNTs synthesized at the higher annealing growth temperature are almost free of defect compared to those synthesized at lower annealing temperature, because the higher growth temperature prevents mobile carbons forming small, physisorbed clusters of CNTs or amorphous carbon on the surface of the growth CNTs.

4.5 Optimization of the Growth Condition Using Response Surface Methodology

4.5.1 Crystallinity Model: I_G/I_D*-Single-Response Optimization*

Investigations of the best variables of camphor oil concentration, annealing process, deposition temperature, and deposition time in the growth conditions of CNTs were

Table 4.2 ANOVA results for CNTs crystallinity

Source	Sum of squares	DF	Mean square	*F*-value	Prob > *F*	
Model	0.095632198	8	0.011954025	12.96935954	<0.0001	Significant
X_1	0.003476379	1	0.003476379	3.771650756	0.0657	
X_2	0.000464015	1	0.000464015	0.503427044	0.4858	
X_3	0.001372742	1	0.001372742	1.489338567	0.2358	
X_4	0.00610947	1	0.00610947	6.628387586	0.0177	
X_1^2	0.079468404	1	0.079468404	86.21818428	<0.0001	
X_2X_3	0.001701563	1	0.001701563	1.846087518	0.1887	
X_2X_4	0.000663062	1	0.000663062	0.719380807	0.4059	
X_3X_4	0.002376563	1	0.002376563	2.578419757	0.1233	
Residual	0.019355969	21	0.000921713			
Lack of fit	0.017355969	16	0.001084748	2.711870133	0.1374	Not significant

analyzed to increase the crystallinity of CNTs during the CVD process. Furthermore, the significance level of the selected parameters in the applied range was also studied using ANOVA analysis. However, the measured response range of the crystallinity value (I_G/I_D ratio) for the experiments is very small (minimum and maximum I_G/I_D ratio is 1.01 and 1.25, respectively), therefore, the effect of the size of the involved parameters is also very small.

As shown in Table 4.2, ANOVA analysis implies that the proposed model is highly significant, due to the Prob > *F* value of the model being less than 0.05. Also, the concentration of camphor oil is the most influenced parameter in the model, due to an acceptable *P*-value. In the case of deposition temperature, the significant level is very close to 0.05. Hence, the deposition temperature is also used as a parameter in capturing the correlation between the growth condition and the crystallinity response of CNTs. The ANOVA analysis clearly shows that the deposition time is insignificant vis-à-vis the crystallinity response of the grown CNTs, which might be due to the analyzed range of deposition times [23]. Moreover, it was reported that the alteration of the deposition time do not affecting the crystallinity of the grown CNTs via the CVD method, but can change the growth rate (length of CNTs as a function of reaction time), which directly affect the architecture (orientation, alignment degree, length, and diameter) of CNTs [24]. In the context of annealing time, the results showed that annealing time has a small effect on the crystallinity of CNTs, due to the high applied temperature range. It is well-known that a long annealing time is required for temperatures under 700 °C [25]. However, by applying an annealing temperature exceeding 750 °C (in the air), the intensity of the Raman shift slightly increases due to the oxidation of carbonaceous particles present on CNTs graphitic domains [26]. Therefore, the duration of the annealing process in the selected annealing temperature range is not significant to the crystallinity model of the grown CNTs. In case of the quadratic term of the parameters (except X_1^2) as well as their interaction terms (X_1X_2, X_1X_3,

X_1X_4, and X_2X_3,) are all insignificant to the crystallinity response of the model, due to *P*-values exceeding 0.05. These terms are regarded as noise, and were removed from the predicted crystallinity model of CNTs. In contrast, X_1^2, X_2X_4, and X_3X_4 with lesser *P* values were retained in the model for an enhanced version that predicts crystallinity.

From the statistical results, an empirical relationship could be presented in the form of a mathematical model for crystallinity of CNTs from (3.2). Indeed, the CNTs of crystallinity can be calculated by developing empirical crystallinity model as (4.1):

$$Y_{IG/ID} = -11.76704 + 0.031337X_1 + 1.58617\text{E} - 003X_4 - 1.88747\text{E} - 005X_1^2 - 2.86111\text{E} - 005X_2X_4 - 8.12500\text{E} - 005X_3X_4 \tag{4.1}$$

where $Y_{IG/ID}$ is the predicted value for the crystallinity of CNTs during the CVD process. A reasonable value of the determination coefficient $R^2 = 0.8317$ estimated the regression coefficients, which provides an indication of an acceptable agreement between the observed and predicted data. Based on the tabulated *F*-values in the ANOVA table (Table 4.2), the quadratic form of deposition temperature resulted in the largest *F*-value of 86.21, indicating that it has the most significant effect on the synthesis of crystalline CNTs. However, when comparing with the deposition temperature, X_1, it has less effect on CNTs' crystallinity, but the quadratic form of deposition temperature (X_1^2) fits the crystallinity model. On top of the quadratic effect of the deposition temperature, the concentration of camphor oil also highly affects CNTs' crystallinity, owing to an *F*-value of 6.62. Moreover, deposition temperature also has a considerable F-value of 3.77, since the *P*-value of X_1 is very close to 0.05.

Figure 4.17 shows the two-dimensional (a) and three-dimensional (b) crystallinity response as a function of annealing time and concentration of camphor oil, which was constructed to show the interaction effects of X_3X_4 on the crystalline growth of CNTs. For this plot, the deposition time and temperature was fixed at zero. As seen from Fig. 4.17, the crystallinity of the synthesized CNTs varied due to the alteration of the camphor oil concentration, while in the case of varied annealing time, the CNTs' crystallinity slightly changes.

The ANOVA table also demonstrated similar statements, since the factor X_4 was highly significant. From the 3D plot of the concentration of camphor oil and annealing time, it can be concluded that CNTs tend to grow in higher crystallinity using a higher ratio of ferrocene to camphor oil (less than 10 mL camphor oil) due to the adequate amount of catalyst for vaporized hydrocarbons.

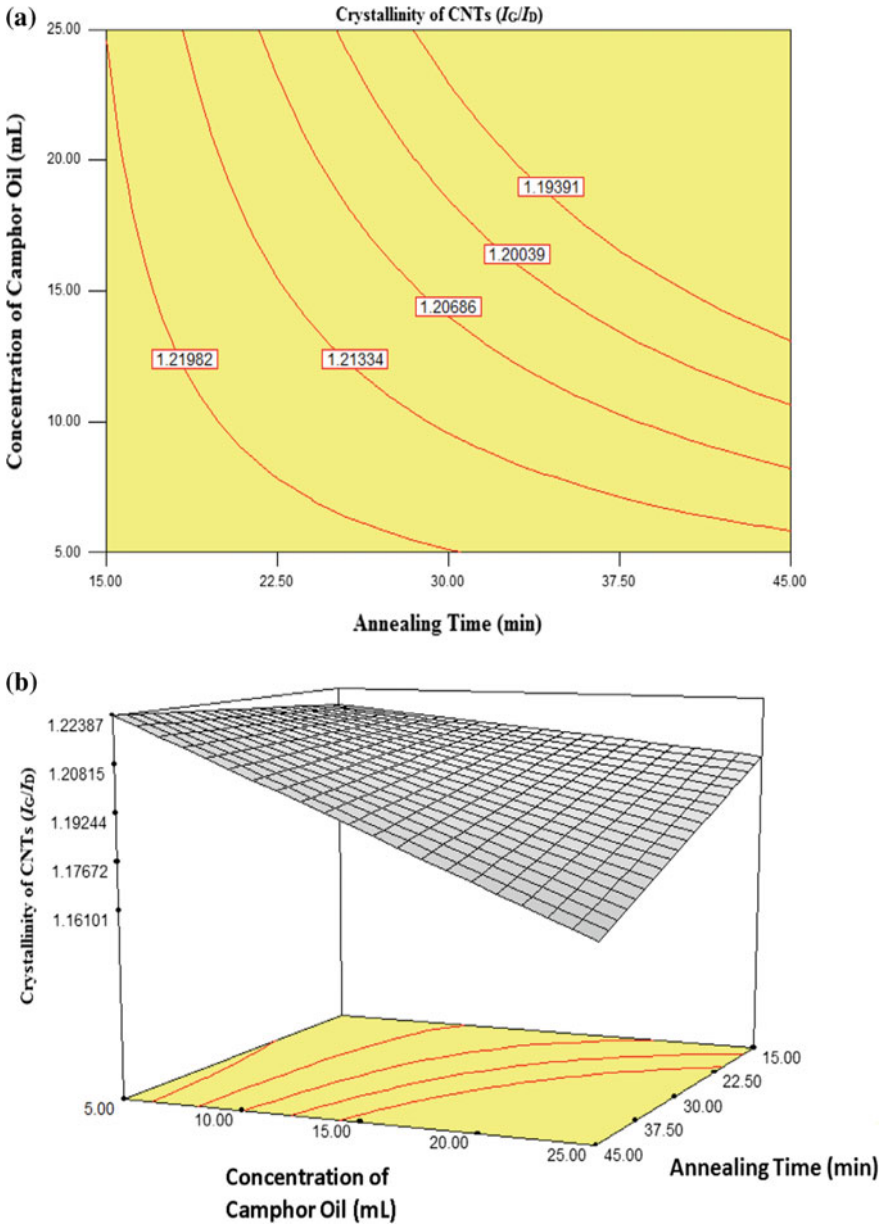

Fig. 4.17 **a** 2D and **b** 3D interaction plot of the concentration of camphor oil and annealing time on the crystallinity of carbon nanotube

4.5.2 *Effect of Deposition Temperature and Concentration of Camphor Oil on Carbon Nanotubes' Crystallinity*

Figure 4.18a shows the Raman spectroscopy results of the grown CNTs at different deposition temperatures. All spectra show two main Raman peaks at ~1300 to 1350 cm^{-1} (*D* band) and ~1580 to 1600 cm^{-1} (*G* band), and also second order Raman signals around 2701 cm^{-1} (*G**-band), corresponding to the overtone mode of the D-band in graphite and CNTs [19]. It was shown that by decreasing the growth temperature, the *D* bands became stronger and broader, which means that a low deposition temperature leads to overlapping *D* and *G* peaks, resulting in low crystalline CNTs, since the *D* peak is explained as a disorder feature of graphitic sheets [27]. According to the growth mechanism of CNTs, carbon atoms diffused into the iron nanoparticles during the CVD process [28].

Therefore, the crystallinity of the CNTs was also significantly affected by the different concentrations of the precursor used to grow CNTs, as shown in Fig. 4.18b [29]. Using low amounts of camphor oil yields fewer CNTs with lower crystallinity, resulting in the CNTs growing in random directions. Achieving

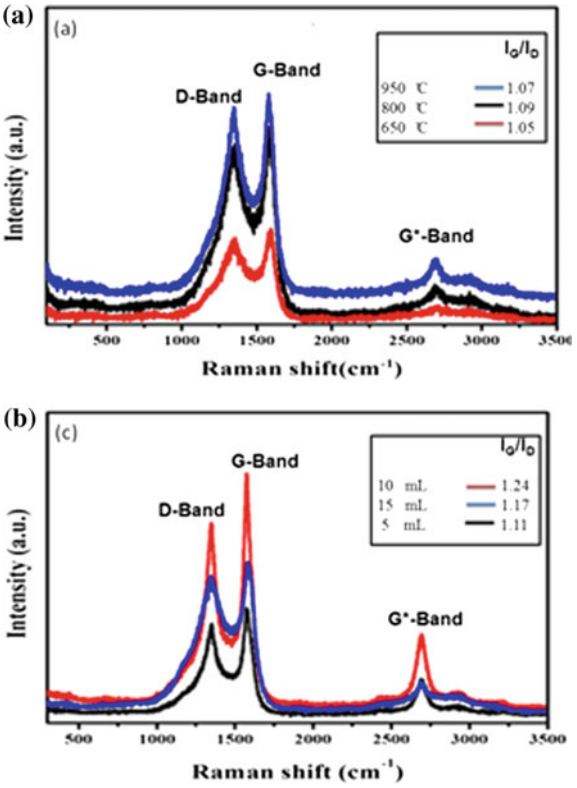

Fig. 4.18 Raman spectra of CNTs based on **a** different deposition temperature: 650, 800, and 900 °C; and **b** different concentration of camphor oil: 5, 10, and 15 mL

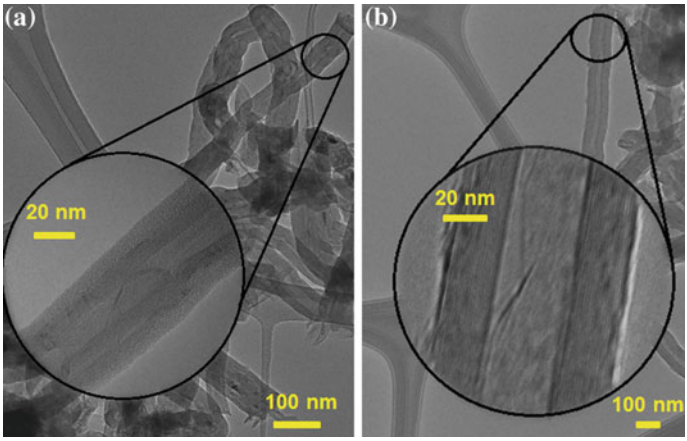

Fig. 4.19 HRTEM images of MWCNTs corresponding to the non-optimized (**a**) and optimized (**b**) conditions of the predominant factors affecting the CVD process

carbonaceous crusts that are not growth oriented due to incomplete evaporation process of ferrocene and camphor oil during synthesis is also possible [30].

The HRTEM results could also be a very useful tool to determine the degree of crystallinity of the grown CNTs, as well as the presence of amorphous carbon coating the outer layers of the tubes. As shown in Fig. 4.19a, the synthesized CNTs, using not optimized condition of the CVD method, display more diffuse spots associated with amorphous carbon, which confirms a lower degree of crystallinity than that shown in Fig. 4.19b, which corresponds to the optimized conditions of predominant factors affecting the CVD process (X_1 = 825 °C and X_4 = 10 mL). Furthermore, the HRTEM results reveal that most of the tubes are closed at their ends and contain a hollow inside that confirms the tubular structure of the grown CNTs. The HRTEM image also confirms the complete removal of catalyst particles.

4.6 Constant Glucose Biosensor Based on Vertically Aligned Carbon Nanotubes Composites

4.6.1 Raman Spectroscopy

Figure 4.20 shows the Raman spectra of MWCNTs. Generally, peak intensities, ranging from approximately 1300 to 1350 cm^{-1}, and approximately 1580 to 1600 cm^{-1}, represent the disordered *D* line and graphitic G line, respectively. The *D* peaks corresponding to the disorder of the multilayer vertical CNTs was 1346.35 cm^{-1}, while the *G* peak(s) was at $\sim$1588.40 cm^{-1} [31].

The I_G/I_D ratio of the optimized crystalline CNTs, which was calculated to estimate the variation in the grown CNTs quality, was 1.22. The absence of the

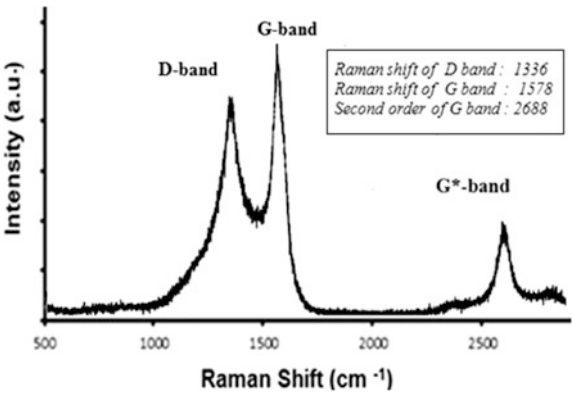

Fig. 4.20 Raman spectra of synthesized MWCNTs. *Inset* is the Raman shifts of D-band and G-band to estimate the I_G/I_D

radial breathing mode which is usually appears below 300 cm^{-1} in the Raman shift, proves that the grown CNTs are more likely to contain more than a single wall, or that the diameter of the growth CNTs exceeds 3 nm [32].

4.6.2 Field Emission Scanning Electron Microscopy

As shown in Fig. 4.21, the FESEM results corresponding to the growth mechanism of MWCNTs highlighted the high aspect ratio and uniformity of the synthesized CNTs using the CVD method. The average diameter of CNTs is enhanced by applying it at higher deposition temperatures, which leads to the growth of more crystalline CNTs with lower than average diameter. Using the data collected from

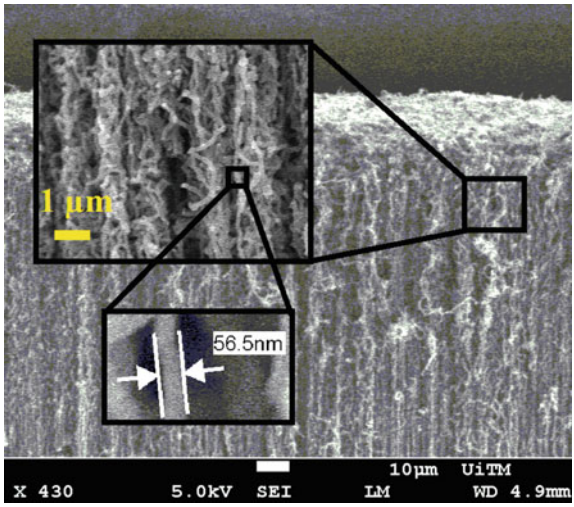

Fig. 4.21 FESEM image of synthesized MWCNTs before dispersal in Gl

the aspect ratio of the FESEM images, the growth rate of the nanotubes can be calculated using the formula $\alpha = \beta$ (μm)/γ (min), where β is the distribution length of the tubes, and γ the deposition time. Therefore, the growth rate of the synthesized CNTs is 3.03 μm/min at 30 min of deposition time, which is included in the optimized temperature and time [33].

4.6.3 Direct Electron Transfer of GOx/MWCNTs/Gl/GCE

The cyclic voltammograms of GOx/MWCNTs/Gl/GCE in nitrogen saturated at pH 7.0 PBS at different scan rates in the range of 20–200 mV/s is shown in Fig. 4.22a. The well-defined and nearly symmetric redox peaks are detected with a formal potential of −0.42 V.

The controlled electrodes illustrated that the redox peaks are derived from GOx, which is similar to the reported results [21, 34]. The peak separation for a reversible process can be calculated as follows:

$$\Delta E_{\mathrm{P}} = E_{\mathrm{Pa}} - E_{\mathrm{Pc}} = \frac{0.059}{n} \tag{4.2}$$

where n is the number of electrons transferred in the reaction, ΔE_{P} is the peak to peak separation, E_{Pa} is the anodic peak potential, and E_{Pc} is the catholic peak potential. In a reversible reaction process, ΔE is greater than ΔE_{P}, whereas in an irreversible reaction process, only one peak will be observed in one of the potential scans.

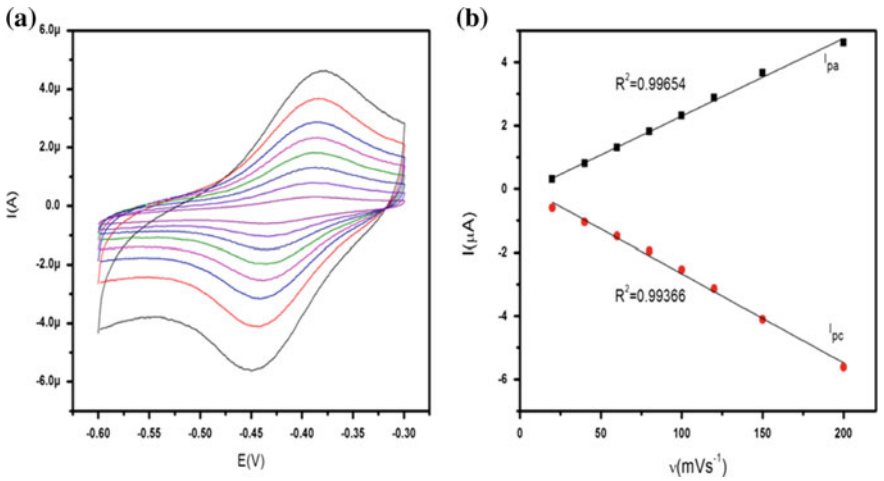

Fig. 4.22 **a** Cyclic voltammograms of the GOx/MWCNTs/Gl/GCE in 0.1 M PBS with nitrogen saturated at different scan rates (from inner to outer curves: 20, 40, 60, 80, 100, 120, 150, and 200 mV/s); and **b** I_{pa} and I_{pc} versus scan rates

The peak separation (ΔE_p) ranges from 25 mV at a scan rate of 20 mV s^{-1} to 65 mV at 200 mV s^{-1}. The redox peaks showed that GOx entrapped in the nanocomposite film undergoes a quasi-reversible electron transfer process [35]. According to the cyclic voltammograms of the GOx/MWCNTs/Gl/GCE, the electron transfer between the electrode and the active site of GOx was not shielded by the globular protein shell of GOx. Figure 4.22b shows a linearity of the anodic or cathodic peak currents at different scan rates, which confirms the surface-confined electrode reactions. Meanwhile, it was also observed that the matrix prominently facilitates active sites of GOx in its approach to the electrode, and confirmed that the GOx/MWCNTs/Gl is stable on the GCE [36]. The K_s (electron transfer rate) between the electrode and GOx was determined to be 8.42 s^{-1} using the Laviron's method [37] as follows:

$$\log k_s = \alpha \log(1-\alpha) + (1-\alpha)\log\alpha - \log\left(\frac{RT}{nFv}\right) - \alpha(1-\alpha)\log\left(\frac{nF\Delta E_p}{2.3RT}\right) \tag{4.3}$$

where α is the transfer coefficient, ΔE_p is the peak separation and n is the number of the transfer electron. T is the absolute temperature; R is the gas constant and v is the scan rate.

4.6.4 Biocatalytic Activity of GOx/MWCNTs/Gl/GC Electrode

Figure 4.23 demonstrates the cyclic voltammograms of the GOx/MWCNTs/Gl/GCE in nitrogen saturated pH 7.0 PBS containing 0.5 mM potassium ferricyanide as its mediator. In Fig. 4.23 curve a describes the redox behavior of potassium ferricyanide on GOx/MWCNTs/Gl/GCE in the absence of glucose, while curve b ascribes the redox behaviors when 2 mM glucose was added into the solution. It was observed that the redox anodic peak current increases. These behaviors demonstrated that GOx/MWCNTs/Gl/GCE is capable of electrocatalyzing the glucose oxidation by taking potassium ferricyanide as a mediator in nitrogen saturated solutions [38].

Studying the dependence of pH from 6.0 to 8.0 on the response, 2 mM glucose in the presence of potassium ferricyanide for the biosensor was explored at an applied potential of +0.3 V, allowing achievement of the highest current response that corresponds to a pH of 7.0. In other words, the appropriate amount of GOx mixed in MWCNTs/Gl composite highly depends on the pH of the buffer solution; in this case, the PBS with pH 7.0 shows the maximum response of 2 mM glucose at an applied potential of +0.3 V. However, the sensitivity and stability of the biosensor by chronoamperometric measurement highly relates to the activity aspect of GOx in the MWCNTs/Gl composite. In the mediator-based glucose biosensor

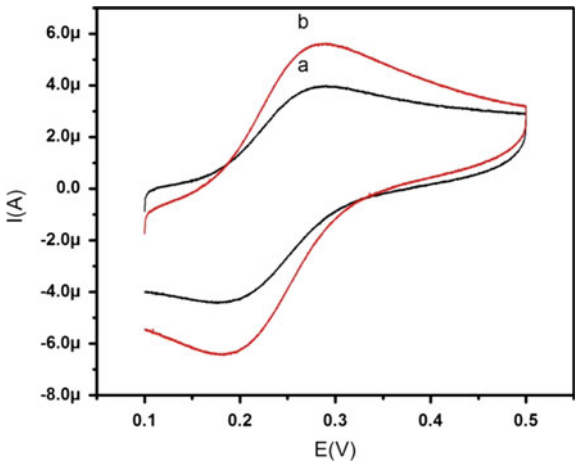

Fig. 4.23 Cyclic voltammograms of the GOx/MWCNTs/Gl/GCE at the scan rate of 20 mV/s in 0.1 M nitrogen saturated PBS and 0.5 mM potassium ferricyanide; *a* in the absence of glucose; and *b* in the presence of 2 mM glucose

the mediator shuttles electrons between the FAD center and the electrode surface by the following scheme [39]:

$$\text{Glucose} + \text{GOx(ox)} \rightarrow \text{gluconic acid} + \text{GOx(red)} \tag{4.4}$$

$$\text{GOx(red)} + 2\text{M(ox)} \rightarrow \text{GOx(ox)} + 2\text{M(red)} + 2\text{H}^+ \tag{4.5}$$

$$2\text{M(red)} \rightarrow 2\text{M(ox)} + 2\text{e}^- \tag{4.6}$$

where M(ox) and M(red) are the oxidized and reduced forms of the mediator, respectively. The reduced form is reoxidized at the electrode, giving a current signal (proportional to the glucose concentration) while regenerating the oxidized form of the mediator, (4.6). Such mediation cycle is displayed in Fig. 4.24.

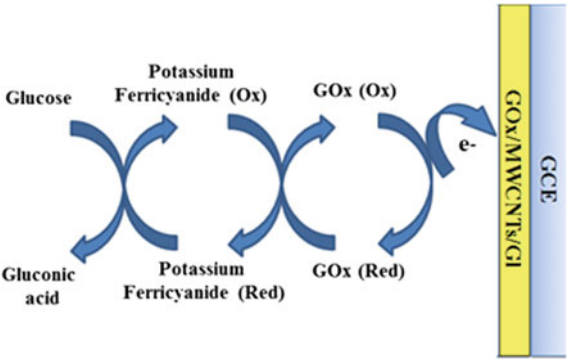

Fig. 4.24 Sequence of events that occur in mediator-based glucose biosensors [44]

4.6.5 Amperometric Determination of Glucose on GOx/MWCNTs/Gl/GC Electrode

Figure 4.25a displays a representative current-time response for the successive addition of 1.5 mM of glucose in each successive adding. The calibration curve in Fig. 4.25b, with a dynamic linear range, spans the glucose concentration from 1 to 8.9 mM, and at higher concentrations, it deviates from linearity, which represents a typical Michaelis-Menten kinetics characteristic. The sensitivity of fabricated modified GCE is 0.644 μA mM^{-1}, which is higher than the reported 0.183 μA mM^{-1} [38].

According to the results, the fabricated biosensor has a higher biological affinity for glucose. The immobilized process might result in the microenvironment changing the enzyme and affecting its intrinsic properties, which could improve its affinity to glucose. The direct electron transfer of GOx in the biosensor exhibits higher stability, and its voltammetric response remains stable after keeping the biosensor for 25 days at 4 °C.

4.6.6 Reproducibility and Stability of the GOx/MWCNTs/Gl/GC Electrode

The storage stability and reproducibility of the modified GOx/MWCNTs/Gl/GC electrode were also studied. The RSD of the modified electrode response to 1.5 mM glucose was 2.6–5.6% for five successive additions. The RSD for detection of

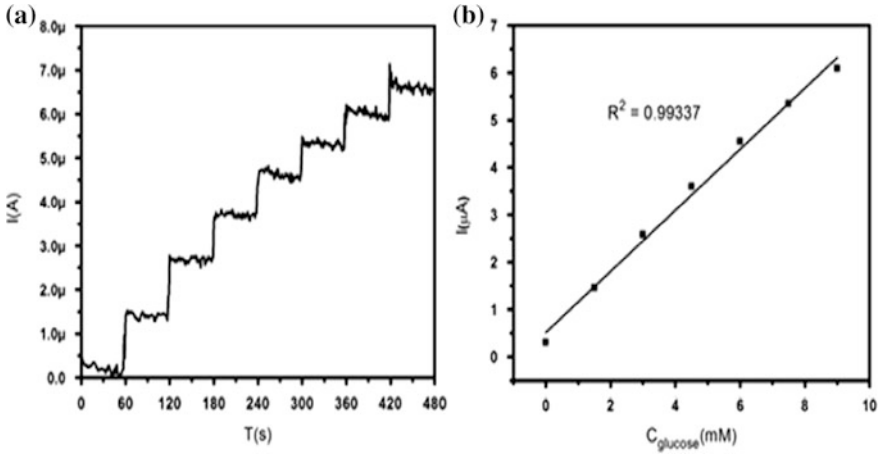

Fig. 4.25 **a** The chronoamperometric response of GOx/MWCNTs/Gl/GCE on the successive addition of 1.5 mM glucose in each successive adding at applied potential of +0.3 V; **b** The calibration curve of the electrocatalytic current on different concentration of glucose

1.5 mM glucose with four modified electrodes prepared under the same conditions was 3.4–6.1%. When the modified GC electrode by GOx/MWCNTs/Gl was stored dry and measured at intervals of 1 week, it retained about 75.4% of its original sensitivity after 25 days.

4.6.7 Determination of Glucose in Human Blood Serum and Analytical Recovery of Glucose

The response of the modified electrode to glucose in human serum of blood was examined. The blood serum sample attained from hospitalized patient was studied. The results were coordinated with reference values gained by the standard colorimetric method obtained from the hospital. Table 4.3 displays the analytical recovery of the glucose solution, which was added to the PBS solution, suggesting the better accuracy of the modified electrode.

Therefore, the entrapment of GOx in MWCNTs/Gl composite matrix was carried out with good film-forming and optimum biocompatibility. By using the surface treated method of CNTs, GOx molecules will more strongly interact with the CNTs' surface (more electrostatically, not only by van der Waals force).

4.7 Brain-Like Taste Bud Circuit Using the GOx/MWCNTs/Gl/GCE Glucose Biosensor

The GOx/MWCNTs/Gl/GCE was superior in maintaining the bioactivity of GOx, rendering it suitable as an amperometric biosensor for glucose detection, with potassium ferricyanide as its mediator. The results indicated that the biosensor possessed excellent stability and acceptable fabrication reproducibility. Such robust sensing information by the glucose biosensor potentially provides useful data not only for diabetes, but also in developing brain-like circuits for electronic tongue. Developing brain-like circuits to design artificial neural networks replicating human abilities is the aim of recent studies, which focus on a combination of nanomaterial and electronic sciences. The human tongue as a whole would be far too complex. Therefore, at the most basic level, the simpler neural network, such as a mouse's

Table 4.3 Assay of glucose in human blood serum sample and recovery of glucose in PBS solution

Sample	Added (mM)	Biochemical analyzer in hospital (mM)	Found mean recovery (mM)	Recovery (%)
Serum of blood	–	4.60	4.47	–
Glucose	1.5	–	1.4	93 ± 2

taste buds, is assumed as a neuron cell that transmits the information signals over the central nervous system and nerve complex.

4.7.1 *Electrical Circuit of a Taste Bud Inspired Network: Single Membrane*

Figure 4.26 shows the output frequency of the electrical circuit of a taste bud inspired network recorded by a GOx/MWCNTs/Gl/GCE according to the variation of the glucose concentration in the electrochemical cell. The glucose concentration is detected as the pulse frequency in the proposed electrical circuit shown, which contains the designed electronic circuit of both second and third layers of the taste bud cell. The input voltage terminal of the circuits was designed for 5 V, which is a high voltage for electrochemical detection of glucose, due to the presence of the potassium ferricyanide [40]. However, the combination of R_1 and R_2 in the circuit design decreases the applied voltage to the electrochemical cell by up to 0.3 V. By adding glucose to the electrochemical cell, the resistivity of the R_2 changes and the operational amplifier will detect a new applied voltage for the circuit, and the multivibrator fixing generated the ON/OFF duration of the frequency [41]. The taste sensory organ identifies sweetness by analyzing the unique patterns of response as a continuous process [42]. Therefore, the modified GCE was designed for a one-time

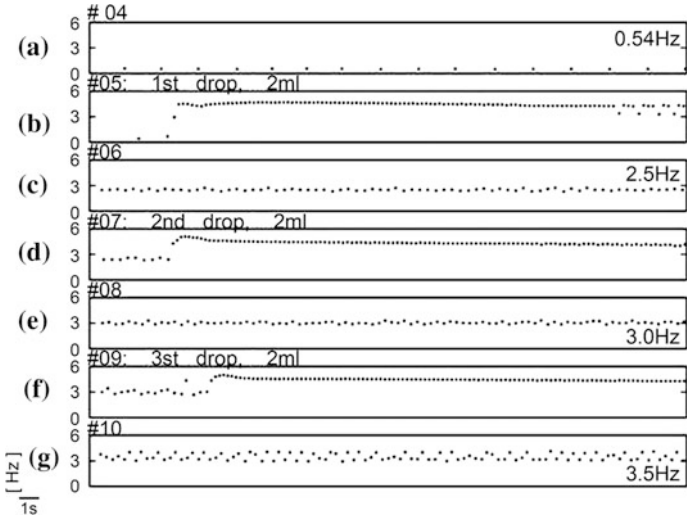

Fig. 4.26 Pulse generator results of the circuit design: **a** before adding glucose; **b** after adding first drop of glucose; **c** stable phase of the reaction in the electrochemical cell after first drop; **d** after adding second drop of glucose to the electrochemical cell; **e** stable phase of the reaction in the electrochemical cell after second drop; **f** after adding third drop of glucose to the electrochemical cell; **g** stable phase of the reaction in the electrochemical cell after third drop

and continuous detection of glucose. Thus, multistep glucose dripping into electrochemical cell tailors the experiment to generate different frequencies according to the concentration of the glucose.

The reduced form is reoxidized at the electrode, giving a current signal (proportional to the glucose concentration) while regenerating the oxidized form of the mediator. Therefore, the glucose concentration is detected as a pulse frequency by a designated electrical circuit. Figure 4.27 shows the pulse frequency results recorded by the oscillator, confirming its results.

According to these hypotheses, the oscillation frequency, F_{osc} of the square wave oscillator is determined by the resistors and a capacitor, based on the following (4.7) [43]:

$$F_{\text{oscillation}} = \frac{1}{2 \times R_t \times C_t \times \text{Ln}(2 \times R_1/R_2 + 1)} \tag{4.7}$$

where R_1 is the resistance between the WE with CNTs and the counter electrode and R_2 is the fixed resistance in fixed time duration (t). The duty ratio of the square wave is determined by a ratio between R_{t1} and R_{t2} ($R_{t1} > R_{t2}$). The resistance depends not only on the glucose concentration, but also applied voltage. Therefore, by adding glucose to the electrochemical cell, the WE resistance is varied, and the voltage is also changed. As a result of this, the output frequency of a square wave becomes a new stable value.

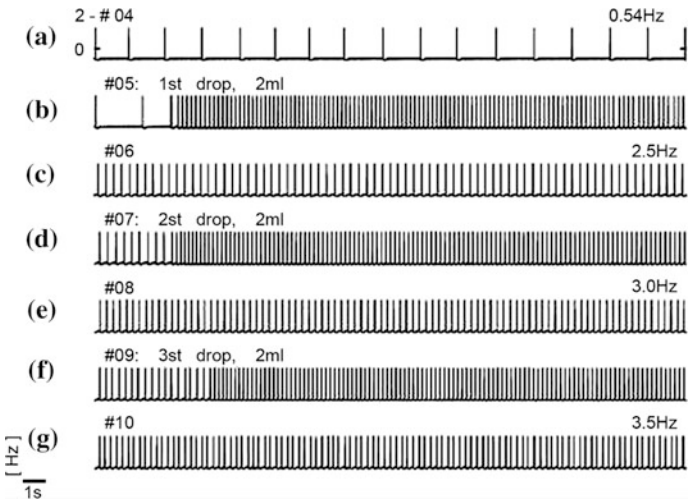

Fig. 4.27 Oscillation frequency results according to the concentration change of the glucose: **a** before adding glucose; **b** after adding first drop of glucose; **c** stable phase of the reaction in the electrochemical cell after first drop; **d** after adding second drop glucose to the electrochemical cell; **e** stable phase of the reaction in the electrochemical cell after second drop; **f** after adding third drop of glucose to the electrochemical cell; **g** stable phase of the reaction in the electrochemical cell after third drop

References

1. Kurenya, A.G., D.V. Gorodetskiy, V.E. Arkhipov, and A.V. Okotrub. 2013. Evaluation of the optimal carrier gas flow rate for the carbon nanotubes growth. *Technical Physics Letters* 39 (3): 258–261.
2. Coville, Neil J., Sabelo D. Mhlanga, Edward N. Nxumalo, and Ahmed Shaikjee. 2011. A review of shaped carbon nanomaterials. *South African Journal of Science* 107 (3–4), 01–15.
3. Chenguang, Lu, and Jie Liu. 2006. Controlling the diameter of carbon nanotubes in chemical vapor deposition method by carbon feeding. *The Journal of Physical Chemistry B* 110 (41): 20254–20257.
4. Lee, Cheol Jin, Seung Chul Lyu, Young Rae Cho, Jin Ho Lee, and Kyoung Ik Cho. 2001. Diameter-controlled growth of carbon nanotubes using thermal chemical vapor deposition. *Chemical Physics Letters* 341 (3), 245–249.
5. Kuo, Chien-Sheng, Allen Bai, Chien-Ming Huang, Yuan-Yao Li, Chi-Chang Hu, and Chien-Chong Chen. 2005. Diameter control of multiwalled carbon nanotubes using experimental strategies. *Carbon* 43 (13): 2760–2768.
6. Morris, James E. 2008. *Nanopackaging: Nanotechnologies and electronics packaging*. Berlin: Springer.
7. DiLeo, Roberta A., Brian J. Landi, and Ryne P. Raffaelle. 2007. Purity assessment of multiwalled carbon nanotubes by Raman spectroscopy. *Journal of Applied Physics* 101 (6), 064307; Vallés, Cristina, Manuel Pérez-Mendoza, Wolfgang K. Maser, M. Teresa Martinez, Laurent Alvarez, Jean-Louis Sauvajol, and Ana M. Benito. 2009. Effects of partial and total methane flows on the yield and structural characteristics of MWCNTs produced by CVD. *Carbon* 47 (4), 998–1004.
8. Kumar, Sunil, Sudip K. Pattanayek, and Gerald G. Pereira. 2014. Organization of polymer chains onto long, single-wall carbon nano-tubes: Effect of tube diameter and cooling method. *The Journal of Chemical Physics* 140 (2), 024904.
9. Aslan, N. 2008. Application of response surface methodology and central composite rotatable design for modeling and optimization of a multi-gravity separator for chromite concentration. *Powder Technology* 185 (1), 80–86.
10. Kastner, J., T. Pichler, H. Kuzmany, S. Curran, W. Blau, D.N. Weldon, M. Delamesiere, S. Draper, and H. Zandbergen. 1994. Resonance Raman and infrared spectroscopy of carbon nanotubes. *Chemical Physics Letters* 221 (1): 53–58.
11. Lehman, John H., Mauricio Terrones, Elisabeth Mansfield, Katherine E. Hurst, and Vincent Meunier. 2011. Evaluating the characteristics of multiwall carbon nanotubes. *Carbon* 49 (8), 2581–2602.
12. Andrews, R., D. Jacques, D. Qian, and E.C. Dickey. 2001. Purification and structural annealing of multiwalled carbon nanotubes at graphitization temperatures. *Carbon* 39 (11): 1681–1687.
13. Kang, Donghun, Noejung Park, Ju-hye Ko, Eunju Bae, and Wanjun Park. 2005. Oxygen-induced p-type doping of a long individual single-walled carbon nanotube. *Nanotechnology* 16 (8): 1048.
14. Maschmann, Matthew R., Placidus B. Amama, Amit Goyal, Zafar Iqbal, Roy Gat, and Timothy S. Fisher. 2006. Parametric study of synthesis conditions in plasma-enhanced CVD of high-quality single-walled carbon nanotubes. *Carbon* 44 (1), 10–18.
15. Veziri, ChM, G. Pilatos, G.N. Karanikolos, A. Labropoulos, K. Kordatos, V. Kasselouri-Rigopoulou, and N.K. Kanellopoulos. 2008. Growth and optimization of carbon nanotubes in activated carbon by catalytic chemical vapor deposition. *Microporous and Mesoporous Materials* 110 (1): 41–50.

16. Botello-Méndez, Andrés, Jessica Campos-Delgado, Aarón Morelos-Gómez, José M. Romo-Herrera, Ángel G. Rodríguez, Hugo Navarro, Miguel A. Vidal, Humberto Terrones, and Mauricio Terrones. 2008. Controlling the dimensions, reactivity and crystallinity of multiwalled carbon nanotubes using low ethanol concentrations. *Chemical Physics Letters* 453 (1), 55–61.
17. Bai, Xiaodong, Dan Li, Ye Wang, and Ji Liang. 2005. Effects of temperature and catalyst concentration on the growth of aligned carbon nanotubes. *Tsinghua Science & Technology* 10 (6): 729–735.
18. Wepasnick, Kevin A., Billy A. Smith, Julie L. Bitter, and D. Howard Fairbrother. 2010. Chemical and structural characterization of carbon nanotube surfaces. *Analytical and Bioanalytical Chemistry* 396 (3), 1003–1014.
19. Meyyappan, Meyya, Lance Delzeit, Alan Cassell, and David Hash. 2003. Carbon nanotube growth by PECVD: A review. *Plasma Sources Science and Technology* 12 (2): 205.
20. Tsai, Yu-Chen, Shih-Ci Li, and Jie-Ming Chen. 2005. Cast thin film biosensor design based on a nafion backbone, a multiwalled carbon nanotube conduit, and a glucose oxidase function. *Langmuir* 21 (8): 3653–3658.
21. Yin, Yajing, Yafen Lü, Wu Ping, and Chenxin Cai. 2005. Direct electrochemistry of redox proteins and enzymes promoted by carbon nanotubes. *Sensors* 5 (4): 220–234.
22. Tanemura, Masaki, K. Iwata, K. Takahashi, Y. Fujimoto, F. Okuyama, H. Sugie, and V. Filip. 2001. Growth of aligned carbon nanotubes by plasma-enhanced chemical vapor deposition: Optimization of growth parameters. *Journal of Applied Physics* 90 (3), 1529–1533.
23. Colomer, J.-F., C. Stephan, Serge Lefrant, Gustaaf Van Tendeloo, Isabelle Willems, Z. Konya, Antonio Fonseca, Ch. Laurent, and Janos B. Nagy. 2000. Large-scale synthesis of single-wall carbon nanotubes by catalytic chemical vapor deposition (CCVD) method. *Chemical Physics Letters* 317 (1), 83–89.
24. Singh, Charanjeet, Milo S.P. Shaffer, and Alan H. Windle. 2003. Production of controlled architectures of aligned carbon nanotubes by an injection chemical vapour deposition method. *Carbon* 41 (2), 359–368.
25. Moon, Jeong-Mi, Kay Hyeok An, Young Hee Lee, Young Soo Park, Dong Jae Bae, and Gyeong-Su Park. 2001. High-yield purification process of singlewalled carbon nanotubes. *The Journal of Physical Chemistry B* 105 (24), 5677–5681.
26. Park, Tae-Jin, Sarbajit Banerjee, Tirandai Hemraj-Benny, and Stanislaus S. Wong. 2006. Purification strategies and purity visualization techniques for single-walled carbon nanotubes. *Journal of Materials Chemistry* 16 (2), 141–154.
27. Hofmann, S., C. Ducati, J. Robertson, and B. Kleinsorge. 2003. Low-temperature growth of carbon nanotubes by plasma-enhanced chemical vapor deposition. *Applied Physics Letters* 83 (1): 135–137.
28. Lee, Cheol Jin, Jeunghee Park, Yoon Huh, and Jeong Yong Lee. 2001. Temperature effect on the growth of carbon nanotubes using thermal chemical vapor deposition. *Chemical Physics Letters* 343 (1), 33–38.
29. Castro, C., M. Pinault, S. Coste-Leconte, D. Porterat, Nedjma Bendiab, C. Reynaud, and M. Mayne-L'Hermite. 2010. Dynamics of catalyst particle formation and multi-walled carbon nanotube growth in aerosol-assisted catalytic chemical vapor deposition. *Carbon* 48 (13), 3807–3816.
30. Hanna Varghese, Saino, Remya Nair, Baiju G Nair, T. Hanajiri, T. Maekawa, Y. Yoshida, and D. Sakthi Kumar. 2010. Sensors based on carbon nanotubes and their applications: A review. *Current Nanoscience* 6 (4), 331–346.
31. Eklund, P.C., J.M. Holden, and R.A. Jishi. 1995. Vibrational modes of carbon nanotubes; spectroscopy and theory. *Carbon* 33 (7): 959–972.
32. Yuan, Dongning. 2008. *Property control of single walled carbon nanotubes and their devices*. ProQuest.

33. Zhang, Xianfeng, Anyuan Cao, Bingqing Wei, Yanhui Li, Jinquan Wei, Xu Cailu, and Wu Dehai. 2002. Rapid growth of well-aligned carbon nanotube arrays. *Chemical Physics Letters* 362 (3): 285–290.
34. Xinman, Tu, Yingjie Zhao, Shenglian Luo, Xubiao Luo, and Li Feng. 2012. Direct electrochemical sensing of glucose using glucose oxidase immobilized on functionalized carbon nanotubes via a novel metal chelate-based affinity method. *Microchimica Acta* 177 (1–2): 159–166.
35. Guiseppi-Elie, Anthony, Chenghong Lei, and Ray H. Baughman. 2002. Direct electron transfer of glucose oxidase on carbon nanotubes. *Nanotechnology* 13 (5), 559.
36. Jenkins, Peter A., Susan Boland, Paul Kavanagh, and Dónal Leech. 2009. Evaluation of performance and stability of biocatalytic redox films constructed with different copper oxygenases and osmium-based redox polymers. *Bioelectrochemistry* 76 (1), 162–168 (2009).
37. Laviron, E. 1979. General expression of the linear potential sweep voltammogram in the case of diffusionless electrochemical systems. *Journal of Electroanalytical Chemistry and Interfacial Electrochemistry* 101 (1): 19–28.
38. Liu, Ying, Mingkui Wang, Feng Zhao, Xu Zhiai, and Shaojun Dong. 2005. The direct electron transfer of glucose oxidase and glucose biosensor based on carbon nanotubes/chitosan matrix. *Biosensors & Bioelectronics* 21 (6): 984–988.
39. Chaubey, Asha, and B.D. Malhotra. 2002. Mediated biosensors. *Biosensors and Bioelectronics* 17 (6), 441–456.
40. Kumar, Arun, Asha Chaubey, S.K. Grover, and B.D. Malhotra. 2001. Immobilization of cholesterol oxidase and potassium ferricyanide on dodecylbenzene sulfonate ion-doped polypyrrole film. *Journal of Applied Polymer Science* 82 (14), 3486–3491.
41. Chen, Kuan-Jung, Chia-Feng Lee, John Rick, Shih-Han Wang, Chung-Chiun Liu, and Bing-Joe Hwang. 2012. Fabrication and application of amperometric glucose biosensor based on a novel PtPd bimetallic nanoparticle decorated multi-walled carbon nanotube catalyst. *Biosensors & Bioelectronics* 33 (1): 75–81.
42. Dias, L.G., António M Peres, Tânia P Barcelos, J. Sá Morais, and A.A.S.C. Machado. 2011. Semi-quantitative and quantitative analysis of soft drinks using an electronic tongue. *Sensors and Actuators B: Chemical* 154 (2), 111–118.
43. Deniz Yildirim, Burak Beşer, Elif Köksal, and Birol Çapa. 2008. Power Electronic Circuits Fall 2008, CRN: 11473.
44. Feng, Xueling, Kaihuan Zhang, Mark A Hempenius, and G. Julius Vancso. 2015. Organometallic polymers for electrode decoration in sensing applications. *RSC Advances* 5 (129), 106355–106376.

Chapter 5
Conclusion

Abstract In this chapter, a summary of the results are presented in brief. Based on results, major fundamental and technological advances have been made for enhancing the capabilities and improving the reliability of glucose measuring devices trough electrochemical glucose monitoring which has contributed significantly to improve the lives of diabetic people. Membrane, mediator, and electrocatalyst were some of the modified activities used to improve the second generation of biosensors based on mediator modified GOx sensors which are still gaining the huge attract by the market leaders.

5.1 Introduction

CNTs have been optimized for biosensing applications, to obtain faster response times and higher sensitivity than traditional electrodes at low working potentials. According to the results, it can be estimated that increasing the amount of immobilized GOx leads to higher active sites on the electrode which has a direct effect on the properties of the fabricated biosensor. Furthermore, the morphology of the CNTs has been improved to obtain the optimized detection sensitivity and selectivity for biosensing compared to conventional biosensing technologies by increasing the total surface area of the CNTs with lower diameter.

5.2 Morphology Optimization of Synthesized Carbon Nanotubes

The synthesized CNTs were optimized by means of effective factors determining the diameter, height, purity, and the orientation of the CNTs.

© Springer International Publishing AG 2018

A. TermehYousefi, *Nanocomposite-Based Electronic Tongue*, Springer Series in Materials Science 259, https://doi.org/10.1007/978-3-319-66848-2_5

5.3 Fast Synthesizing of the Multilayer Carbon Nanotubes

The single-step developed as a new method that allows for the control of the diameter of CNTs on silicon substrate. The FESEM results coupled with HRTEM images clearly indicate that the multilayer MWCNTs were successfully synthesized on the substrate in a one-step process using renewable natural camphor oil via CVD. The diameter of CNTs produced through the optimized growth condition is limited by controlling the diffusion of the feedstock.

5.4 Well-Crystalline Multi-walled Carbon Nanotubes

According to this method, the carbon feeding rate was controlled by altering the carrier gas in the diffusion of nanotube feedstock to neutralize the formation of disorders in the cooling step of CVD. Among the candidate carrier gases, argon and oxygen have advantageously exhausted the feedstock into the quartz by invariable acceleration with a flow microcontroller. Oxygen, as a carrier gas in the cooling process, prevents highly mobile carbons from forming small, physisorbed clusters of CNTs or amorphous carbon. The results demonstrate that different cooling methods for synthesizing CNTs will affect the structural defects and naturalize the impurities to yield CNTs with diverse crystallinity.

5.5 Highly Oriented Carbon Nanotubes

In this contribution, high VACNTs arrays based on CVD method were reported. The length of the nanotubes, the uniform orientation, and extra high purity are some of the advantages of synthesized CNTs. The correlation of parameters involved in the growth mechanism was studied in an attempt to determine the interactions between the variables. The results can be used to easily scale up CNTs in continuous or semicontinuous production. The FESEM results supported by Raman spectroscopy and TGA confirm the optimized condition of growth CNTs, which can display impressive architecture in different applications.

5.6 Selective Aspect Ratio of Carbon Nanotubes

In this contribution, growth temperature was described as an effective parameter in the CVD method to optimize the aspect ratio of CNTs. The correlation of growth temperature and annealing time on the growth mechanism was examined to determine the complex interactions between the annealing process and aspect ratio

of CNTs. According to the results, increasing the growth temperature up to 950 °C will increase the axial alignment as well as increasing the crystallite size, which indicates that the developing graphitic domains are still continuing in the annealing process. The FESEM images indicate that the nanotubes are approximately perpendicular to the surface of the silicon substrate and CNTs form in different aspect ratios according to the applied growth temperature. HRTEM images also confirm that CNTs were successfully made up of 10–15 graphitic sheets.

5.7 Vectorial Crystal Growth of Oriented Vertically Aligned Carbon Nanotubes

Research reports the utilization of response surface methodology to provide a model to synthesize low defect CNTs by designating a set of experiments to understand the overall response for each effective factor. Regression analyses coupled with ANOVA were used to form a mathematical model to obtain the correlation between crystallinity and influencing factors. However, to focus the discussion, four effective explanatory variables on crystallinity of CNTs during CVD process were studied, denoted by deposition temperature, deposition time, annealing temperature, and concentration of precursor. According to lowest *p*-values and highest *t*-student test values, also the quadratic term of deposition temperature, annealing time, and the concentration of precursor show significant effects on the crystallinity of CNTs as well as the interaction term of deposition time with annealing time and concentration of precursor.

5.8 Constant Glucose Biosensor Based on Vertically Aligned Carbon Nanotubes Composites

As-optimized CNTs were modified to reclaim the oxidation or reduction of biological molecules during the adsorbent and interaction of biosensors. The total charge carrier of CNTs density will change by adsorbent biomolecules and the alteration of the conductance, making the CNTs-based biosensor capable of powering a full device in continuous monitoring of biological molecules. Polymeric entrapment or covalent immobilization methods enhance the direct and fast electron transfer of enzymes, and are rapidly emerging as a new research area in the functionalization of CNTs. The resulting electrode exhibits a fast response, wide linear range, and good stability for glucose sensing. The entrapment of GOx in MWCNTs/Gl composite matrix was carried out with good film-forming and optimum biocompatibility. The GOx/MWCNTs/Gl/GCE was superior in maintaining the bioactivity of GOx, rendering it suitable as an amperometric biosensor for glucose detection with potassium ferricyanide as its mediator. The fabricated

biosensor exhibited a wide linearity range of 0.1–8.9 mM glucose, with the detection limit of 0.54 mM and a stability of 75.4% current diminish after 25 days.

5.9 Brain-Like Taste Bud Circuit Using the GOx/MWCNTs/Gl/GCE Glucose Biosensor

Besides improving the carbon-based electroconductive platform of biosensors, the brain-like circuit design can also be changed for the integration of a complete categorized artificial tongue by the electrochemical detection of all types of tastes. The proposed electronic tongue, namely artificial taste bud, consisted of neuron-like circuits attached to the amperometric glucose biosensor. The circuit design consists of two layers. In the first layer, the glucose concentration was transduced to a spiking pattern. The spiking pattern was conducted to the second layer via paracrine-like optical transmission, and induced synchronization of neural spiking activity in the second neuron layer. The glucose concentration was represented by the degree of synchronization of the output spike. The resistance of the modified GC electrode depends not only on the glucose concentration, but also on the applied voltage at the electrode. When the electrode resistance is reduced due to high glucose concentration, the fraction between R1 and R2 changes and the electrode resistance is reassigned a new value. This tuning process automatically occurs, and the output impulse frequency approaches multiple stable states. The results clearly confirm that by adding glucose to the circuit design, the output oscillation frequency changes and the square wave frequency becomes new stable value.

5.10 Research Contribution

The contributions of this research were detailed in previous sections, where it can be classified into theoretical and experimental contributions. Generally, the study contributes to the body of knowledge on glucose biosensor-based CNTs. The experimental contribution particularly emphasizes the synthesis of MWCNTs using the double-furnace CVD method. Several parameters were studied to obtain the best response of CVD, which is comparable to the results of other researchers. Meanwhile, a detailed literature review related to the synthesis of CNTs was described that is useful for anyone intending to follow up on this study. A theoretical model was also developed for CNTs' growth using statistical analyses, which include updated references of recent findings.

The main contribution of this book is to suggest two different applications for optimized MWCNTs based on the modification of the GC electrode in an electrochemical cell. The correct detection of glucose using a fabricated CNTs-based biosensor is a significant practical objective, which shows the role of

electroconductive material to the biosensing approach. Furthermore, integration of electronic tongue based on the modified GCE opens a new filed of research in artificial brain-like circuits, which is experimentally significant for future research planning.

5.11 Recommendations and Future Work

Carbon nanotube is a promising material for many applications, due to its perfect physical and chemical properties in the context of glucose sensing. This book emphasizes the morphological improvements of MWCNTs as a platform for glucose biosensing. There should be improvements in the biosensors' properties by using optimized SWCNTs or DWCNTs, which can be synthesized by the application of higher temperatures in the CVD, followed by the gas phase hydrocarbons. SWCNTs and DWCNTs show superior electrical properties to MWCNTs, due to their lower number of walls. However, synthesizing SWCNTs and DWCNTs is more costly than MWCNTs, and fast and easy growth of vertically aligned SWCNTs and DWCNTs remains a challenge. Furthermore, graphene nanoribbon, which can be produced by longitudinal unzipping of SWCNTs and DWCNTs (by sonication method), can also be a good electroconductive material, due to its high surface area for the immobilization GOx.

Besides improving the carbon-based electroconductive platform of biosensors, the brain-like circuit design can also be changed for the integration of a complete categorized artificial tongue by the electrochemical detection of all types of tastes. In fact, the electronic tongue fabricated to detect sweetness can be developed for other tastes via the electrochemical detection of hydrogen chloride (sourness), sodium chloride (saltiness), caffeine (bitterness), and disodium guanylate (savoriness) in liquids.

Index

A
Acceptor, 21
Acid, 4
Agitation, 39
Amorphous, 4, 66–68, 71, 73, 74, 76, 81, 94
Analytes, 2
Animal tissue, 5
Annealing, 16, 74–79, 94, 95
Anode, 14
Antibody, 5
Anticancer agents, 28
Antifungal amphotericin, 30
Antigen, 5
Antimicrobial, 29
Antimicrobial biocomponents, 30
Argon, 41, 63, 64, 66, 68, 71, 94
Armchair CNTs, 2
Aryl diazonium, 20
Atmosphere, 14
Atoms, 17, 68, 74, 80
Authentic, 8

B
Bacteria, 29
Biocompatibility, 20, 87, 95
Biocomponents, 74
Biological, 1, 86, 95
Biological devices, 6
Biomolecules, 2, 95
Biosensing, 1, 93, 97

C
Camphor oil, 19, 63, 70, 71, 73, 76–78, 80, 81, 94
Cancer, 28
Carbonaceous, 4, 81
Carbon nanotube, 1, 65, 79, 97
Carbon nanotube spearing, 29
Carboxylation, 20
Catalyst, 15, 70, 71, 78, 81
Cathode, 14
Chamois, 54
Chemically Modified Electrodes (CMEs), 5
Chemistry, 1
Chiral CNTs, 2
Co, Ni, and FeS, 14
Components, 6
Composites, 54
Conductivity, 2
Constitution, 18
Convenient, 8
Counter electrode (Pt wire), 55
Covalent, 4, 95
Crystallinity, 4, 63, 66–68, 71–74, 77–81, 94, 95
CVD, 3, 63, 67, 69–71, 73, 74, 77, 78, 80–82, 94–97
Cycloadditions, 20
Cylinder, 13

D
Decomposes, 18
Decomposition of carbon, 3
Defects, 4, 67, 68, 71, 94
Deionized (DI), 39
2-deoxy-d-glucose, 21
d-fructose, 21
Diabetes, 1, 6, 87
Diabetes mellitus, 5
Diameter, 13, 63, 64, 66, 68–73, 75, 76, 82
Dimethylformamide, 23
Direct Current (DC), 14
Discharge, 14
Dispersing, 54
d-mannose, 21
DNA manifestation, 29
Double-walled Carbon Nanotube (DWCNTs), 2, 97

© Springer International Publishing AG 2018

A. TermehYousefi, *Nanocomposite-Based Electronic Tongue*, Springer Series in Materials Science 259, https://doi.org/10.1007/978-3-319-66848-2

Drug delivery, 28
Drugs, 28

E
Economical, 8
Efficacy, 7
Electrical signals, 2
Electrocatalyst, 93
Electrochemical, 1, 63, 74, 88, 89, 93, 96, 97
Electrochemical system, 56
Electrode, 5, 74, 83–87, 89, 95–97
Electron, 6, 63, 74, 82–86, 95
Electron beam, 49
Electron-transfers, 20
Electrophilic, 20
Embracing mass, 7
Enzymatic biosensors, 19
Enzyme, 5, 86, 95
Escherichia coli, 29
Ethanol, 54
Exohedral derivatizations, 5

F
IV, 56
Faradaic, 57
Feedstock, 41, 64, 69, 71, 94
Ferrocene, 18, 42, 70–73, 78, 81
Field Emission Scanning Electron Microscope (FESEM), 49, 50, 63, 64, 66, 68–70, 75, 82, 83, 94, 95
Flask, 21
Folic acid, 29
Fourier Transform Infrared (FTIR) spectrometer, 51, 52, 64–66
Frequency, 58
Fullerene, 31
Function, 17, 76–78
Functionalization, 5, 95
Functionalized, 4, 29

G
GCE, 39, 63, 83–86, 95, 97
Gelatin, 54
Genes, 28
Glucose, 1, 63, 84–89, 93, 95–97
Glucose biosensors, 5, 85
GOx, 19, 63, 83–88, 93, 95, 96
Graphene, 2, 68, 97
Graphite, 14, 80
Graphitized, 18

H
Halogenation, 20
HNO_3, 23
Horizontal quartz tube, 41
Hottest zone of, 17
HRTEM, 49, 71, 75, 81, 94, 95
Hybridization, 26
Hydrocarbon, 15, 71, 74
Hydrogen, 15, 97
Hydrogenation, 20
Hydrogen peroxide (H_2O_2), 21
Hydrophobic, 3, 63
Hydroxybutyrate, 20

I
Immobilized, 6
Impurities, 4, 66, 67, 94
Interference, 20
Interferogram, 51

L
Laser beam, 14
Lifetime, 6
Light Emitting Diode (LED), 58
Linkage, 25
Liquid medium, 29
Lymph node cancers, 29

M
MΩ, 39
Mechanism, 18, 67, 80, 82, 94
Mechanistic, 18
Metallic (conductors), 31
Microfiltration, 4
Micromolar, 23
Molecules, 28, 87, 95
Morphology, 17, 69, 93
Multi-walled Carbon Nanotubes (MWCNTs), 2, 24, 63, 64, 69, 71, 73, 75, 81, 82, 84, 87, 94, 96, 97

N
Nanoelectronics/nanospintronics, 2
Nanoparticles, 15
Nanotechnology, 1
Negative, 14
Non-covalent, 4
Nucleophilic carbenes, 20

O
Operating potential, 20
Optical, 96
Optical sensors, 7
Oscillation, 58
Oscillation frequency, 63, 89
Oscilloscope, 59, 63
Oxygen, 19, 66, 68, 94

P
Pathogenic, 29
Physics, 1
Pi-stacking, 5
Plant, 5
Polymers, 25
Poly Methyl Methacrylate (PMMA), 24
Polynomial model, 43
Polypyrrole (PPy), 21
Potentiometric, 7
Powder, 14, 64
Practical, 14, 96
Proteins, 28
Pyrolyzed, 54

Q
Quadratic, 43, 77, 78, 95
Quartz tube, 41, 66

R
Radicals, 20
Radius, 2
Raman spectroscopy, 48, 74, 80
Redox, 19, 83, 84
Reference electrode ($Ag|AgCl|KCl_{3M}$), 55
Relative Standard Deviation (RSD), 56
Resistances, 16
Resistivity, 13, 88

S
Scaffold, 5
Selective, 25, 74, 94
Semiconducting, 31
Sensitive, 25
Sequential experimental strategies, 3
Silicon, 14, 63, 64, 68, 71, 94, 95
Single-walled Carbon Nanotubes (SWCNTs), 2, 69, 97
Solubility, 20
Soot carbon, 14
Sorption, 5
Sp^2, 26
Sp^3, 26
Spectroscopic, 51
Spectrum, 51, 64–66
Square wave, 58, 89, 96
Stability, 7, 73, 74, 84, 86, 87, 96
π–π stacking, 20
Sulfanilic acid, 21
Sulfo-NHS, 21
Supramolecules, 20
Sweetness, 57, 63, 88, 97

T
Tert-butyl nitrite, 21
Theories, 17
Therapeutic materials, 29
Thermal Interface Materials (TIMs), 26
Thermogravimetric Analysis (TGA), 47, 73, 74, 94
Thermogravimetric analyzer, 47, 48
Thin film, 14
Three-electrode, 55
Three-electrode system, 56
Transmission electron microscope, 49, 51
Tumor targeting, 28

V
VACNTs, 19, 74, 94
Van der Waals, 5, 87
Vaporization, 17
Variables, 44, 76, 94
Voltage, 14, 88, 89, 96
Voltammetric, 7, 86

W
Working electrode, 55

Y
Yield strength, 3
Young's modulus, 3

Z
Zigzag CNTs, 2